FACULTÉ DES ÉTUDES SUPÉRIEURES ET POSTOCTORALES

uOttawa

L'Université canadienne
Canada's university

FACULTY OF GRADUATE AND POSDOCTORAL STUDIES

Jacqueline Cormier
AUTEUR DE LA THÈSE / AUTHOR OF THESIS

M.A.Sc. (Civil Engineering)
GRADE / DEGREE

School of Information Technology and Engineering
FACULTÉ, ÉCOLE, DÉPARTEMENT / FACULTY, SCHOOL, DEPARTMENT

Laboratory Studies of Near Surface Permafrost Conditions in Fine-Grained Soils from the Mackenzie Valley, N.W.T.

TITRE DE LA THÈSE / TITLE OF THESIS

Baolin Wang
DIRECTEUR (DIRECTRICE) DE LA THÈSE / THESIS SUPERVISOR

CO-DIRECTEUR (CO-DIRECTRICE) DE LA THÈSE / THESIS CO-SUPERVISOR

EXAMINATEURS (EXAMINATRICES) DE LA THÈSE / THESIS EXAMINERS

P. Simms

M. Fall

Gary W. Slater
Le Doyen de la Faculté des études supérieures et postdoctorales / Dean of the Faculty of Graduate and Postdoctoral Studies

Laboratory Studies of Near Surface Permafrost Conditions in Fine-grained Soils from the Mackenzie valley, N.W.T.

Jacqueline Cormier

Thesis submitted to the
Faculty of Graduate and Postdoctoral Studies
In partial fulfillment of the requirements for the degree of

MASTER'S OF APPLIED SCIENCE
in Civil Engineering

Ottawa-Carleton Institute for Civil Engineering
University of Ottawa
Ottawa, Canada

Your file Votre référence
ISBN:978-0-494-63016-7
Our file Notre référence
ISBN: 978-0-494-63016-7

Table of Contents

List of figures

List of tables

List of symbols

A: cross-sectional area of a soil element (cm^2);

AE: actual vertical evaporative flux (mm/day);

c_v: coefficient of consolidation (cm^2/s);

erf ( ): error function;

f(u): function dependent on wind speed;

k: hydraulic conductivity (cm/s);

k_x: thermal conductivity in the x-direction (kJ/hr/m/°C);

k_y: thermal conductivity in the y-direction (kJ/hr/m/°C);

m_v: coefficient of volume compressibility (cm^2/s);

P_0: load applied at the surface (kPa);

Q: applied boundary flux (kJ/hr);

Q_n: net radiant energy available at the surface (mm/day);

R: thaw consolidation ratio;

M1: Model 1;

M2: Model 2;

t: time;

T: temperature (°C);

T_s: temperature at the soil surface (°C);

T_a: temperature of the air above the soil surface (°C);

u: excess pore pressure (kPa);

ΔV: change in volume;

x: depth measured from the ground surface (m);

X: distance to the thaw plane from the soil surface (m);

W_r: ratio of the relative magnitude of the applied load and the effective overburden pressure at the thaw line;

α: thermal constant determined in the solution of the heat conduction problem ($m/yr^{1/2}$);

γ: unit weight of soil (kN/m^3);

γ' : submerged unit weight of the soil (kN/m^3);

γ_w: unit weight of water (kN/m^3);

λ: capacity for heat storage;

σ: total stress (kPa);

σ'_0: soil initial effective stress in the soil (kPa);

υ: psychrometric constant;

ω: gravimetric water content of the soil.

Abstract

Laboratory studies were conducted on fine-grained soils from the Mackenzie valley, N.W.T., Canada, to study the transient layer. Two laboratory models simulating repeated freeze-thaw cycles were placed in a walk-in freezer. Temperatures and pore water pressures were monitored along the soil columns during eleven freeze-thaw cycles. At the end of the testing program, soil moisture conditions and cryostructures were examined. Temperature and pore water pressure data were compared to computed results and the thaw consolidation theory, respectively.

In both laboratory models, an ice-rich zone developed at the active layer and permafrost interface as a result of moisture migration to the freezing front. The high ice content zone was altered under extreme air temperature conditions. Distinct cryostructures were created after repeated freeze-thaw processes. The formation and shifting of the ice-rich zone provide useful information on moisture conditions and the cryostructures for further understanding the transient layer.

Résumé

Une étude expérimentale a été effectuée sur un sol fin près de la surface de pergélisol provenant de la vallée du Mackenzie, T.N.O, Canada afin d'étudier la zone de transition. Deux appareils de laboratoire simulant des cycles répétés de gel-dégel ont été placés dans un réfrigérateur. À la fin du test, la distribution de glace et les cryostructures furent examinées. Les données de températures et de pressions interstitielles ont été comparées à des résultats numériques et à la théorie de consolidation, respectivement.

Dans les deux modèles, une zone à teneur élevée en eau fut créée à l'interface de la zone active et du pergélisol résultant de la migration de l'eau vers l'isotherme 0°C. La zone riche en eau fut altérée sous des conditions extrêmes de températures. Des cryostructures distinctes furent créées à la suite de cycles répétés de gel-dégel. La formation et le

déplacement de la zone riche en glace fournissent de l'information utile concernant la distribution d'eau et les cryostructures afin de mieux comprendre la zone de transition.

Acknowledgements

Very special thanks to Dr. Baolin Wang for guiding me during my Masters degree. I want to thank him for his valuable input throughout my studies and to have given me the opportunity to write a research paper. Thank you for providing me with a job and a space to work at the Geological Survey of Canada.

Thanks to the Natural Science and Engineering Research Council for awarding me with research funds necessary to complete my degree.

Thanks to the GSC library staff for all the help and for always greeting me with a smile. The staff was always keen on assisting me in finding those hard-to-find papers.

Thanks to Dr. Fall for offering me a directed studies course and for giving me the opportunity to be a teacher in the laboratory. It was a great teaching experience!

Thanks to Kenneth Lalonde for helping me with the installation and removal of the soil samples in the laboratory and for adjusting the lab apparatus to the testing requirements.

Thanks to the "coffee club" at the end of the hall on the fifth floor. Especially Denis and Scott for giving me guidance, expert advice on oral presentations and making me laugh all the time!

Last but not least, thank you Pape, Mame, my sister Martine and all of my friends for their support, advice and love throughout my studies.

1 Introduction

1.1 General

Cold region engineering is gaining more attention given the interest of the energy sector in the north. In addition, there are concerns that climate change may contribute to the degradation of permafrost, which can lead to landslides and excessive ground settlements. Natural disasters have major implications on the integrity of engineering structures such as roads and pipelines. A significant number of landslides have been recorded in the Mackenzie valley which mostly occur in fine-grained soils (Aylsworth et al. 2000a). Such slope failures are linked to the thawing of near surface permafrost. However, the current state of knowledge on this topic is still limited. It is necessary to study permafrost terrain under extreme climate conditions in order to better understand landslide triggers and thaw consolidation to assist engineers in developing appropriate solutions when dealing with permafrost-related geotechnical problems.

Currently, permafrost underlies approximately 50% of the Canadian territorial surface (Johnston 1981; Heginbottom and Radburn 1992). Permafrost consists of earth materials that remain continuously at or below 0°C for at least two consecutive years (Andersland and Ladanyi 2004). Geographically, permafrost is divided into three categories: continuous, discontinuous and sporadic, as outlined in Figure 1.1.

Permafrost varies from continuous and thick (greater than 100 m) in the north to sporadic and thin (less than 5 m) in the extreme south of the Mackenzie valley (Aylsworth et al. 2000a). The layer of soil overlying permafrost is called the active layer and thaws annually. The thickness of this layer varies from 15 cm in the far north to 1 m or more in the south of the N.W.T. (Andersland and Ladanyi 2004). Extreme weather can cause thawing to greater depths than normal which may result in various geotechnical concerns.

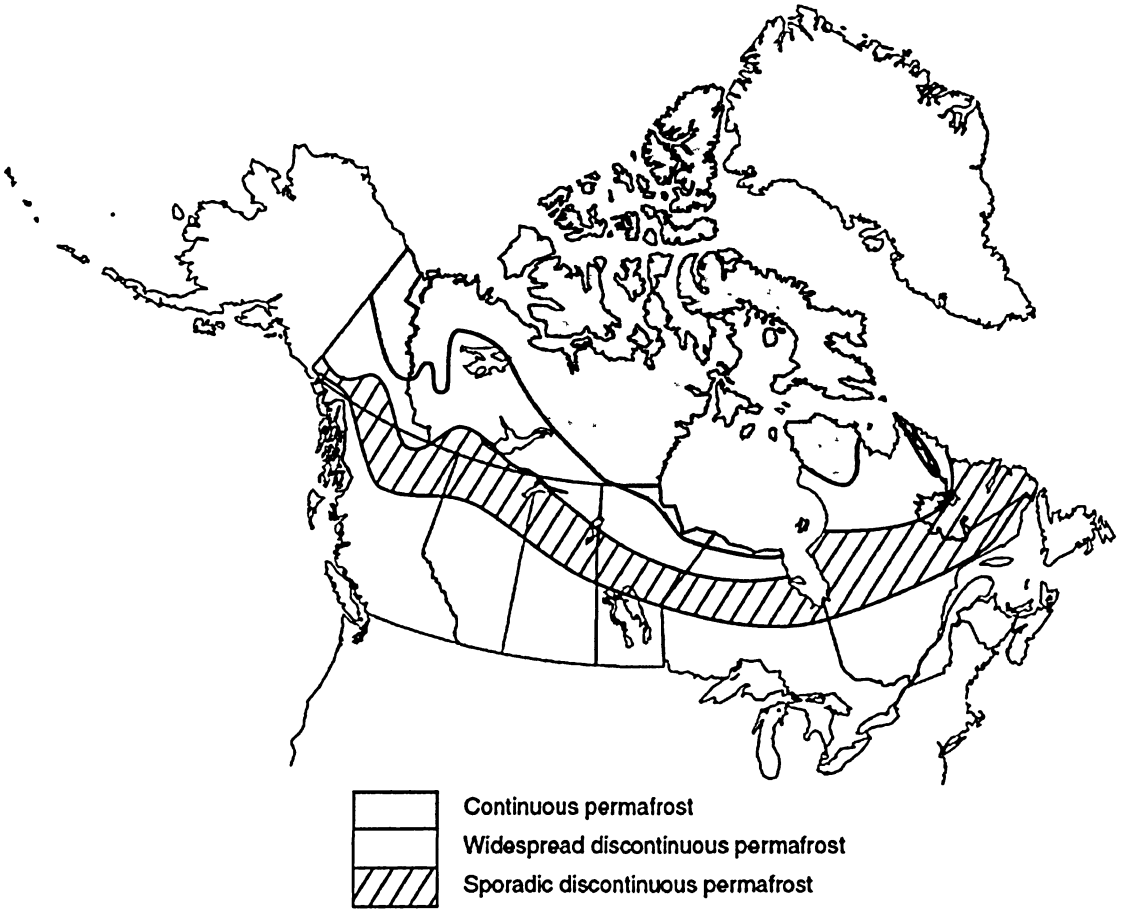

Figure 1.1 Types of permafrost in Canada (Source: Smith and Riseborough 2002, adapted from Brown 1972)

Much of the Mackenzie valley has a thin and discontinuous to thick and continuous cover of glacial ground moraine, also referred to as till (Aylsworth et al. 2000a). These fine-grained sediments generally have 10-25% segregated ice occurring as thin, irregular seams in the upper 2 to 3 m, with thicker lenses or irregularly distributed large masses of segregated ice at greater depths. Research shows that areas containing ice-rich sediments are most susceptible to landsliding as a result of permafrost degradation (Aylsworth et al. 2000b). An inventory of 3400 landslides have been identified from historical air photos along the Mackenzie valley, the Mackenzie Delta and Tuktoyaktuk (Aylsworth et al. 2000a). A flow-type of failure, such as the one shown in Figure 1.2, is the most common type of slope failure occurring in thawing fine-grained soils in the Mackenzie valley (McRoberts and Morgenstern 1974; Aylsworth et al. 2000a; Dyke 2000, 2004; Harris and

Lewkowicz 2000; Wang et al. 2005). Many failures occurring on slopes of less than 15° have been recorded (Dyke 2000).

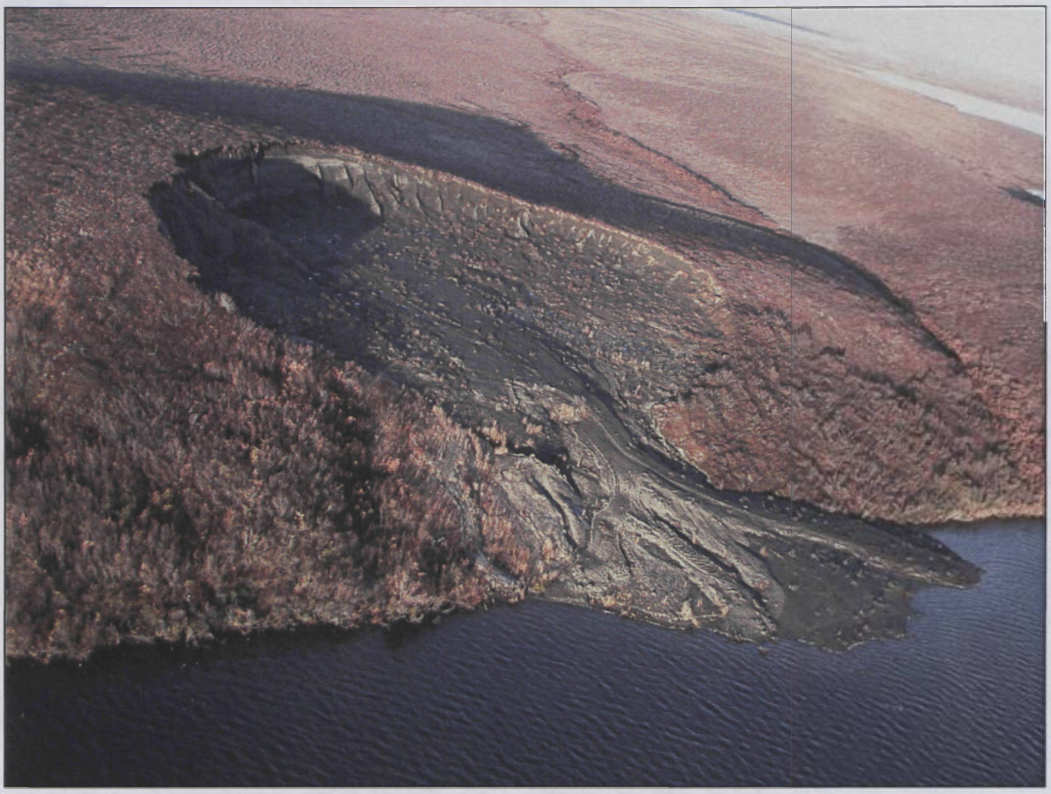

Figure 1.2 A typical retrogressive thaw flow in the Mackenzie valley (Wang et al. 2005)

1.2 Transient layer

Traditionally, permafrost ground is defined as a two-layered system: a seasonally frozen zone, called the active layer, and underlying permafrost (Andersland and Ladanyi 2004). However, this two-component model fails to adequately explain the behaviour of frozen ground, especially in ice-rich soils (Shur 1988; Shur et al. 2005; Nelson et al. 2008). A third layer, located between the active layer and subjacent permafrost, called the transient layer (or transition zone) is often overlooked. This layer thaws periodically, but not every year. It appears that the transient layer is present throughout the permafrost region (Shur 1988), but can sometimes be difficult to visually identify in field investigations (Wang et al. 2005). By definition, this layer is still classified as permafrost (Everdingen 2002). However, the intermediate layer has characteristics that differ from the active layer and long-term permafrost (Shur et al. 2005).

The moisture regime of the transient layer can be an important factor in determining soil strength during thawing. In ice-rich fine-grained permafrost, when ground ice transforms into water, soil shear strengths are significantly reduced. Based on a field investigation conducted by Wang et al. (2005), fine-grained soils generate a significant amount of water when thawed and may even become liquid. Consequently, the soil is unable to sustain shear stress. Under these circumstances, it can be assumed that soil shear strength reduction of a fine-grained soil is related to its water content. Several geotechnical related problems may arise in the event that thawing occurs. Wang et al. (2008) indicated that the total water content is one of the most important characteristics of permafrost soils.

The transient layer is believed to play a key role in slope stability (Wang et al. 2005). It also promotes thermal stability for the underlying permafrost (Shur et al. 2005). In other words, the latent heat properties of the transient layer cause the ice-rich zone to resist thaw and tend to encourage thermal stability at greater depths. If thawing occurs beyond the transient layer into the underlying permafrost, shear strength will most likely decrease (Nixon and Morgenstern 1973), which could possibly lead to slope instability and excessive thaw consolidation (Morgenstern and Nixon 1971). Thus, thawing of transient layer soils could be critical in geotechnical implications. Nonetheless, this layer has been the focus of very few studies; therefore, the impact of extreme climate conditions on its thermal regime requires further study.

Understanding the causes of landslides and excessive thaw consolidation in permafrost and developing appropriate mitigation measures are of great interest to engineers. Therefore, gaining more knowledge on near surface permafrost in regards to these issues is of prime importance. More specifically, it is essential to shed some light on the thermal and moisture regimes of the transient layer in order to have a better understanding of its implications in permafrost terrain. Additionally, if the transient layer can be more clearly defined, only then can it be identified with more accuracy when conducting a soils investigation. In the event that this is achieved, the transient layer can

then be a part of slope stability analyses which may reduce risks associated with its thawing. In some field studies, one of the criterions used for determining the bottom of active layer has been the identification of cryostructures (Höfle et al. 1998; Bockheim and Hinkel 2005).

1.3 Cryostructures

The term cryostructure refers to the shape and distribution of ice and sediment within frozen soils. The three zones of soil found within permafrost ground – active layer, transient layer and permafrost – contain varying amounts of ground ice. This is mainly due to the particular thermal regime of permafrost soils in comparison to non-permafrost soils. As a result, a range of sediment arrangement can be found in permafrost terrain. Various terms have been used to identify the cryostructures found in permafrost ground. To end the confusion, Murton and French (1994) put forth a detailed description of typical cryostructures encountered in a periglacial environment. The identification of cryostructures could assist engineers and scientists in delineating the active layer, transient layer and permafrost zones (Höfle et al. 1998; Bockheim and Hinkel 2005).

1.4 Thaw consolidation

From an engineering point of view, thaw settlement is one of the most common geotechnical problems resulting from the thawing of permafrost. It is crucial for engineers to understand the process of thaw consolidation in cold regions prior to developing mitigation methods.

Thawing of fine-grained soils may lead to consolidation which is defined as a volume reduction or change in void ratio that results in soil settlement. Soils that are most sensitive to thaw settlement are moraine, fine-grained lacustrine and organic bog (Aylsworth et al. 2000a). Such soils are commonly found in the Mackenzie valley, making this area susceptible to landslides and excessive thaw settlements. The thaw consolidation behaviour of a soil depends on many factors, including the physical properties of the soil, water supply, amount and distribution of ice in the soil, load, thaw rate, the rate of pore water dissipation, etc. Higher ice content in the soil results in higher

values of thaw consolidation which produce greater settlements. The generation of excess pore water pressures leads to a decrease in shear strength, bearing capacity and stability of the soil (Nixon 1973; Wu and Tong 1991; Harris et al. 2001). Excess pore water pressures are mainly dependant on thaw rate and the rate of pore water dissipation within the soil matrix (Morgenstern and Nixon 1971). In order to evaluate the excess pore water pressures generated in a compressible soil, Morgenstern and Nixon (1971) developed a thaw consolidation theory based on heat conduction and linear consolidation. Solutions for two special loading conditions were developed: a weightless material with surface loading and a soil consolidating under its own weight. The thaw consolidation behaviour for a thawing soil consolidating under its own weight has been investigated by Lesage and Wang (2008) which was intended to verify the theory using laboratory models subjected to one freeze-thaw cycle. In general, theoretical predictions and experimental results agreed. As part of the current research, the Morgenstern and Nixon theory is further evaluated for a soil consolidating under its own weight during eleven freeze-thaw cycles.

It should be noted that the coupled mechanical, hydraulic and thermal behaviour of a soil matrix under freeze-thaw cycle is a highly complex issue. Several soil characteristics may change if any conditions change. For example, freezing and thawing processes cause soil moisture migration and soil structure change, which in turn causes hydraulic conductivity change. Changes in ice/water content affect the thermal conductivity and heat capacity. Furthermore, thermal and hydraulic changes within the soil matrix influence pore pressure conditions and therefore soil strength. To date, no model or theory is capable of modeling the fully coupled behaviour. Discussions about the complex mechanical-hydraulic-thermal behaviour are beyond the scope of this study.

1.5 Objectives of the study

The main objective of this research is to better understand geotechnical characteristics of fine-grained soils near the permafrost table. The study investigates geothermal and geotechnical characteristics and the behaviour of a transition zone that thaws under

abnormal climate conditions. The ultimate goal is to contribute to knowledge regarding this zone for better design of engineering projects in permafrost.

1.6 Scope of the investigation

A laboratory study was conducted on two fine-grained soil samples from the Mackenzie valley, N.W.T. Two identical laboratory apparatuses were specifically designed to simulate soils under repeated freezing and thawing. Variation of thawing temperatures was applied to one of the samples during later thawing cycles. Soil temperatures, moistures, and pore water pressures were measured and cryostructures inspected.

A finite element analysis was carried out to investigate soil thermal conditions. Soil moisture conditions and cryostructures were evaluated along with temperature history. As well, the pore water pressure data were compared to the consolidation theory developed by Morgenstern and Nixon (1971).

1.7 Thesis outline

In the second Chapter, a literature review on the transient layer, cryostructures and thaw consolidation is presented. In Chapter 3, the laboratory apparatus used in this study is introduced. A description of the soil samples tested and the method of testing are also discussed in this chapter. Chapters 4, 5, 6 and 7 present results and analyses of temperatures, moisture contents, cryostructures and pore water pressures, respectively, of the two samples tested in the laboratory. Finally, conclusions form Chapter 8.

2 Literature Review

2.1 Transient layer

In general, permafrost terrain is described as a two-layered system. However, the active layer/permafrost system fails to adequately explain the behaviour of frozen ground (Shur 1988; Shur et al. 2005). There is a third component in frozen soils which is believed to play a key role in slope stability: the transient layer (Shur et al. 2005; Wang et al. 2005). Nonetheless, this layer has yet to be defined quantitatively since it is a relatively new concept in permafrost engineering.

According to Grechishchev and Grechishcheva (1997), V.K. Yanovsky in 1933 was the first researcher to identify the so-called "transitive" layer. He stated, "By a transient layer of permafrost region we call its very upper bed which under favorable conditions thaws, joining the active soil layer, and under unfavorable conditions remains frozen, representing the upper layer of permafrost". Several authors have noted the presence of an intermediate layer between the active layer and the permafrost. In 1972, Mackay was referring to the transient layer when he stated that an ice-rich zone can develop where an aggrading permafrost table traps ice lenses that have formed at the base of the active layer during two-sided freeze-back. Lewkowicz and Clarke (1998) confirmed the importance of a basal ice-rich layer by demonstrating enhanced rates of slope movement throughout the active layer during summers with deep thaw. Within the basal ice-rich layer, the soil thaws and moves in some years and remains frozen and stationary in others. In general, higher rates of movements developed in years with deeper thaw. Based on field monitoring conducted by Harris and Lewkowicz (1993 and 2000), active layer soils close to maximum thaw are subjected to progressive shear strains which take place over a thin basal ice-rich zone. The displacements cause the shear strength values to gradually decrease from peak to residual. Shur et al. (2005) defined the transient layer as having different characteristics from the active layer and permafrost. These authors believe the transition zone has a great impact on certain periglacial processes, on the thermal stability of the underlying permafrost and on the formation of cryogenic structures (or cryostructures). Wang et al. (2005) emphasized the likelihood of the

transient layer playing a key role in permafrost slope stability by studying landslides in the Mackenzie valley. Field observations lead to the conclusions that soil shear strength at the base of the active layer is generally lower in comparison to that of the upper active layer soils after being thawed. Kokelj et al. (2007) examined how changes in the transient layer affect the active layer thermal regime and surface morphology in Inuvik, N.W.T. They concluded that ice-enrichment in the transient layer is the principal mechanism driving hummock form modification. A study conducted by Wang and Saad (2007) correlates slope failure, ice content and the transient layer by suggesting that thawing of the transient layer may or may not trigger landslides depending on its water content, rate of thaw, pore water pressure and material strength. In many arctic field investigations, an ice-enriched zone has been identified and described as being either within the transient layer (Shur 1988; Shur et al. 2005; Bockheim and Hinkel 2005; French 2007; Nelson et al. 2008b) or at the base of the active layer (top of permafrost) (Mackay 1971, 1983; Pollard and French 1980; Cheng 1983; Kokelj and Burn 2003a, 2005; Morse et al. 2009). All of these studies highlight the importance of the transient layer and the need to better understand its role in permafrost terrain.

The transient layer is located between the active layer and the long-term permafrost as conceptualized by Figure 2.1. It is a layer that thaws only occasionally. Bockheim and Hinkel (2005) state that the lower boundary of the transient layer delineates the position of maximum thaw over time. This boundary can be considered the long-term permafrost table.

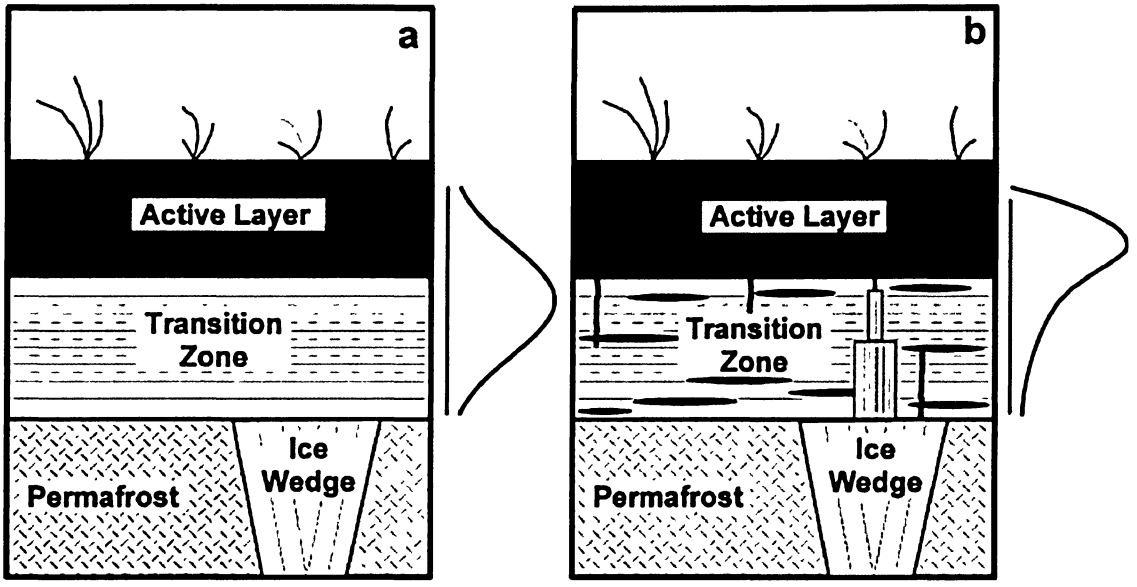

Figure 2.1 Conceptual permafrost stratigraphy with curves showing probability of annual thaw depth (a) immediately following a very deep thaw and (b) with ice enrichment of the transition zone after several centuries (Shur et al. 2005). *Figure not to scale.*

On a time scale ranging from sub-decadal to multi-centennial, all or some of the transition zone thaws. Shur et al. (2005) put forth a hypothesis that estimates the transient layer thawing probability based on average thawing recurrence. Figure 2.1a illustrates this concept by showing a normal distribution curve (Gaussian form) with 43% thawing probability located at the base of the average annual active layer. Beyond the curve peak (50%), where the ground is frozen for two or more years, the probability of thaw decreases. However, this symmetric curve is only valid immediately following a very deep thaw. Ice accumulation in this zone in-between maximum thaw events will diminish the probability of thaw beyond the ice-rich zone. As such, the curve becomes skewed and higher probability of thawing will gradually progress toward the surface (Fig. 2.1b). The lower transient layer thaws less frequently and occurs in response to extreme climate conditions or disturbance of the surface vegetation (Shur et al. 2005).

Shur et al. (2005) report a transient layer thickness varying mostly from 3% to 28% of the active layer thickness in Russia. It is believed that the transient layer thickness plays a critical role in evaluating the response of the active layer and near surface permafrost to climate change and for the development of thermokarst processes (Shur 1988).

The transition zone is believed to play an important role in a periglacial environment. It stabilizes the subjacent permafrost and serves as a barrier between the active layer and the underlying permafrost. In other words, it protects the permafrost from thaw during most warm periods (Shur et al. 2005). The transient layer is believed to have a high ice content and a high resistance to thaw due to the latent heat required to melt the ice. Hence, the transient layer has a tendency to encourage thermal stability at greater depths (Shur 1988). The extent of latent heat required to thaw this ice-rich layer inhibits rapid thaw and tends to govern the active layer thickness (Nelson et al. 1998, 2008). More specifically, a succession of warm thawing periods could thaw the ice-rich layer and reset the active layer at a position deeper in the soil. In the same manner, during a colder year, the active layer may not reach the ice-rich zone. As such, ice segregation will occur at shallower depths which will tend to govern the active layer thickness in subsequent years. The melting of an "intermediate ice-rich" layer was recorded by Gavriliev and Efremov (2003) and had several consequences on the overlying active layer. These consequences ranged from the destruction of the cryogenic structure, a significant change in composition and hydrothermal regime to the strength and stability loss of active layer soils.

During unusually warm summers with deep thaw penetration, the ice-rich soils thaw and a substantial amount of pore water pressures are generated. According to Morgenstern and Nixon (1971), in fine-grained soils, excess pore water pressures develop at the thawing front. Field observations in the Mackenzie valley conducted by Wang et al. (2005) reveal the near surface permafrost has a high ice content and turns into liquid when completely thawed for which shear stress cannot be sustained. It was observed that shear strength of active layer materials decreased with depth, which is linked to an increase in moisture content.

Despite its importance, relatively little research has been done on the transient layer. There is still no conclusive definition on where to draw the boundaries of the transient layer. Bockheim and Hinkel (2005) delineated the transition zone boundaries of 138

samples by means of criteria such as sample location (between active layer and permafrost), ice content and cryostructures.

2.2 Cryostructures

The cryostructure refers to the structural characteristics of frozen earth materials (Everdingen 2002). Cryostructures describe the form, distribution and volume of ice in soil (Shur and Jorgenson 1998). The cryogenic structure of a soil varies depending on the conditions under which it was deposited and frozen (Bray et al. 2006). An analysis conducted by Shur and Zhestkova (2003) in fine-grained permafrost soils in different parts of the world reveals that cryostructures are generally the same regardless of their geographical location. According to Shur and Jorgenson (1998), ice-rich near surface permafrost has distinctive cryostructures within the active layer, the intermediate layer and underlying permafrost. The cryostructural differences can generally be explained by the variation in thermal and moisture patterns of each zone. For example, layered ice may represent periods when the active layer was stationary, therefore ice accumulated at a certain depth; consequently, the cryostructure at that location is different compared to the upper and subjacent soils.

The active layer may have a different structure since it undergoes yearly thawing. Gavriliev and Efremov (2003) described the active layer as having cavities and cracks resulting from the melting of ice lenses and streaks. It is typically unsaturated, with either visible or non visible pore ice. Field studies conducted by Leshchikov and Ryashchenko (1978) depicted the active layer as being structureless since ice is not visible within frozen sediments.

Numerous terms have been used to describe the cryostructures within the transient layer or top of permafrost. Bockheim and Hinkel (2005) referred to it as platy while Gavriliev and Efremov (2003) deemed it as being layered-reticulate or massive agglomerate. Mackay (1972) named this ice-rich region as aggradational ice. Some researchers have described it as being cloudy and misty (Cheng 1983). Several authors have defined it as an ataxitic grid-shaped or net-like structure (Shur 1988; Hinkel et al. 1996; Shur and

Jorgenson 1998; Shur et al. 2005). To end the ambiguity of cryostructural terms, Murton and French (1994) established a nomenclature describing cryostructures that are typically encountered in permafrost terrain. Figure 2.2 illustrates the classification for the most common types of cryostructures found in frozen ground. The equivalent term used for an ataxitic cryogenic structure in the Murton and French classification is the *suspended* cryostructure (Shur et al. 2005). Suspended (or ataxitic) ground ice structures are a strong form of ice nets in which ice makes up the majority of volume and soil appears as small islands. In essence, soil sediments appear to be suspended in the ice and the ice content is usually high in the suspended structure. Figure 2.3 displays a permafrost sample from a recent field investigation in the Mackenzie Delta carried out by Morse et al. (2009). This section of soil corresponds to the interface between the base of the active layer and the top of permafrost. From this figure, it is apparent that different cryostructures are present within this section of soil. The authors described the section of soil between 7 cm and 10 cm as segregated ice.

In research conducted by Höfle et al. (1998), ice wedges, ice lenses and cryostructures were used to estimate the depth of annual thaw. These authors believe that the average depth of summer thaw is often marked by ice-rich layers containing ice lenses, ice nets, and suspended or ataxitic ground ice fabrics located at the base of the active layer. These features may also occur below the current active layer, indicating that the depth of thaw was greater at some point. This study established the active layer depth by means of morphological characteristics such as cryostructures. Moreover, Bockheim and Hinkel (2005) used the cryostructures as one of the criteria to delineate the transient layer in field investigations. Cryostructures could be useful for identification of transient layers. However, the literature lacks a clear validation for this method.

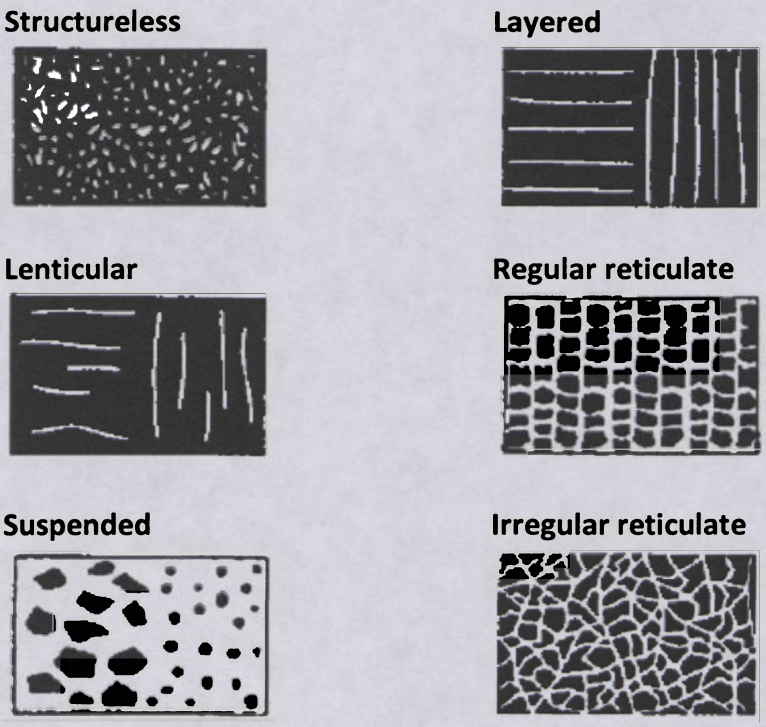

Figure 2.2 Cryostructural classification established by Murton and French (1994). Ice is shown in white and sediment in black.

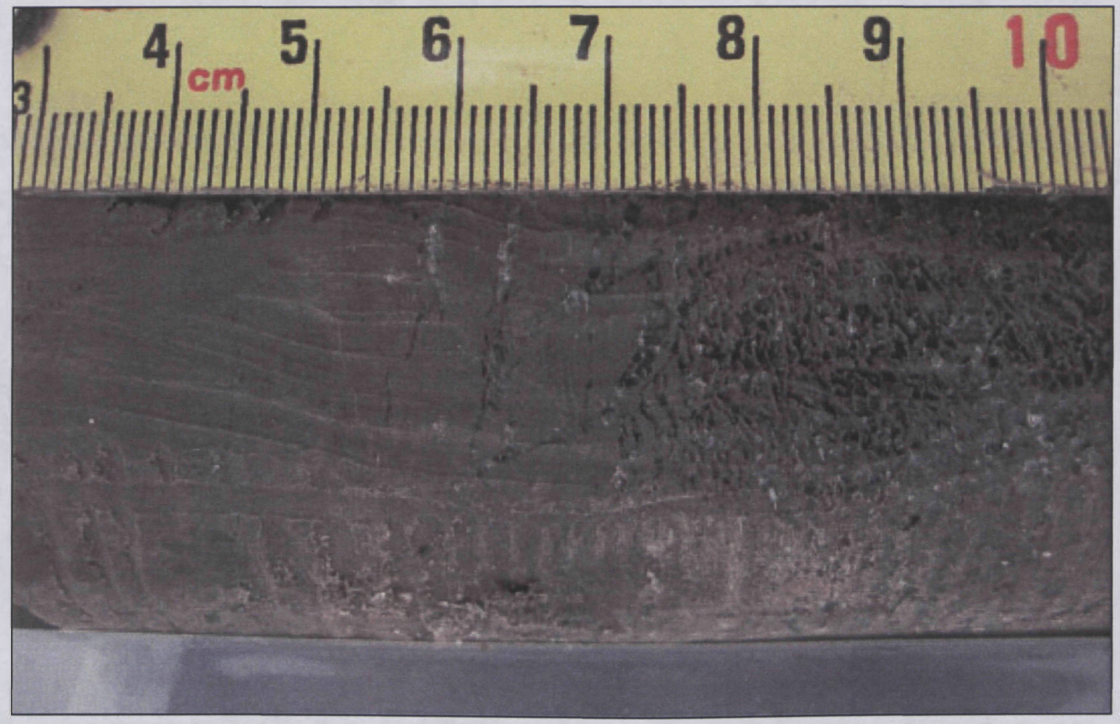

Figure 2.3 The interface between the base of the active layer and the top of permafrost (at approximately 7 cm on the scale). Segregated ice lenses appear darker than the ice-bonded sediment (Morse et al. 2009)

Mackay (1973) stated that the engineering behavior of permafrost soils may vary considerably depending on the cryostructure of the soil. Field investigations conducted by this researcher indicate that ice structures are considered to be important in thaw consolidation and differential settlement.

2.3 Ice lens formation and ice content

Moisture content distribution in fine-grained permafrost soils are very distinct and quite different from what is found in non-permafrost terrain. In permafrost regions, most moisture profiles are characterized by a peak in total moisture content at the permafrost table which has been recorded in many field investigations (Mackay 1971; Pollard and French 1980, 1983; Cheng 1983; Burn et al. 1986; Burn 1988; Burn and Michel 1988; Harris 1988; Kokelj and Burn 2003a, b, 2005; Wang et al. 2008). Mackay reported that the ice-rich zone is a typical feature of the Western Arctic Coast and Lower Mackenzie River valley. This distinctive permafrost feature can be explained by the two-sided freezing nature of permafrost and the mechanism of moisture migration which leads to ice lens formation (Konrad and Morgenstern 1980; Cheng 1983; Mackay 1983). Pollard and French (1980) compiled data form The Mackenzie valley Geotechnical Data Bank and constructed a typical distribution of ground ice versus depth as shown in Figure 2.4.

Mackay (1983) noted upward and downward water migration in active layer soils in the Mackenzie valley during a 1967 field program studying freeze-thaw processes within the active layer. It was concluded that water moves from the thawing active layer into the subjacent permafrost. In general, moisture migration is the result of processes such as capillary suction, gravity, osmotic gradient and temperature gradient, where the latter is the most influential in moisture redistribution within permafrost soils. As such, moisture in frozen ground moves in the direction along which the ground temperature decreases in response to an imposed thermal gradient (Mageau and Morgenstern 1980; Penner and Goodrich 1981; Smith 1985). Hence, moisture will generally migrate downward in spring and summer (Mackay 1980; Cheng 1983; Zhao et al. 2000) and will tend to migrate upward in autumn and winter as shown in Figure 2.5. Essentially, moisture is attracted to the cold front.

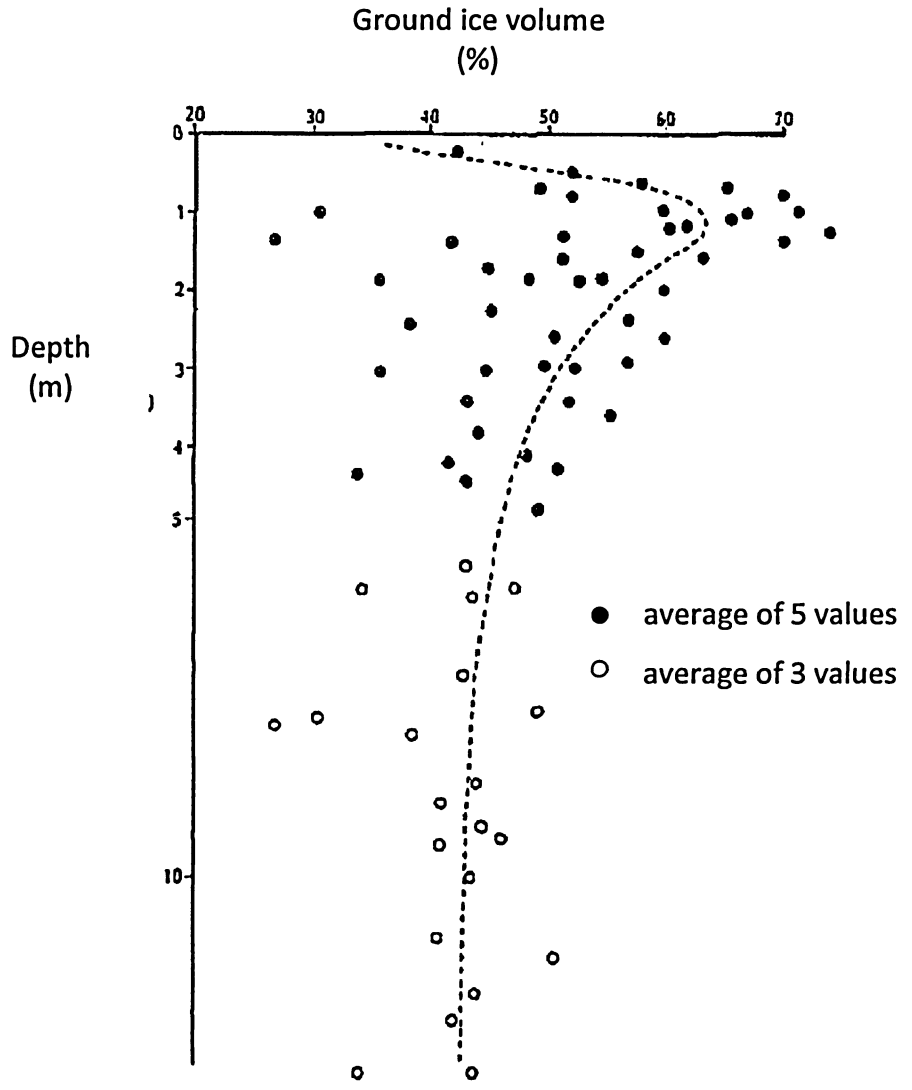

Figure 2.4 Typical ground ice versus depth curve (dotted line), Richards Island, N.W.T., Canada (Pollard and French 1980)

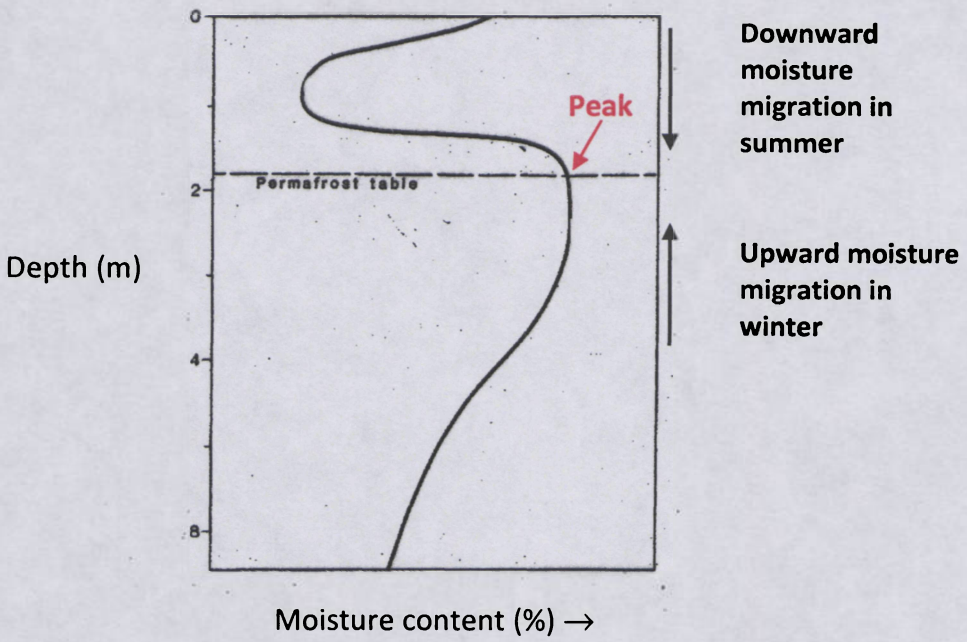

Figure 2.5 Typical ice content profile in permafrost (adapted from Harris 1988)

Unfrozen moisture migrates upwards when ground surface begins to freeze. This process is considered to be a closed system. On the other hand, downward moisture migration is viewed as an open system since water comes from an external source of water such as snowmelt, rain and groundwater flow (Mackay 1983; Cheng 1983). Typically, there is more downward water migration during thawing than upward water migration during freezing given that the thaw cycle is an open system. This results in an unequal upward and downward moisture migration occurring in fine-grained permafrost terrain and a yearly moisture increase at the permafrost table (Cheng 1983; Hinkel et al. 1996; Kokelj and Burn 2003a; Bockheim and Hinkel 2005). Field studies have indicated that the ice content at the active layer base and top of permafrost increases in the summer due to downward water migration coming from the thawed active layer (Mackay 1983; Burn and Michel 1988).

Kokelj and Burn (2003a) established a relationship between tree leaning and near surface ground ice in the Mackenzie Delta. The leaning of trees was more prominent in areas where ice content was greater. The same authors linked forest type with ground ice content. For example, spruce/feathermoss trees are more likely to be underlain by moderate to high ice content permafrost whereas spruce/alder-bearberry forests appear to

grow on soils containing low ice contents (Kokelj and Burn 2005). Several authors have indicated that the thawing of ice lenses also has a significant influence on slope stability due to a drop in soil shear strength (McRoberts and Morgenstern 1974; Harris and Lewkowicz 2000; Gerchishchev 2003).

Research conducted by Harris et al. (2008a, c) highlights the importance of ice lensing in permafrost terrain. These studies were carried out on fine-grained soils placed on a slope subjected to two-sided freezing. They concluded that shear strain and thaw consolidation are concentrated within ice-rich zones developed at the base of the active layer. Pore water pressures noted during basal thawing were sufficiently high to allow significant shear strains.

2.4 Thaw consolidation theory and pore water pressure

When thawing occurs in ice-rich permafrost, water is released and pore pressures are generated. The strength of thawed soil depends upon the magnitude of these pore pressures and the rate of settlement will vary with the rate of pore water dissipation. It is fundamental to consider the excess pore pressure conditions during thawing of fine-grained soils when designing foundations of structures and slopes. There is a need to verify the thaw consolidation theory which can be used to assess settlement and excess pore water pressure conditions when frozen soils are subject to thawing.

In 1971, Morgenstern and Nixon formulated a thaw consolidation theory based on theories of heat conduction and linear consolidation of a compressible soil. This theory considers a one-dimensional configuration. The position of the thaw front at a certain time during the course of thawing is described by the Neumann solution:

$$X(t) = \alpha\sqrt{t} \qquad [2.1]$$

Where:

X: depth to the thaw plane;

α: a thermal constant;

t: time.

Two solutions for excess pore water pressures were derived for two special loading conditions. Equation [2.2] presents the solution for a material under surface loading and Equation [2.3] is the solution for a soil consolidating under its own weight. The complete derivation of the formulated equations can be found in Appendix A.

$$\frac{u(Z,t)}{P_0} = \frac{erf(RZ)}{erf(R) + \frac{e^{-R^2}}{\sqrt{\pi}R}} \qquad [2.2]$$

$$\frac{u(Z,t)}{\gamma' X} = \frac{Z}{\left(1 + \frac{1}{2R^2}\right)} \qquad [2.3]$$

Where:

u: excess pore water pressure;

erf( ): error function;

Z: x/X(t);

x: depth measured from the ground surface;

X: depth to the thaw plane;

P_0: load applied to the surface;

R: thaw consolidation ratio;

t: time;

γ': submerged unit weight of the soil.

Morgenstern and Nixon (1971) state that the excess pore pressures and the degree of consolidation in thawing soils are dependant principally on the thaw consolidation ratio *R*. This parameter is calculated with the following equation:

$$R = \frac{\alpha}{2\sqrt{c_v}} \qquad [2.4]$$

Where c_v is the coefficient of consolidation.

The thaw consolidation ratio is a measure of the relative rates of thaw and expulsion of excess pore water. Figure 2.6 plots the normalized excess pore water pressure with respect to depth for thaw consolidation ratios from 0.1 to 10 for the case of soil consolidating under its own weight.

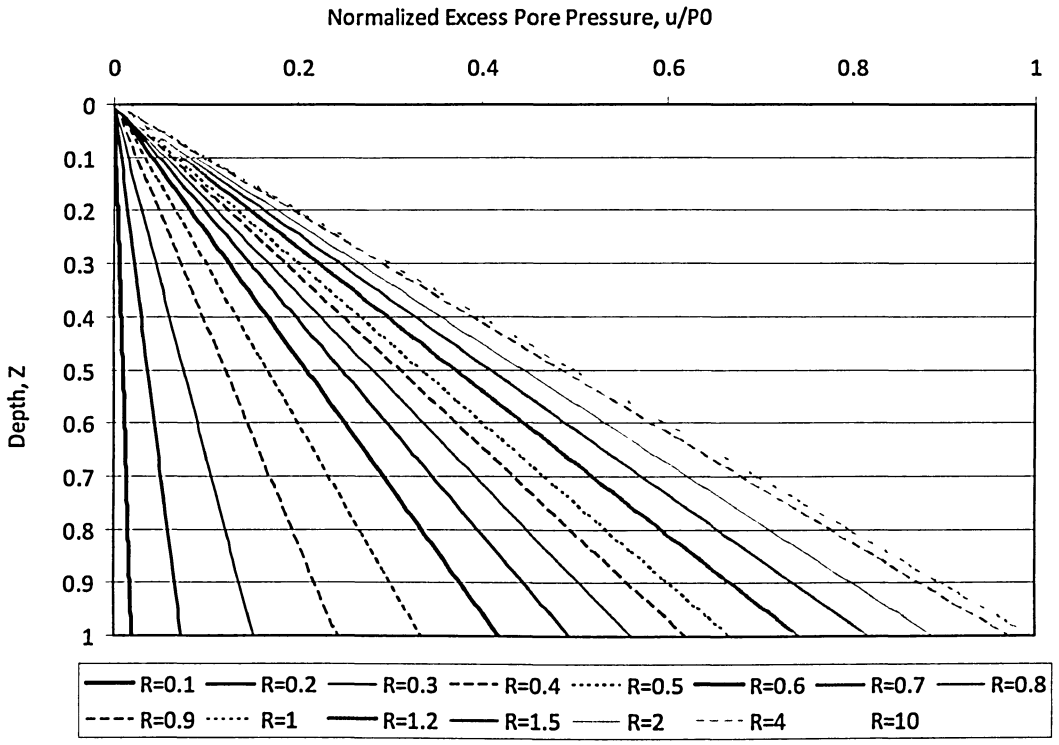

Figure 2.6 The normalized excess pore water pressure with respect to normalized depth for different values of R (soil consolidation under its own weight)

Several laboratory studies were conducted in order to validate the Morgenstern and Nixon theory (Morgenstern and Smith 1973; Morgenstern and Nixon 1975; McRoberts and Morgenstern 1975; Ryden 1985). However, these studies were to verify the soil consolidation under an applied load at the surface. Lesage and Wang (2008) conducted a laboratory test to verify the thaw consolidation theory for the case where soil consolidates under its own weight. The laboratory study featured a remoulded silty clay sample

extracted from the Mackenzie valley. The soil specimen had a height of 95 cm and a diameter of 15 cm. It was found that the experimental pore pressures and the theoretical results from the thaw consolidation theory by Morgenstern and Nixon (1971) were generally agreeable. The test was done under one cycle of freezing and thawing.

2.5 Other experimental studies

Numerous laboratory studies have been conducted on repeated freezing and thawing of fine-grained soils. However, the majority of these studies were done on hydraulic conductivities or strength parameters of the soil (Chamberlain and Gow 1979; Yong et al. 1982, 1985; Wong and Haug 1991; Bergeron et al. 1995; Viklander 1998) while others were limited to only one freeze-thaw cycle conducted on the soil specimen (Mageau and Morgenstern 1980; Ryden 1985; Cheng and Chamberlain 1988; Solomatin and Xu 1994; Eigenbrod et al. 1996; Murton and Harris 2003; Harris et al. 2005; Lesage 2008). Below is a brief description of previous experimental research studying moisture and ice patterns, pore water pressures and temperatures. All of the studies were conducted on repeated freeze-thaw cycles of fine-grained soils.

In 1998, Harris and Davies studied pore water pressures, temperatures, heave and thaw settlement in saturated silty soil samples during seven unidirectional freeze-thaw cycles. The soil sample had a height of 30 cm and was placed on a 12° slope in a refrigerated container. Results showed that variations in pore pressures and temperatures during freezing and thawing were consistent during each cycle. Negative pore pressures were measured during the zero curtain period – the period in which the ice is undergoing phase change – and positive pressures were noted during the freezing of the soil. Moreover, during thaw consolidation, excess pore water pressures were induced in the soil and downward slope displacements were observed. Heave and thaw settlement increased with increasing cycles.

Harris et al. (2001) presented results of a scaled physical modeling of thawing slopes undertaken in a geotechnical centrifuge at angles of 12°, 18° and 24°. The 12° slope model was subjected to four cycles of freezing and thawing, the 18° slope model to two

cycles and the 24° slope model to one cycle for which the soil samples had a height of 30 cm. As expected, slope movement occurred during each thaw phase, and was higher for an increased slope angle. Pore water pressures were similar in all models and behaved similarly to those reported by Harris and Davies (1998). Pore water pressures decreased more rapidly in higher slope gradients. The analysis of the data focussed on the comparison of slope gradient increase and pore water pressure results with increasing number of freeze-thaw cycles. Harris along with several others conducted a series of laboratory tests using the same experimental setup as described above (Harris et al. 2003; Harris et al. 2008a, b). Once again, pore water pressure data were generally consistent in the experiments except for one soil sample having a lower slope gradient (4°) and higher clay content (20%) than other soil samples. This sample recorded higher excess pore water pressures. In similar laboratory experiments (Kern-Luetscheg and Harris 2008; Kern-Luetschg et al. 2008), temperature, frost heave, thaw settlement and solifluction were studied for fine-grained permafrost and non-permafrost slopes during 4 to 6 freeze-thaw cycles. It was concluded that within the permafrost slope, an ice-rich zone developed at the base of the active layer and top of permafrost following two-sided freezing.

2.6 Summary

The transient layer between the active layer and long-term permafrost is an important part of permafrost ground; although, few have studied it. Thus far, no laboratory study has been conducted on soil samples to gain more knowledge on the transient layer. This research focuses on the transient layer of fine-grained soil samples and its behaviour under extreme climate condition. This study is intended to improve the current state of knowledge on the transition zone by investigating thermal, moisture and cryostructural conditions of fine-grained soil samples subjected to eleven freeze-thaw cycles. As part of the experiment, excess pore water pressures are also investigated in order to verify a part of the thaw consolidation theory.

3 Laboratory Testing

3.1 Laboratory apparatus

The laboratory equipment used for the testing was built in 2007 for a previous study (Lesage 2008) verifying pore pressure conditions of thawing soils. The equipment was slightly modified for the current study which is shown in Figure 3.1. Two identical laboratory apparatuses were used to measure pore water pressure and temperature changes along a soil column under repeated freeze-thaw actions. Thus, two tests were conducted simultaneously.

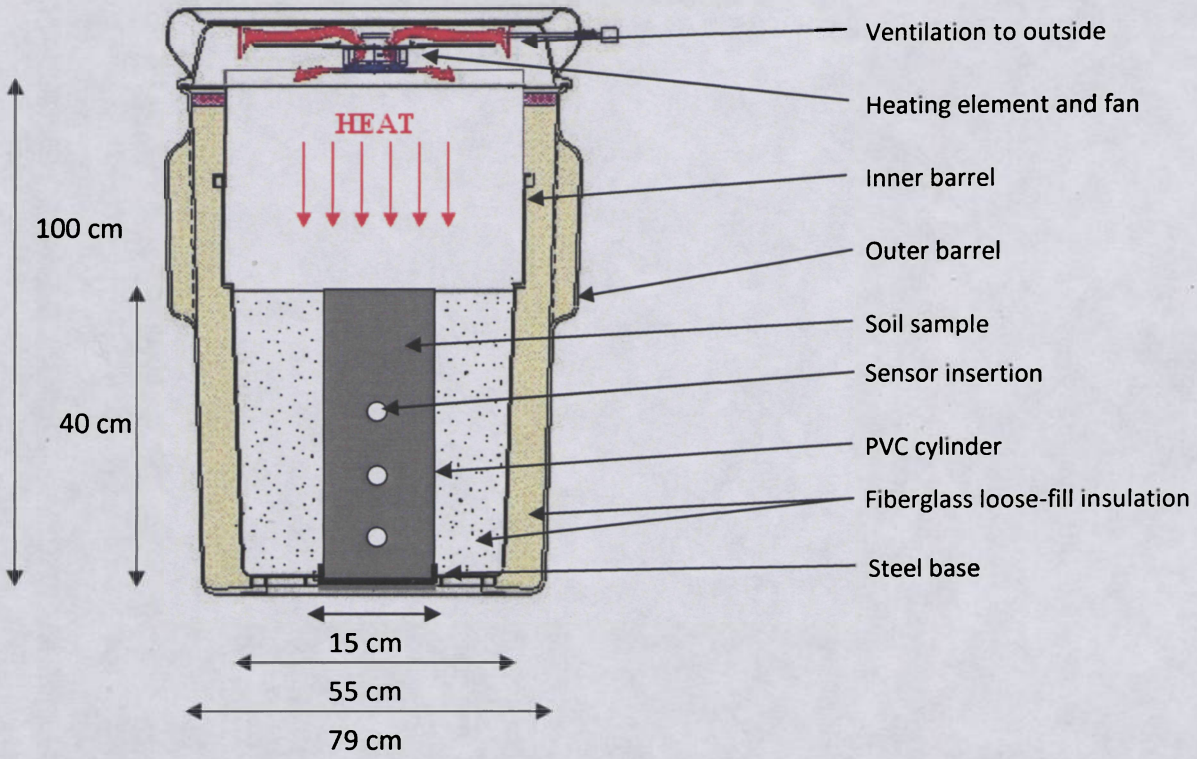

Figure 3.1 Sketch of the laboratory setup (modified from Lesage 2008) – *not to scale.*

The soil column was contained in a 6 mm thick PVC cylinder. The cylinder was contained in a 55 cm diameter plastic barrel (inner barrel) that was placed in a 79 cm diameter barrel (outer barrel). In order to minimize lateral heat flow and ensure vertical heating and cooling of the sample, two layers of insulation (a total of 32 cm thickness) were integrated in the design of the apparatus. The inner layer of insulation was placed around the perimeter of the PVC cylinder and consisted of fibreglass loose-fill insulation.

The loose fill insulation was used so that it could be removed easily to access of the frozen sample for inspection later. It should be noted that the insulation was to reduce the boundary effect. However, it is impossible to eliminate the boundary effect. The effectiveness was investigated and discussed later.

A plastic sheet was placed on top of the insulation to serve as an air barrier. The outer layer of insulation was fitted in-between the inner and outer barrel and was also fibreglass loose-fill insulation. This section was then sealed off at the top with fitted Styrofoam. The areas where the insulation was placed are shown in Figures 3.1 and 3.2. The PVC cylinder was secured on a metal base as illustrated in Figure 3.1. The metal base held the soil sample and provided high thermal conductivity between the soil sample and the ambient environment outside the system.

Both model assemblies were placed in a walk-in freezer. The base of the soil column was exposed to the freezer room temperature and the top of the sample to an encapsulated heating chamber. The heating chamber was composed of ventilation and heating systems. The ventilation system is a fan and a plastic tube that connect the heating chamber to the office environment outside of the cold room. This setup ensured proper air circulation and allowed the excess moisture to be evacuated. The heating system consists of four heating elements and is regulated by a controller located outside the cold room. Both the freezer and the heating chamber temperatures are adjustable. The heating and ventilation systems are presented in Figure 3.3. Figure 3.4 shows the outside view of the assembled system. Two of these devices were used in the testing.

A pore pressure transducer and a thermistor were inserted at depths of 5, 15 and 25 cm. The top sensors were inserted from the upper surface of the sample, while the lower sensors were inserted from the side. A thermistor was also installed at a depth of 32 cm. No pressure transducer was installed at this location since it was expected to be frozen at this depth throughout the laboratory testing.

Each soil column had a total of four K-type thermocouples and three PDCR-81 miniature pore pressure transducers inserted at the specified depths. The sensors were connected to a data acquisition system (DT500 dataTaker), with an overall system accuracy of ±1.5°C for the thermocouples and ±0.28 kPa for the pressure sensors. The depths at which the sensors were inserted are shown in Figure 3.5. As shown in the figure, no holes were drilled at the 5 cm location; the sensors were inserted in the sample from the top of the soil sample.

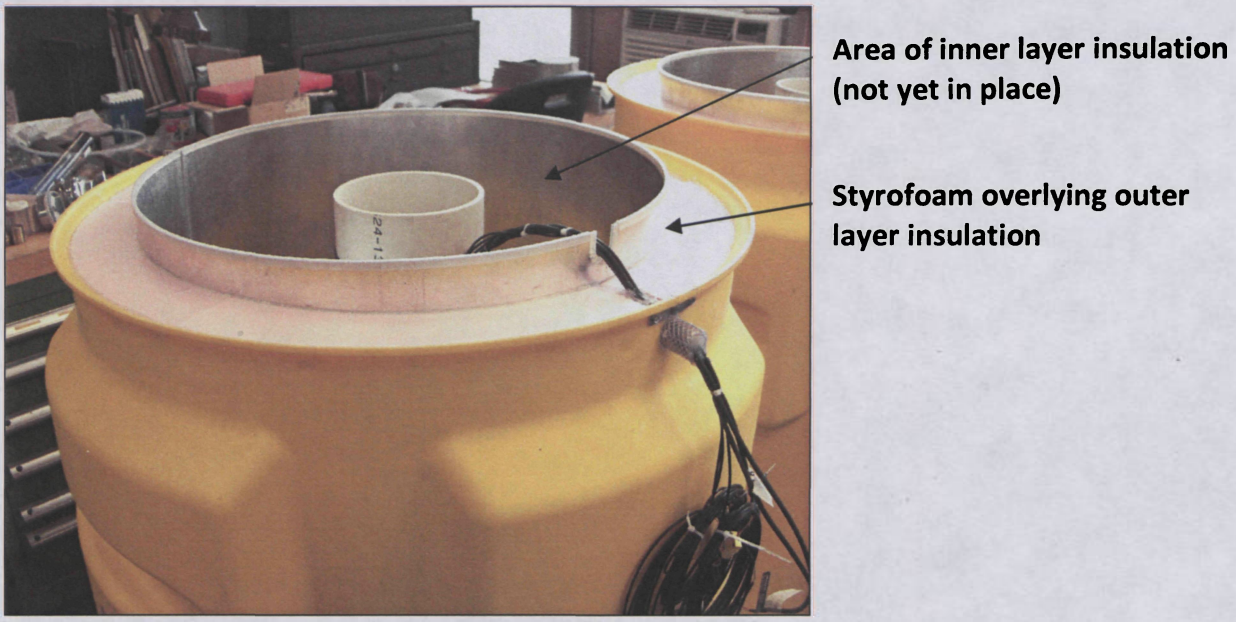

Figure 3.2 Areas where insulation is placed (Lesage 2008)

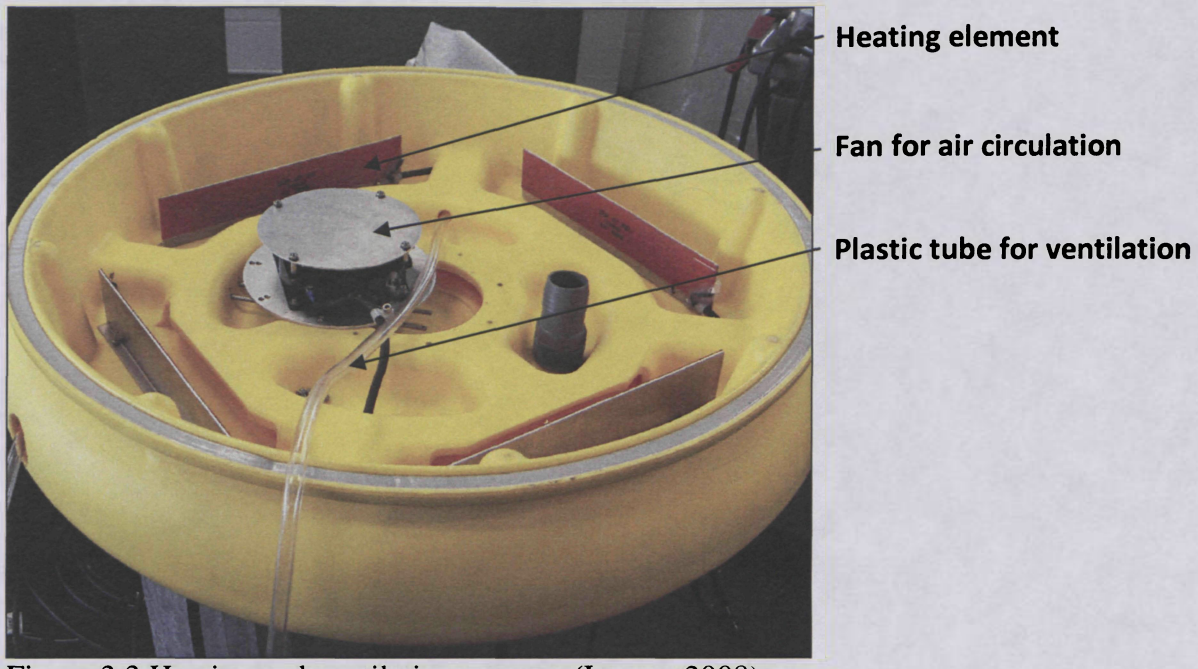

Figure 3.3 Heating and ventilation systems (Lesage 2008)


Figure 3.4 Laboratory apparatus (two were used in the test)

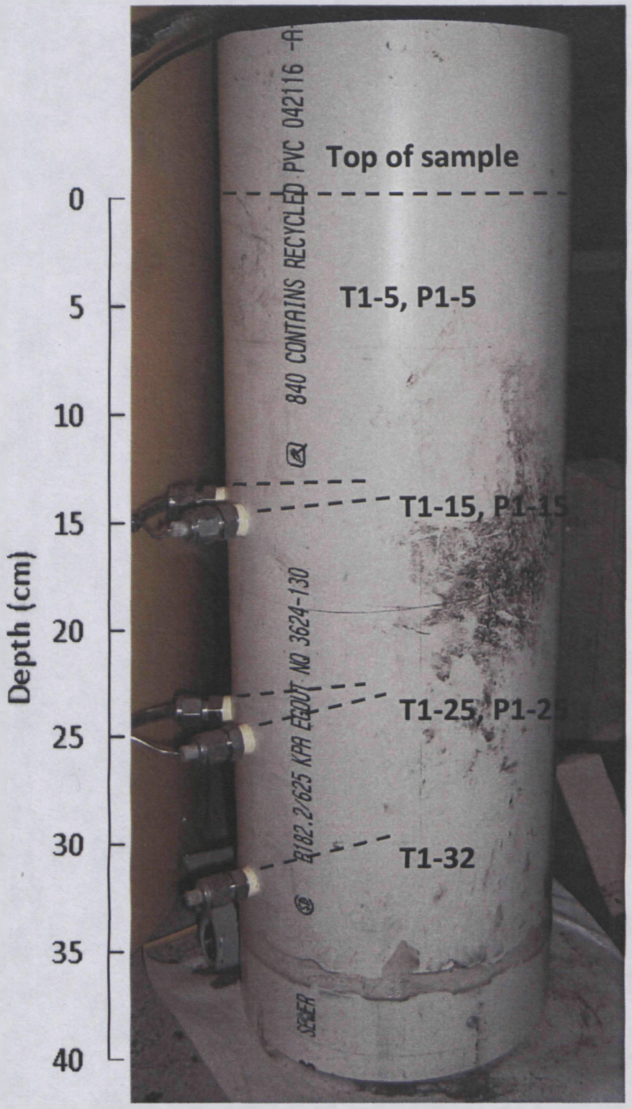

Figure 3.5 Depths where sensors are inserted (5, 15, 25, and 32 cm). *T* refers to the thermistor and *P* refers to the pressure sensor.

3.2 Temperature and pressure sensors

3.2.1 Temperature sensors

The temperature of the soil is measured by means of four stainless steel K-type thermocouples shown in Figure 3.6. In both samples, a thermocouple is inserted at depths of 5, 15, 25 and 32 cm. Each sensor has a length of 30 cm and a diameter of 1.57 mm. The thermocouples were calibrated by taking several measurements in ambient temperature water and comparing the readings to two mercury thermometers also placed in the water. The temperature differences between the thermocouples and thermometers

are presented in Table 3.1. For instance, thermocouple T1-5 measures an average of 1.99 C° higher than the thermometer temperatures. It should be noted that T1-5 refers to the thermocouple in model 1 at a depth of 5 cm. According to Nanmac Corporation (maker of the thermocouple used), the calibration at subzero temperatures should be within the same calibration range as shown in Table 3.1.

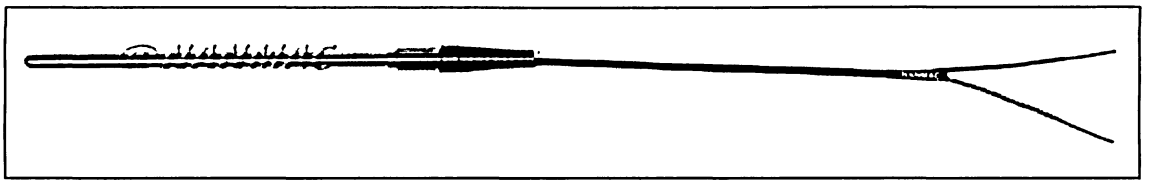

Figure 3.6 K-type thermocouple (source: www.nanmac.com)

Table 3.1 Thermocouple calibration

Sensor	Temperature correction (Cº)
T1-5	1.99
T1-15	1.94
T1-25	2.08
T1-32	2.04
T2-5	2.09
T2-15	1.96
T2-25	1.92
T2-32	2.13
T2 - Chamber temperature	1.85

3.2.2 Pressure sensors

PDCR-81 miniature pressure transducers as shown in Figures 3.7 and 3.8 were inserted at depths of 5, 15, and 25 cm in both models. The pressure transducer consists of a 0.09 mm thick, single crystal, silicon diaphragm with a fully active strain gauge bridge diffused into the surface. A high air entry porous stone is placed at the tip of the transducer just over the diaphragm. The deformation of the diaphragm causes a change in voltage measured across the strain gauge which is translated into pressure. The PDCR-81 has a pressure range of 350 mbar and a temperature range of -20°C to 120°C.

Figure 3.7 PDCR-81 miniature pore water pressure transducer

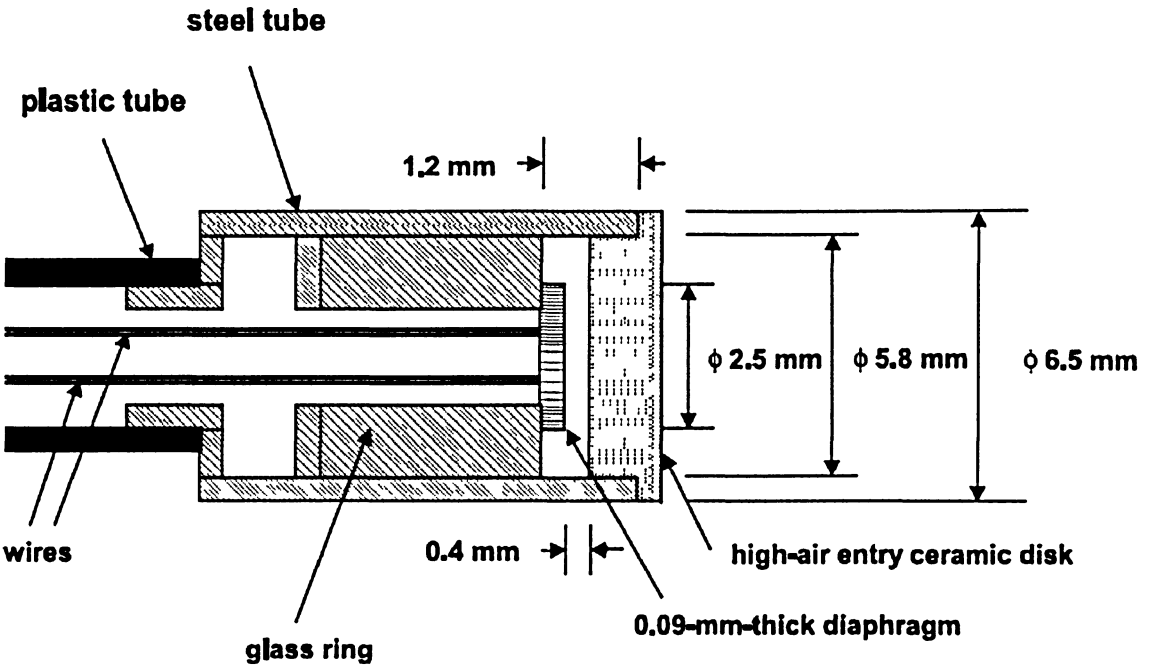

Figure 3.8 Dimensions of the PDCR-81 miniature pore pressure transducer (Meilani et al. 2002)

Prior to the installation into the soil sample, the PDCR-81 sensors were submerged in ethylene glycol antifreeze. The submerged sensors were placed in a vacuum chamber to de-air the porous stone for a period of 24 hours. This was to allow the ethylene glycol solution to enter the porous stone to avoid damage caused by ice accumulation (Harris and Davies 1998). Once the saturation was completed, the sensors were ready to be calibrated.

The calibration of the pressure transducers was done by taking readings in water at depths of 10, 20 and 30 cm. Table 3.2 lists the measured pressure for each sensor at all three depths. Figure 3.9 plots the relationship between measured pressure and theoretical values. A relationship was established between the readings and the theoretical

hydrostatic pressures in order to correct the actual sensor readings. This relationship is referred to as *Corrected pressure* in Table 3.2 and the value of H in the equation is the measured pressure in cm.

Table 3.2 Pressure sensor calibration

Water depth (cm)	Measured pressure, H (cm)					
	P1-5*	P1-15	P1-25	P2-5	P2-15	P2-25
10	14.62	20.26	13.15	10.35	-5.78	19.97
20	23.80	29.97	22.77	19.52	4.12	29.68
30	32.97	39.68	32.38	28.70	14.02	39.39
Corrected pressure	1.09H - 5.94	1.03H -10.87	1.04H - 3.68	1.09H - 1.28	1.01H+ 15.84	1.03H- 10.57

*(i.e. P1-5 refers to the pressure transducer in model M1 at a depth of 5 cm)

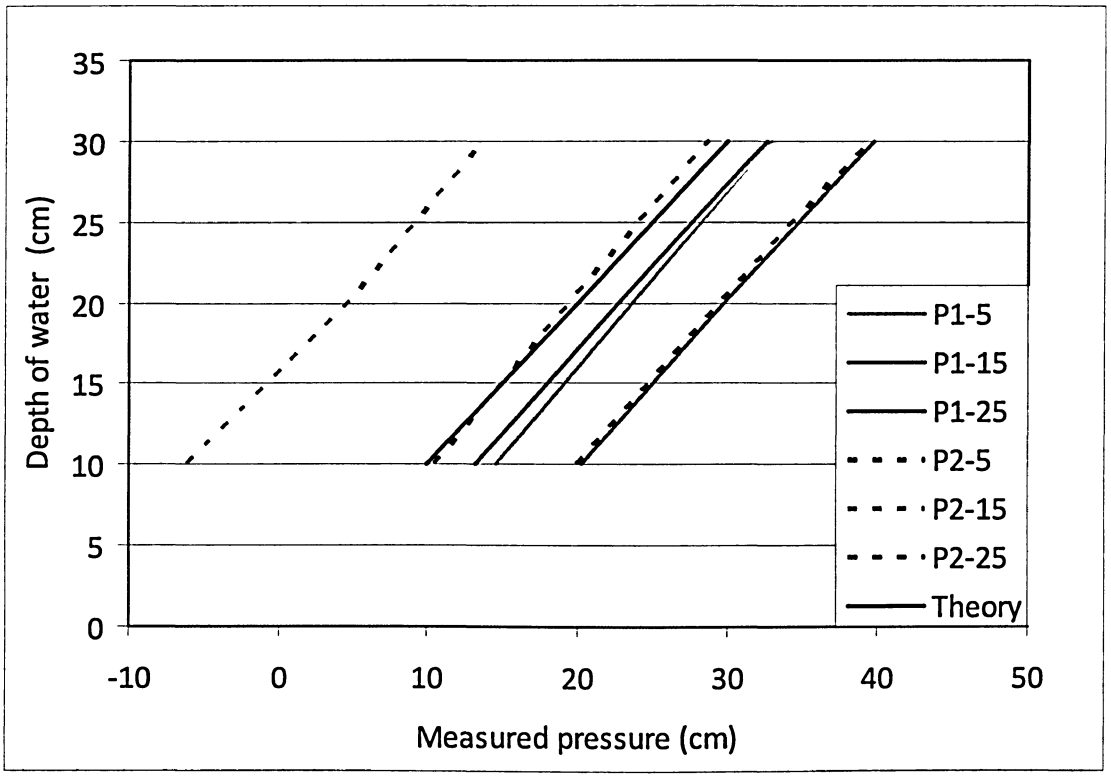

Figure 3.9 Depth of water vs. measured pressure

3.3 Soil samples

The soil samples used in the laboratory testing were collected in June 2006 during a geotechnical investigation in the Travaillant Lake area, 120 km southeast of Inuvik, in the N.W.T. (Fig. 3.10). Laboratory results indicate that the material is a high plasticity silty clay with a liquid limit of 61%, a plastic limit of 28% and a plasticity index of 33% (Su et al. 2006). The grain size curves for this site are presented in Figure 3.11 and the location of sample extraction (G1) is shown in Figure 3.10.

Figure 3.10 Inuvik sample location (adapted from Wang et al. 2008)

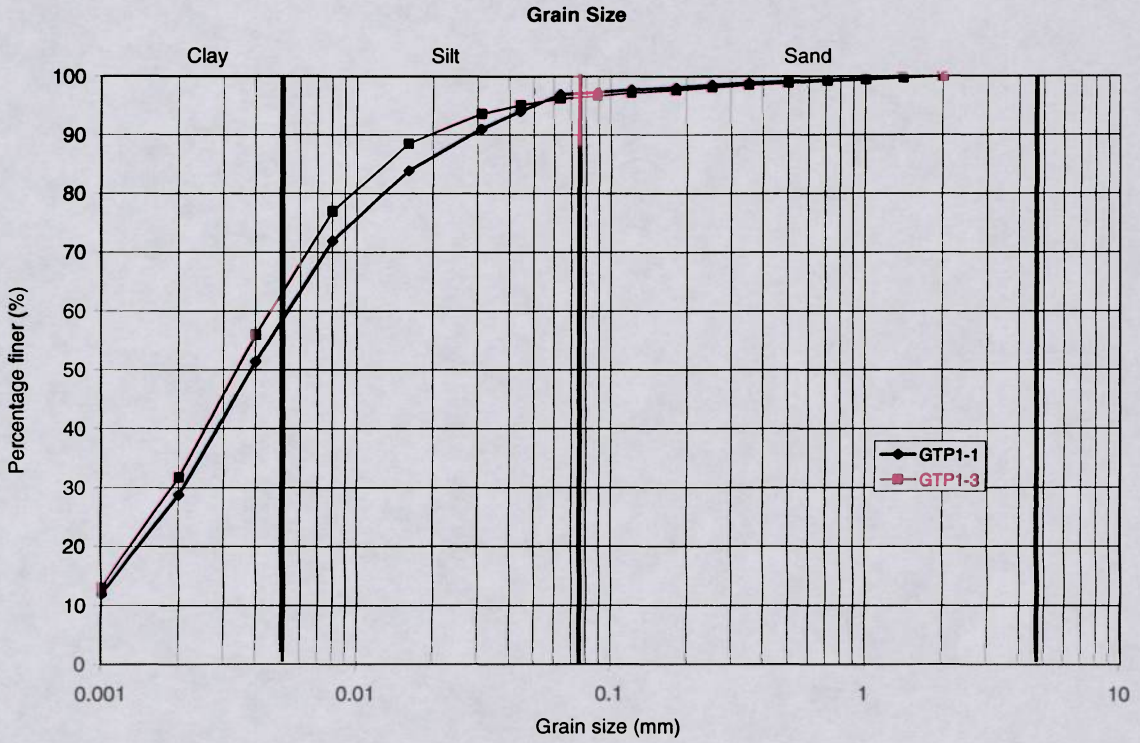

Figure 3.11 Grain size curves (adapted from Wang et al. 2008)

Field testing from Su et al. (2006) established that gravimetric moisture contents in the active layer increase with depth from about 27% near the top of the active layer to about 40% at the bottom. Wang et al. (2008) determined a broader range of moisture content of soils in the northern Mackenzie valley region. The typical moisture contents increase with depth, varying from 20% in the active layer to more than 100% into the permafrost. An average gravimetric moisture content of 50% for the laboratory model was determined to represent typical moisture conditions near the permafrost table in the Mackenzie valley. Both soil models were prepared at 50% moisture content.

3.4 Assembling of soil samples and test procedures

Prior to soil placement, the interior walls of the PVC cylinder and the metal steel base were coated with lithium grease to minimize friction during heaving or consolidation of the soil sample. After, the sensors were installed at specific depths in the predrilled holes within the PVC cylinders. The soil sample was then carefully placed into the cylinders and effort was made to minimize potential air trapping in the samples.

Freezing of the soil columns from both the top and the bottom was initiated after the models were assembled. Freezing at the top of the sample was achieved by keeping the heating chamber open to the freezer environment with the heating elements turned off. After the soil temperature reached the target freezing temperature, the heating chamber was closed and heating was initiated at the top while the bottom of the column was maintained at the freezer room temperature.

It is recognized that, ideally, other climatic factors, e.g., precipitation, runoff, evaporation and wind, etc., should be simulated. However, simplification is necessary to isolate the temperature effect. It should be noted that the duration of the laboratory modeling was compressed to carry out many cycles of repeated freezing and thawing within a reasonable time frame. For this reason, water was added at the top of the columns every day of the thawing cycle. The amount of water added was just enough to compensate for moisture losses and to avoid soil desiccation that may create direct water flow paths.

A total of eleven freeze-thaw cycles were tested for both models. Table 3.3 lists the upper and lower boundary temperatures applied on both models. A colder bottom boundary temperature (-7°C during thawing) was used in Cycle 1 as a trial cycle for which thawing reached only the sensors at 5 cm depth. It was also an accuracy check of the freezer temperature control to make sure that the lower portion of the samples were not operating near the melting point at any time. Adjustments were made in subsequent cycles to maintain the bottom boundary temperature at -5°C during thawing and -10°C during freezing, which is within the proximity of the average ground temperature in permafrost in the Mackenzie valley (Taylor and Judge 1974; Smith and Burgess 2000; Andersland and Ladanyi 2004; Wang and Saad 2007). The heating chambers were maintained at a temperature of 25°C for the repeated thawing cycles, which is within the proximity of normal summer high temperatures in the Mackenzie valley region. The temperatures of 20°C and 30°C were used for model M1 in Cycles 9 and 11, respectively, to simulate extreme weather variations from normal conditions. Once the freeze-thaw cycles were complete, the samples were cut open. Soil moisture specimens were taken at

1 and 2 cm intervals along the entire depth of the soils column. Final moisture content profiles and cryostructures were determined for each model.

Table 3.3 Temperature boundary conditions for each model

Cycle	Thermal state	Lower boundary (ºC)	Upper boundary (ºC)	
			Model M1	Model M2
1	*Freezing*	-10	-10	-10
	Thawing	-7	25	18
2 to 8	*Freezing*	-10	-10	-10
	Thawing	-5	25	25
9	*Freezing*	-10	-10	-10
	Thawing	-5	20	25
10	*Freezing*	-10	-10	-10
	Thawing	-5	25	25
11	*Freezing*	-10	-10	-10
	Thawing	-5	30	25

4 Temperature

Soil temperature data were recorded at sensor locations throughout the entire freeze-thaw cycles. During the test, model M2 was subjected to eleven thawing cycles of 25°C, whereas model M1 was subjected to eight thawing cycles of 25°C and to extreme temperature conditions: a colder cycle of 20°C followed by a "normal" temperature cycle of 25°C then by an extremely warmer cycle of 30°C. The temperature results are discussed as follows.

4.1 Results

4.1.1 Temperature history

The temperature history for the entire laboratory experiment is shown in Figures 4.1a and 4.1b for M1 and M2, respectively. In both charts, the temperature history is presented for each sensor inserted at 5, 15, 25 and 32 cm depth from the top surface. Data for the sensor located at the 32 cm depth in sample M2 are not shown due to sensor malfunction. Temperatures were recorded in the heating chamber of models M1 and M2 by means of a mercury thermometer and a thermistor, respectively which are also depicted in the charts. Due to a lack of datalogger channels, no thermistor was placed in the heating chamber of M1 or directly in the cold room. However, cold room temperature monitoring was achieved by means of a temperature recorder for the cold room.

According to Figure 4.1b, it can be observed that some thawing cycles recorded a heating chamber temperature below 25°C although the heating control unit was operating at 25°C. This is likely caused by shifting of the sensor or obstruction of air flow around the sensor. In both models, temperature jumps were noted in the sensor located at 5 cm. These jumps can be attributed to the addition of water to the soil surface during thawed cycles.

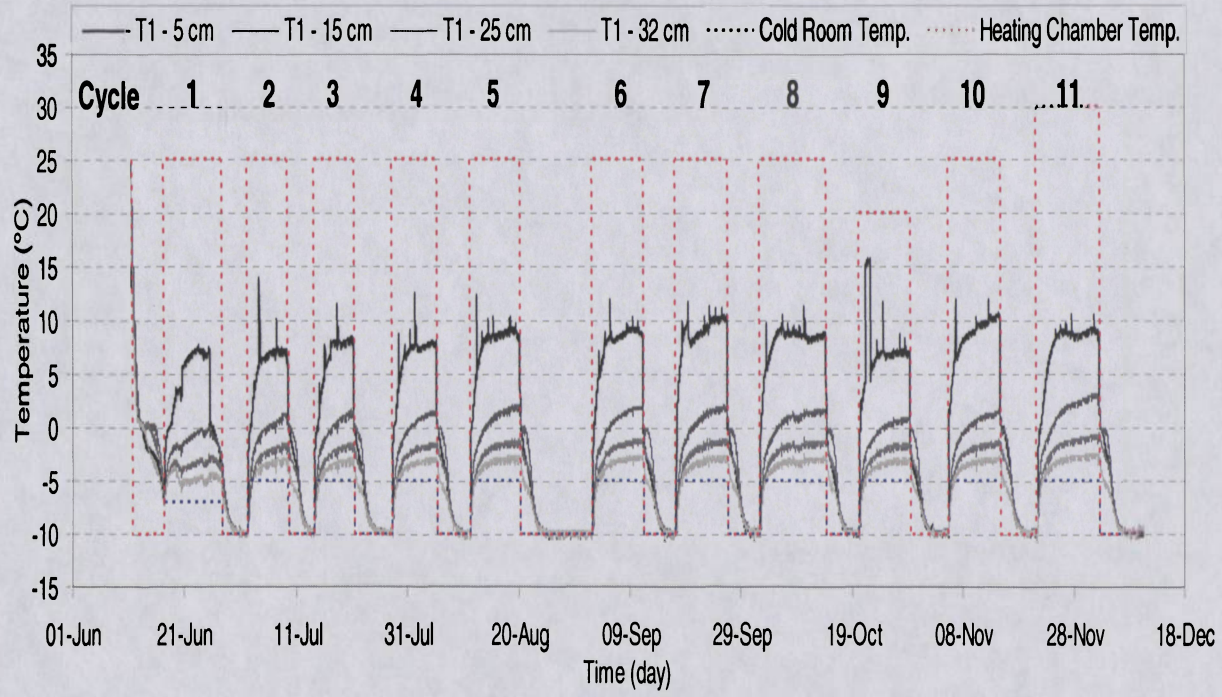

(a) Model M1

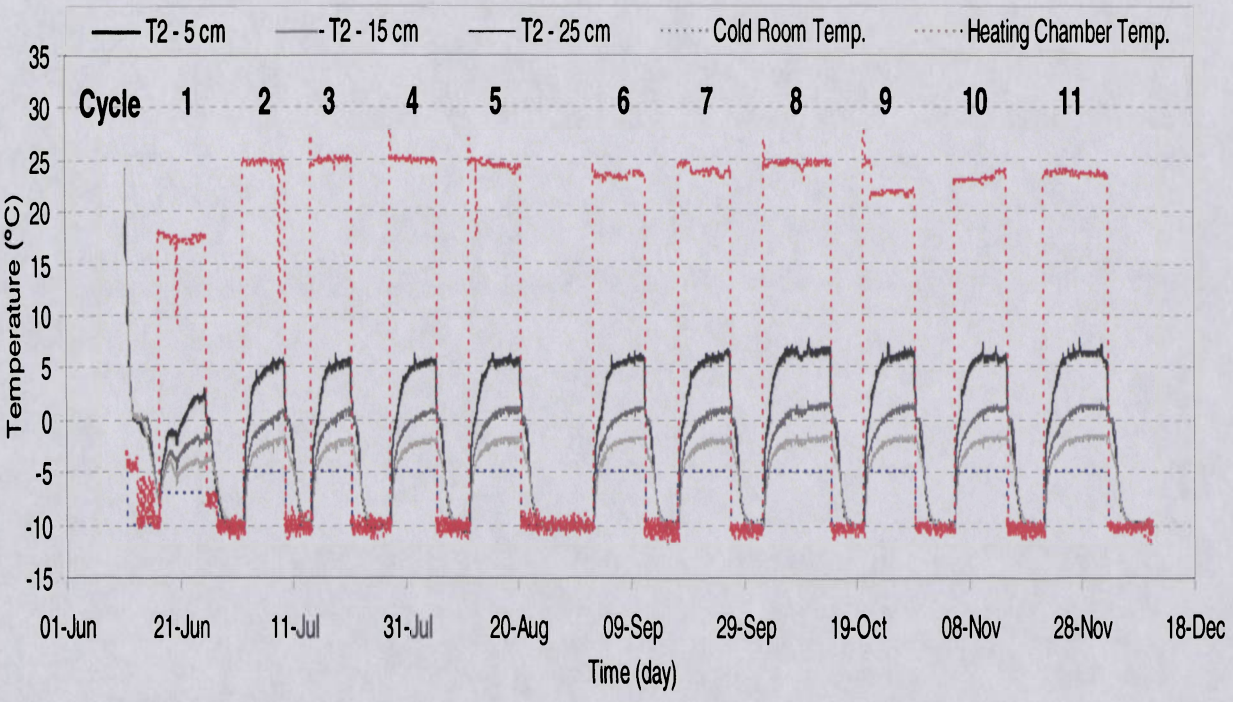

(b) Model M2

Figure 4.1 Temperature history for (a) model M1 and (b) model M2

After completion of the test, an inspection revealed that the temperature sensor at 5 cm depth shifted up by 1.5 cm during testing of M1. This difference is accounted for in subsequent results.

Soil settlement is another factor possibly impacting temperature results. Settlements were measured at the end of each thawed cycle and are shown in Figure 4.2. During the eleven cycles, M1 and M2 have a total settlement of 2 and 3 cm, respectively, which occurred during a period of 174 days. It is possible that thermistors may record higher temperatures as settlement increases (i.e. less soil covering sensors) and as the soil becomes denser. However, no temperature corrections were made to account for soil settlement.

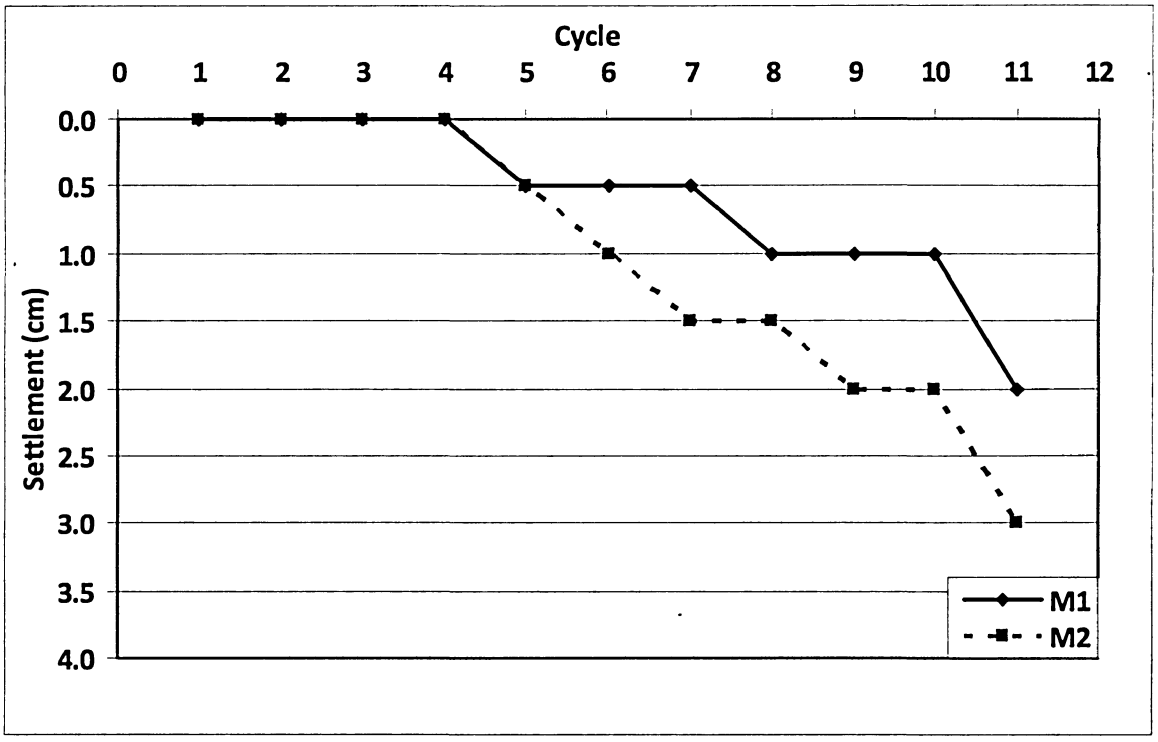

Figure 4.2 Soil settlement at the end of each thawing cycle in both models

4.1.2 Temperature profiles

Figures 4.3 and 4.4 depict the temperature profiles along the soil columns for M1 and M2 at the end of each freezing and thawing cycle. From these figures, it can be seen that

both soil columns were at a temperature of approximately -10°C at the end of each freezing cycle. For the thawed cycles, it can be observed from both figures that Cycle 1 has lower temperatures in comparison to other cycles. This is due to different boundary temperatures used during this cycle (Table 3.3). Temperatures for model M1 recorded during colder (20°C) and warmer (30°C) cycles are lower and higher, respectively, than the average 25°C cycles. According to the enlarged figure at the bottom right of Figures 4.3 and 4.4, the temperatures recorded during the 25°C thawing cycles slightly vary, which can be attributed to experimental noise or the accuracy of the system (±1.5°C). It should be noted that in Figures 4.3 – 4.5, the temperature data for the sensor at 5 cm depth (in M1) has been corrected to a depth of 3.5 cm since this sensor shifted upwards by 1.5 cm during testing.

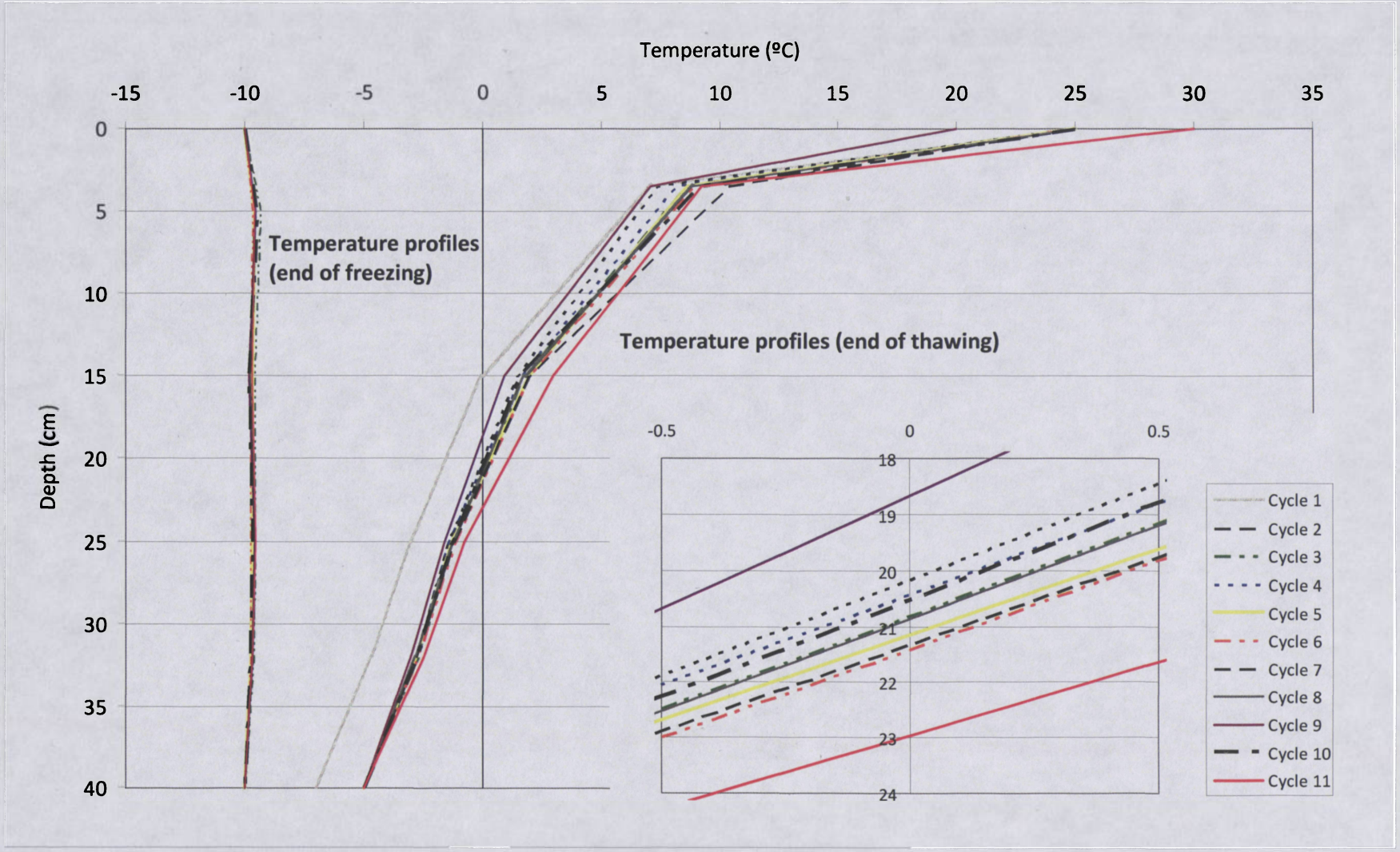

Figure 4.3 Temperature profiles of model M1 at the end of freezing and thawing cycles

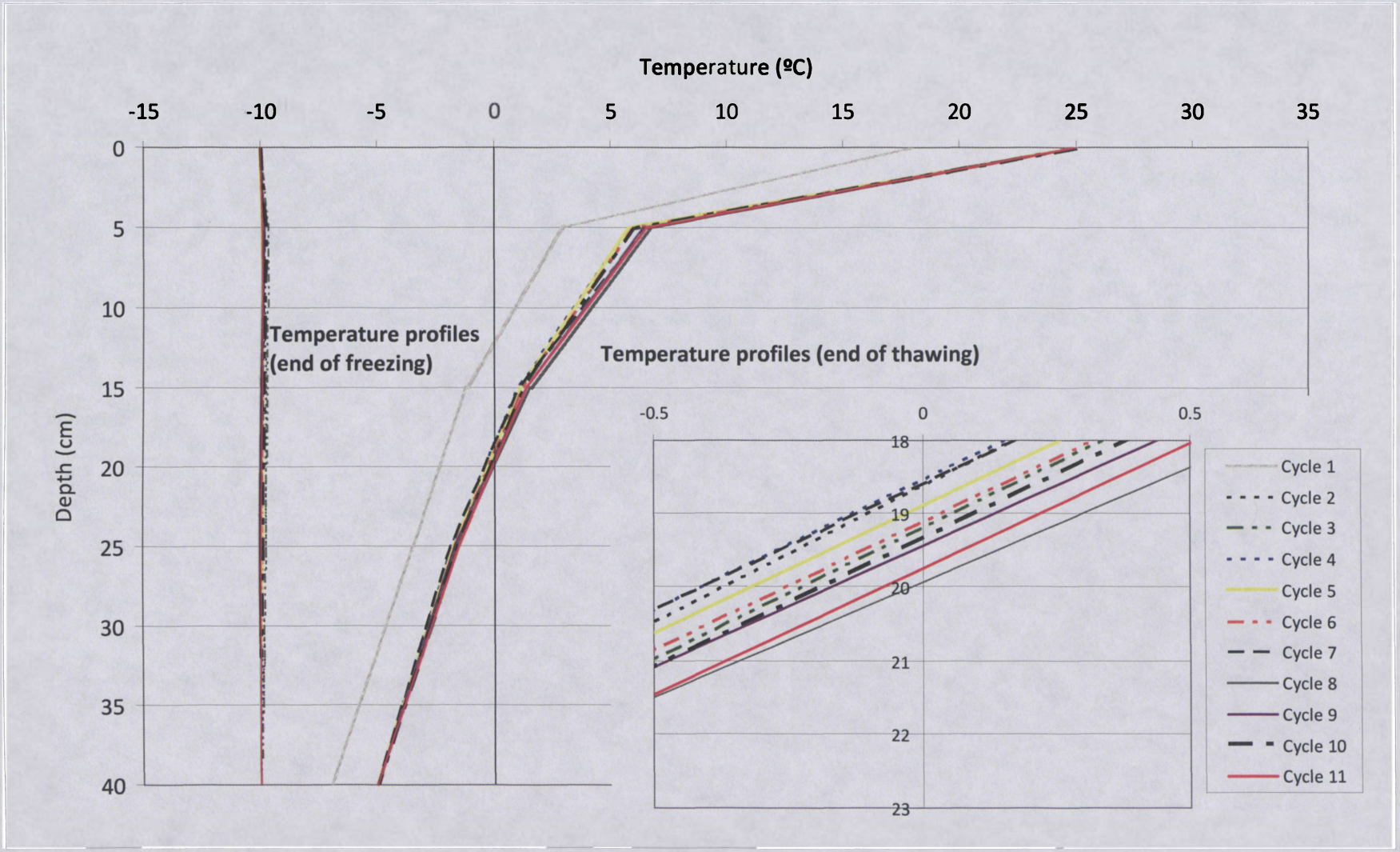

Figure 4.4 Temperature profiles of model M2 at the end freezing and thawing cycles

The temperature profiles of the thawed cycles for M1 and M2 are compared in Figure 4.5. Based on linear interpolation between two adjacent sensors at depths of 15 and 25 cm, at the end of thawing, the maximum cryofront depths (or 0°C isotherms) in M1 are 18.7 cm, 20.5 cm and 23.0 cm for air temperatures of 20°C, 25°C and 30°C, respectively; whereas in M2, it is 19.2 cm for thawing cycles of 25°C. These maximum cryofront depths are the average for cycles having the same thawing temperature and are depicted in Figure 4.5. In M1, the average cryofront depth for 25°C thawing cycles is calculated based on thermal profiles in Cycles 2 to 8 when boundary conditions are the same. As for M2, the average cryofront is calculated based on Cycles 2 to 11.

Riseborough (2008) examined several methods of determining the 0°C isotherm. The study concluded that extrapolations from above or below data points are more accurate for establishing active layer depths. The temperature profiles with the extrapolated cryofront depths are shown in Figure 4.6. According to this figure, the 0°C isotherms are elevated to 16.7, 17.8 and 20.5 cm depths for thawed cycles of 20°C, 25°C and 30°C, respectively. For M2, the cryofront is elevated to a depth of 17.4 cm.

The cryofront reached a greater depth during extreme thawing conditions (cycle of 30°C air temperature) compared to that of the 25°C "normal" cycle. According to the extrapolated version, the results indicate that the cryofront moved down by 15.2% from its normal depth for an air temperature increase of 5°C. It moved up by 6.2% for an air temperature decrease of 5°C. If the normal cryofront depth is used as reference, the 15.2% deepening of cryofront due to the extreme air temperature is in general agreement with the active layer variation of 3 to 28% reported by Shur et al. (2005).

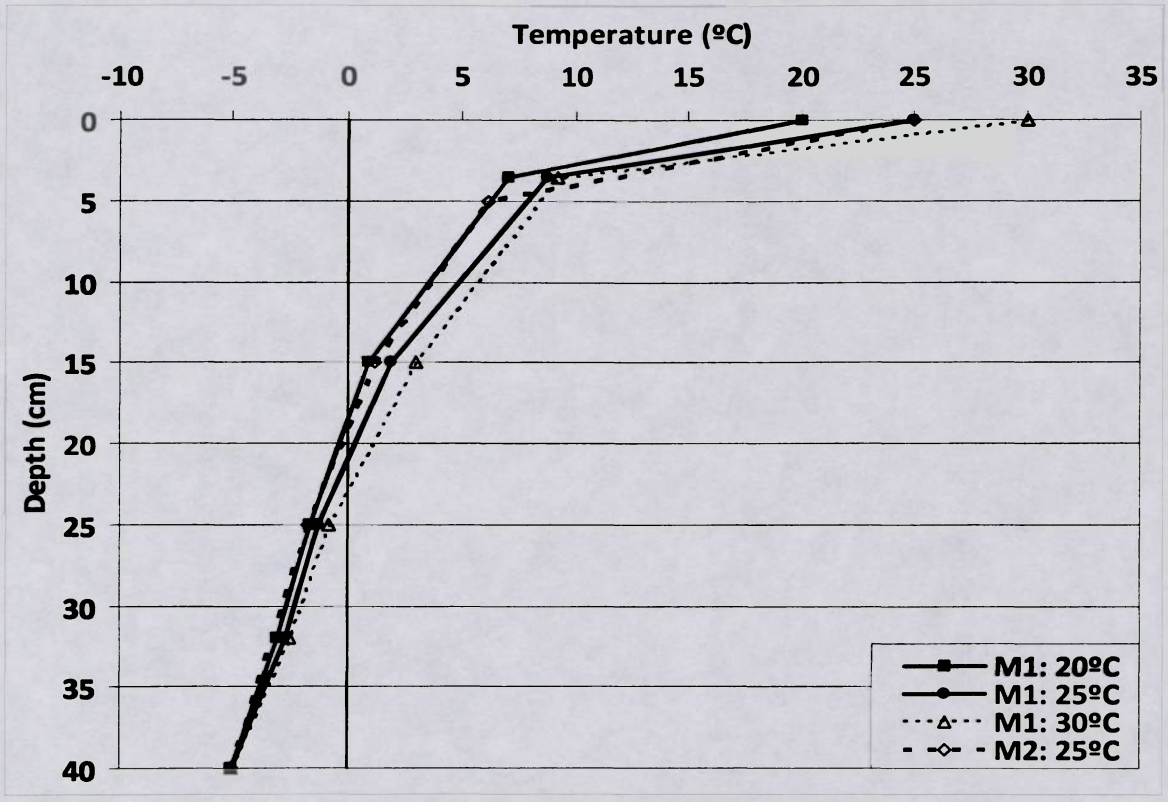

Figure 4.5 Average temperature profiles at the end of thawing

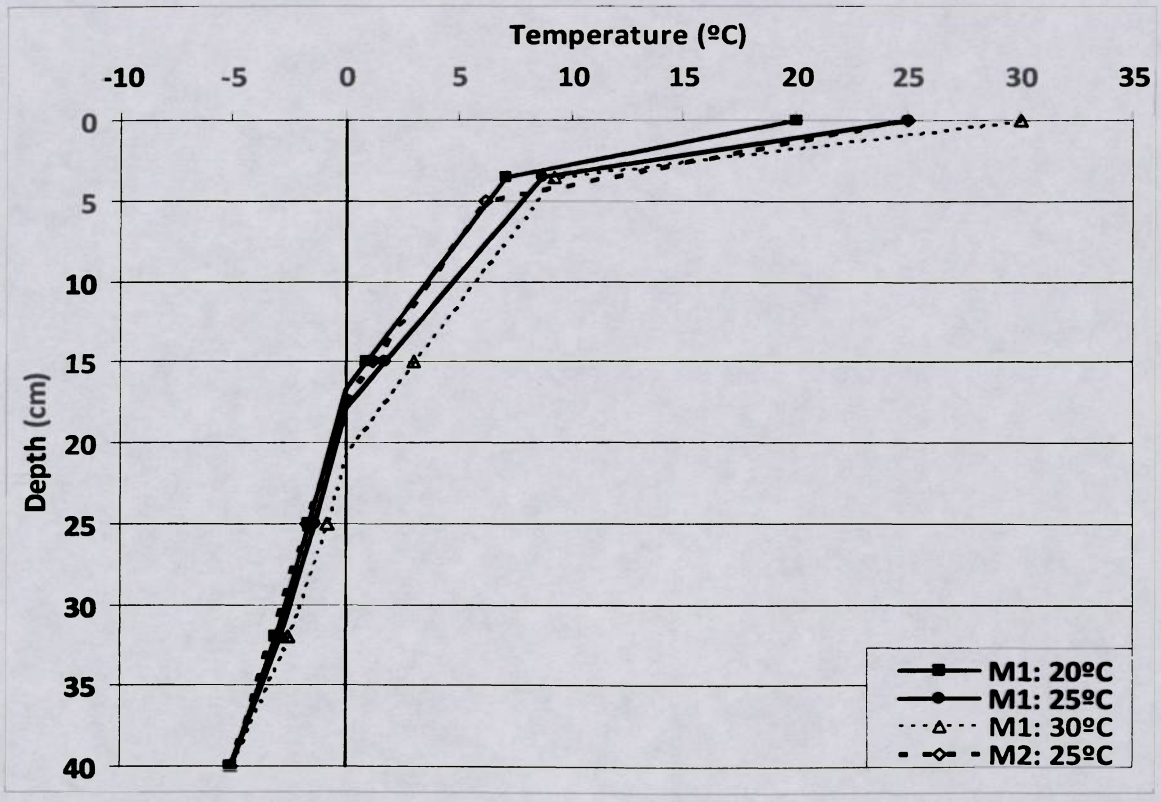

Figure 4.6 Extrapolation of temperature profiles at the end of thawing to determine depth of the 0°C isotherm

4.2 Numerical model verification of insulation effectiveness

A numerical analysis was carried out to simulate the soil column thermal conditions. A finite element software, Temp/W developed by Geo-slope International Ltd. (2007), was used for the analysis. The main purpose of the numerical analysis was to verify the effectiveness of the lateral insulation of the soil columns in the laboratory model.

4.2.1 Model description

Temp/W is a two-dimensional finite element program that can be used to simulate thermal behaviour of geo-materials. The governing differential equation used in Temp/W is expressed as:

$$\frac{\partial}{\partial x}\left(k_x \frac{\partial T}{\partial x}\right)+\frac{\partial}{\partial y}\left(k_y \frac{\partial T}{\partial y}\right)+Q=\lambda \frac{\partial T}{\partial t} \qquad [4.1]$$

Where:

T:	temperature;
k_x:	thermal conductivity in the x-direction;
k_y:	thermal conductivity in the y-direction;
Q:	applied boundary flux;
λ:	capacity for heat storage;
t:	time.

This equation states that the difference between the heat flux entering and leaving an elemental volume of soil at a point in time is equal to the change in the stored heat energy (Geo-Slope International Ltd. 2007).

In this study, it is important to determine the time required for the 0°C isotherm to reach its maximum. As such, a transient analysis was carried out to simulate the time dependant behaviour.

A radially symmetric model was set up to simulate the freeze-thaw conditions applied to the soil columns in the physical test. The dimensions of the model were chosen based on the sample setup used in the laboratory testing. The soil sample has a height of 40 cm and a diameter of 15 cm and is laterally insulated with a 32 cm thick layer of loose-fill insulation. As discussed later in Chapters 5 and 6, soil moisture conditions changed in the physical models tested. Therefore, a two-layered system was simulated with the numerical model.

The two soil layers were assumed as follows: (1) the active layer to a depth of 20 cm and (2) permafrost from 20 cm to 40 cm depth. A sketch of the Temp/W model developed in the thermal analysis is depicted in Figure 4.7. A total of 1755 elements were discretized (Fig. 4.7). The materials and boundary conditions assigned to the model are discussed in the next sections.

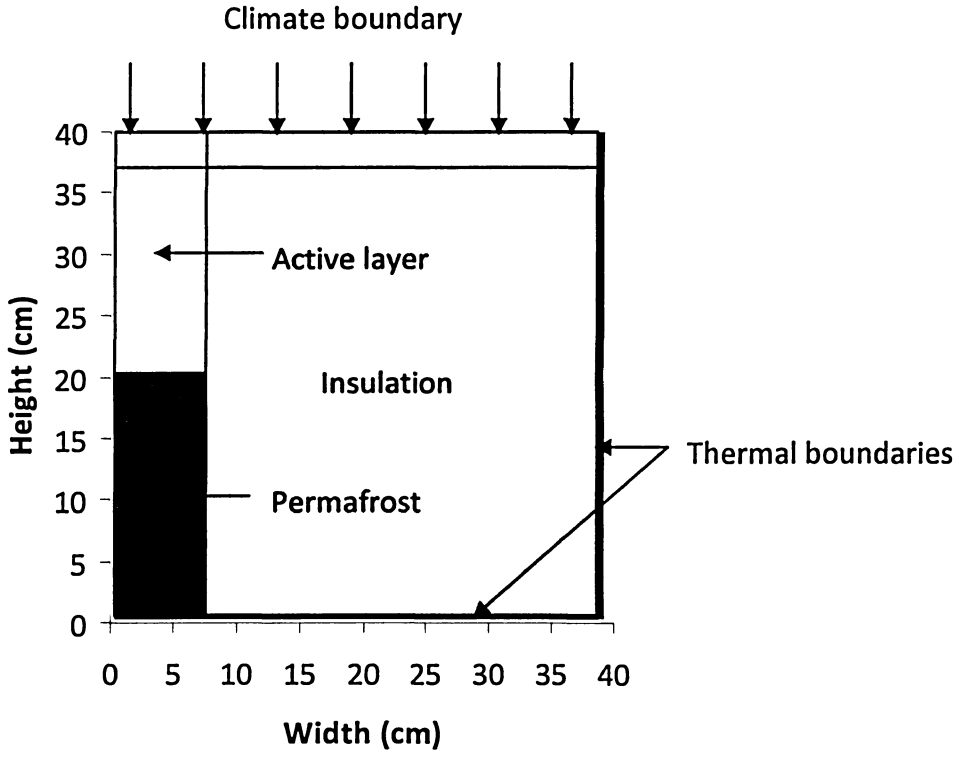

Figure 4.7 Sketch of the Temp/W model developed in the thermal analysis

4.2.2 Material properties

Three different materials were defined in this analysis: active layer, permafrost and insulation. Table 4.1 lists the frozen and unfrozen volumetric heat capacities, the unfrozen volumetric water contents and the frozen and unfrozen thermal conductivities properties input in the Temp/W analysis. These properties were established based on several sources: Penner (1970), Penner et al. (1975), Goodrich (1982), Riseborough and Smith (1993), Riseborough (2002), Andersland and Ladanyi (2004), Overduin et al. (2006), Geo-Slope International Ltd. (2007) and Wang and Lesage (2007). The unfrozen volumetric water content defined for the active layer was based on the final water content measured in the laboratory. For the permafrost material, an unfrozen volumetric water content of 0.57 was modeled since this value corresponds to a gravimetric water content of 50% – the initial water content of the samples used in the laboratory experiment.

Table 4.1 Input thermal properties in Temp/W analysis

Material	Volumetric heat capacity ($kJ/m^3/°C$)		Unfrozen volumetric water content (m^3/m^3)	Thermal conductivity ($kJ/hr/m/°C$)	
	Frozen	Unfrozen		Frozen	Unfrozen
Active layer	1950	2350	0.43	6.9	4.4
Permafrost	2050	2450	0.57	9.9	5.6
Insulation	43.5	43.5	0	0.7	0.7

The heat capacity and thermal conductivity of the insulation material shown in Table 4.1 were assumed based on the manufacturer's suggested values. Two cases of insulation thermal conductivity were modeled in the numerical analysis: the sample has no lateral insulation and the sample is fully insulated laterally.

The thermal conductivity functions input in the model are given in Figure 4.8. These functions were generated by the Temp/W software by inputting frozen and unfrozen heat conductivities and specifying the type of material simulated. Figure 4.9 plots the volumetric unfrozen water content functions for the soils modeled in the analysis. The unfrozen water content functions were determined based on the literature.

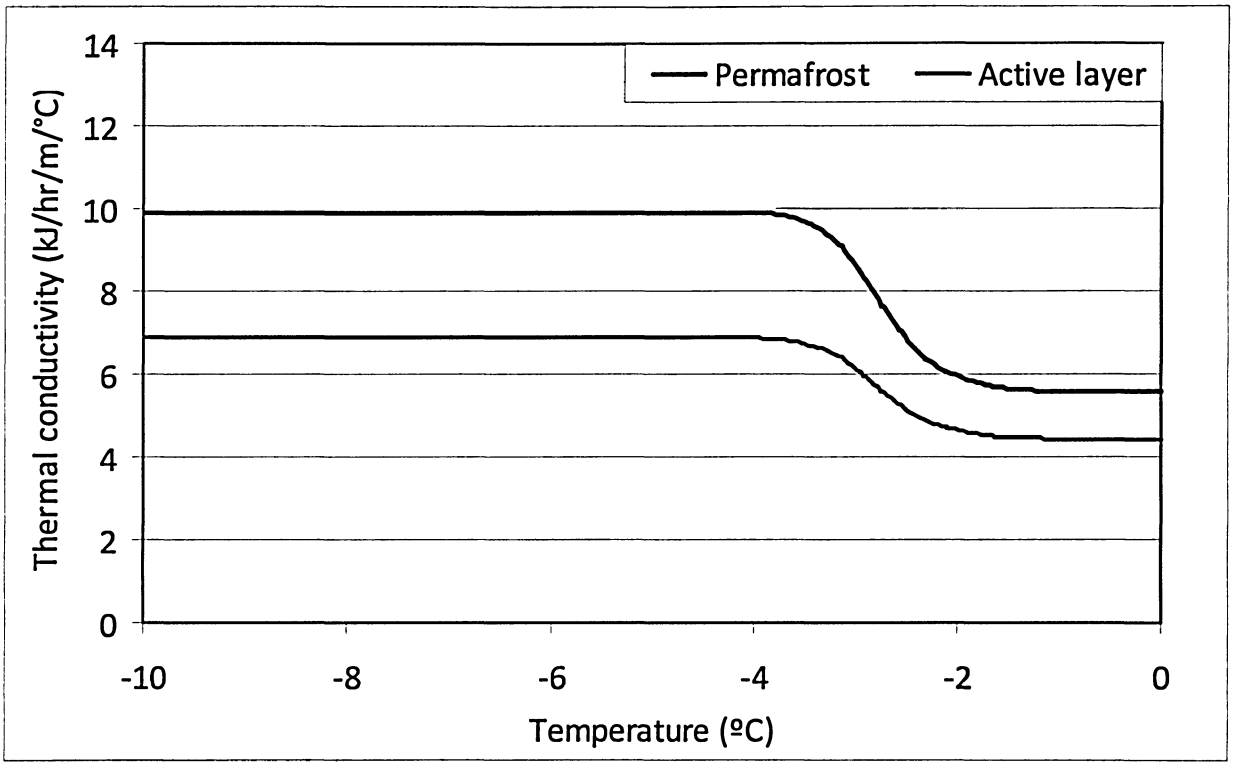

Figure 4.8 Thermal conductivity functions input in Temp/W

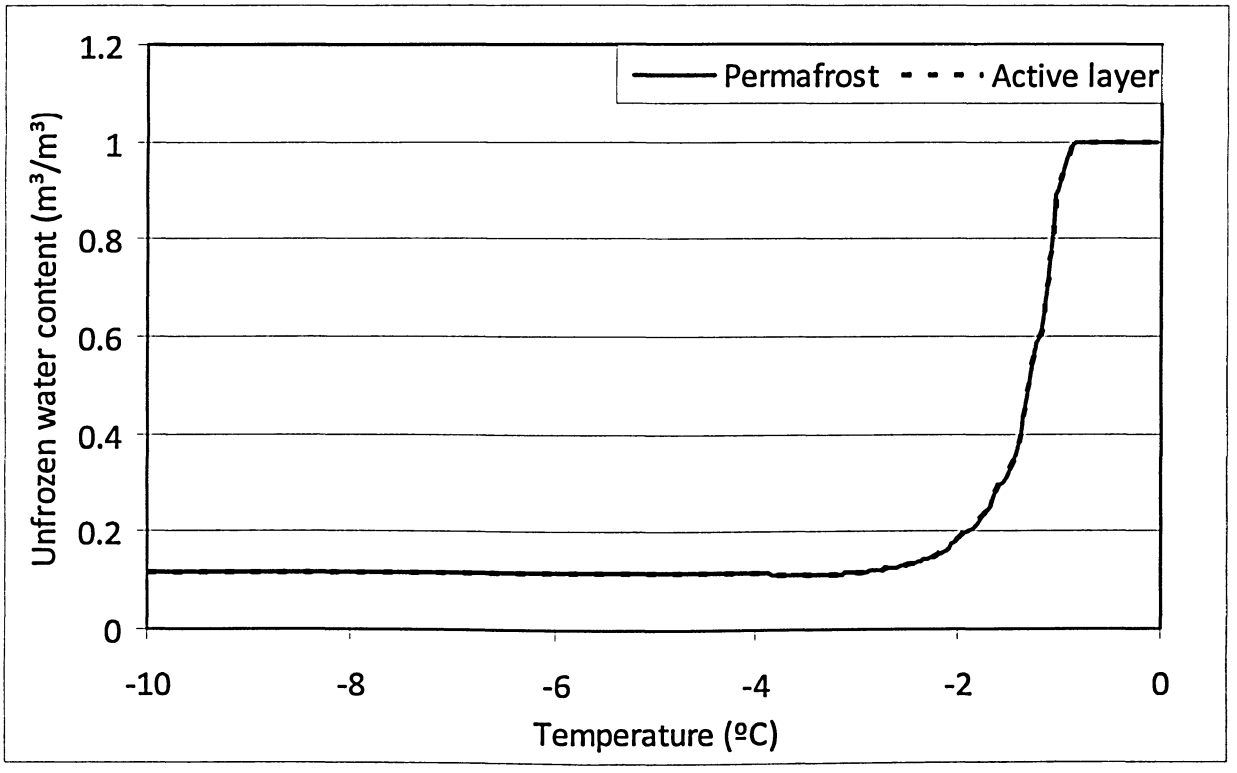

Figure 4.9 Unfrozen water content functions input in Temp/W

4.2.3 Boundary conditions

The boundary conditions input in the numerical model simulate the laboratory experiment. All nodes were assumed to have an initial temperature of -10°C, which represents the temperature condition during the freezing period. In addition, nodal heat flux is assumed to be zero for the lateral boundaries.

The lower and lateral boundaries were defined as an alternation of -10°C and -5°C, which corresponds to the laboratory testing conditions (Table 3.3). These thermal boundary conditions are depicted in Figure 4.10. The time interval for each temperature was based on the temperatures imposed on the physical model.

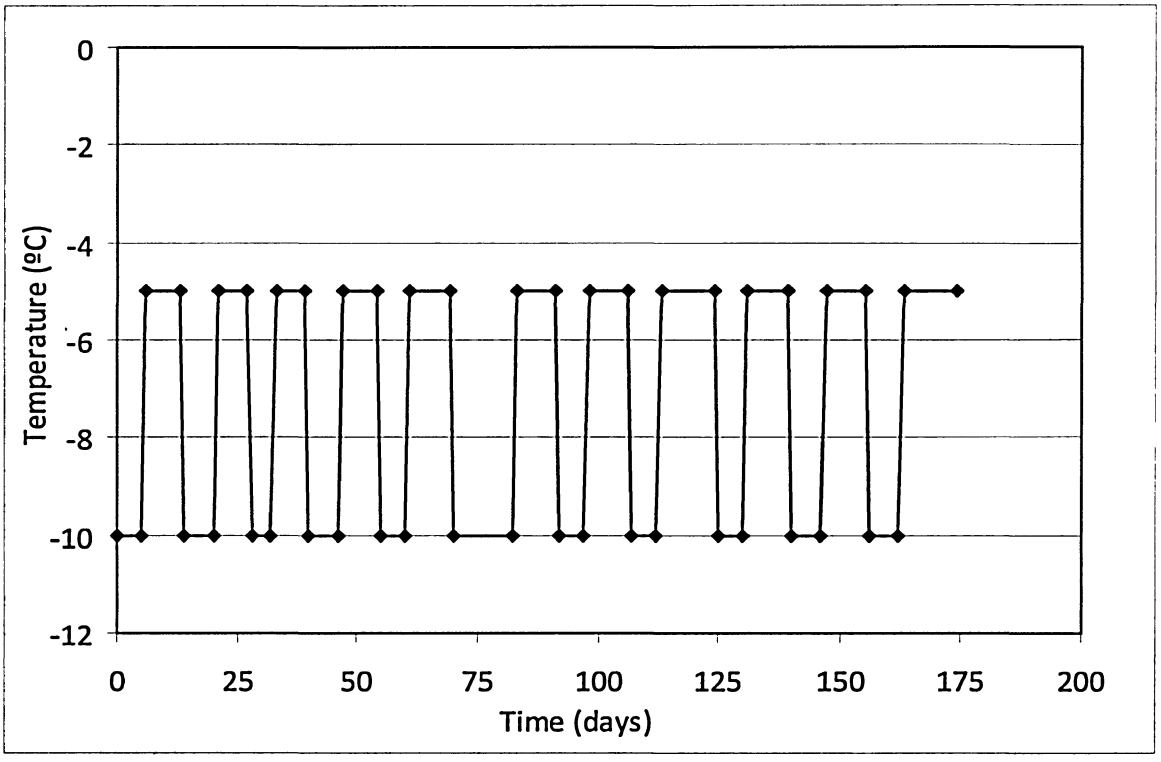

Figure 4.10 Thermal function used for lateral and lower temperature boundaries

The soil temperature at the ground surface is an important boundary condition. In Temp/W, it is determined by air temperature and other climatic conditions as follows (GeoSlope 2007):

$$T_s = T_a + \frac{1}{\upsilon f(u)}(Q_n - AE) \qquad [4.2]$$

Where:

T_s: temperature at the soil surface (°C);

T_a: temperature of the air above the soil surface (°C);

υ: psychrometric constant;

f(u): function dependent on wind speed;

Q: net radiant energy available at the surface (mm/day);

AE: actual vertical evaporative flux (mm/day).

Basically, this equation states that the ground temperature is increased by energy that was not consumed in the evaporation or transpiration process (GeoSlope 2007). When calculating the actual evaporation (AE) component of the above equation, the model assumes that the soil is saturated at 80% and that AE is approximately equal to the potential evaporation (input in the climate boundary). The AE requires the input of mean air temperature, relative humidity and precipitation (if applicable to the simulated soil). Furthermore, the function f(u) accounts for the wind speed also input in the climate boundary. It should be noted that Temp/W does not consider the water stress state in its computations.

A climate boundary condition was applied at the top surface of the model. The climate data used in the analysis during one freeze-thaw cycle are presented in Table 4.2. In the table, the temperature column refers to the applied temperature at the top of the soil column during the laboratory testing. The relative humidities and the wind speed were assumed. The potential evaporation was measured in the laboratory by placing a beaker of water under the heating chamber where the soil sample is located, and allowing the water to evaporate for 24 hours. An average of 10 mm of water evaporated during one day. Water was added every day of the thawing cycle to avoid desiccation of the samples caused by the heat and fan located in the heating chamber. The amount of water added to

the sample equals the total amount evaporated due to the wind and heat originating from the heating chamber. A precipitation of 10 mm/day was therefore simulated in the numerical model. Altogether, eleven freeze-thaw cycles were input in the climate boundary condition, which is a total of 174 days.

Table 4.2 Climate surface boundary condition for one freeze-thaw cycle

	Temperature (°C)	Relative humidity (%)	Wind speed (m/s)	Precipitation (mm)	Potential evaporation (mm/day)
Thawing	25	79	3	10	10
Freezing	-10	72	3	10	10

4.3 Numerical results and comparison with laboratory data

The temperature profiles obtained in the laboratory and the numerical analysis for thawed conditions are shown in Figure 4.11. These profiles are the result of maximum thawing for Cycles 9, 10 and 11. As shown in the figure, the black-dotted line is the computed temperature results for a model that has no lateral insulation whereas the other lines correspond to a simulation having full lateral insulation with different upper boundary temperatures. According to this figure, the measured temperatures are generally within the temperature range computed from the insulated and uninsulated cases. The comparison indicates that there could be heat losses at the lateral boundary of the soil columns. Nonetheless, it should be noted that the thermal conductivity value of the insulation material determined by the manufacturer is likely based on ideal conditions, which are not usually the case due to a number of factors (e.g. placement method, compression or separation of the insulation sheets). Thus, the thermal conductivity of the insulation is most likely not as optimal as the manufacturer specifies. The lower temperature readings from the upper two sensors in model M2 (at depths of 5 cm and 15 cm) were further exaggerated by a lateral shift of the sensors towards the cylinder wall that was noticed during inspection after the test. Figure 4.12 depicts the results of the experimental and numerical models in reference to the progression of 0°C isotherm depth over time. This figure also shows that the physical experiment represents a case between the fully insulated and uninsulated lateral boundary conditions.

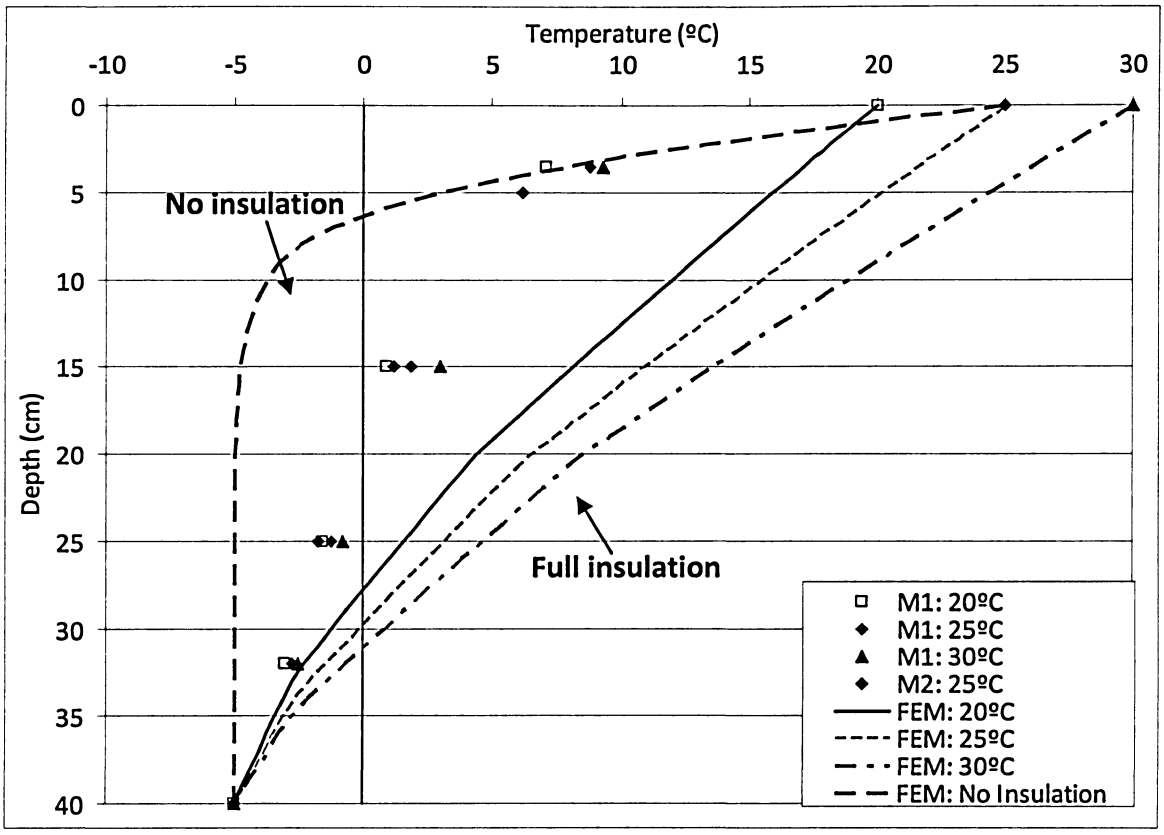

Figure 4.11 Comparison of maximum temperature profiles from physical and numerical (FEM) models

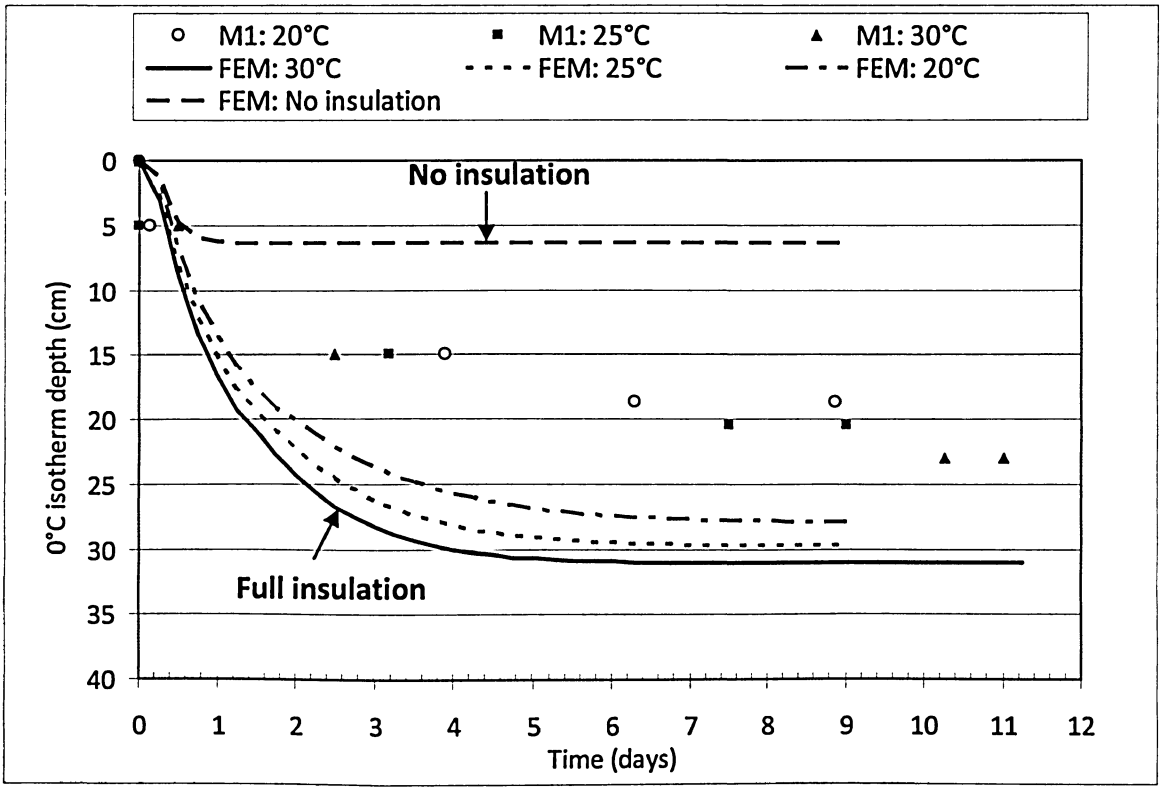

Figure 4.12 Comparison of 0°C isotherm progression in numerical and laboratory models

5 Moisture Content

5.1 Observations

Gravimetric moisture contents of soil samples taken along the soil columns after the laboratory test was completed are shown in Figure 5.1. In both laboratory models, the initial gravimetric water content was set at 50% (Fig. 5.1). The figure also illustrates the extrapolated maximum cryofront depths (Fig. 4.6) for M1 (left of profiles) and for M2 (right of profiles).

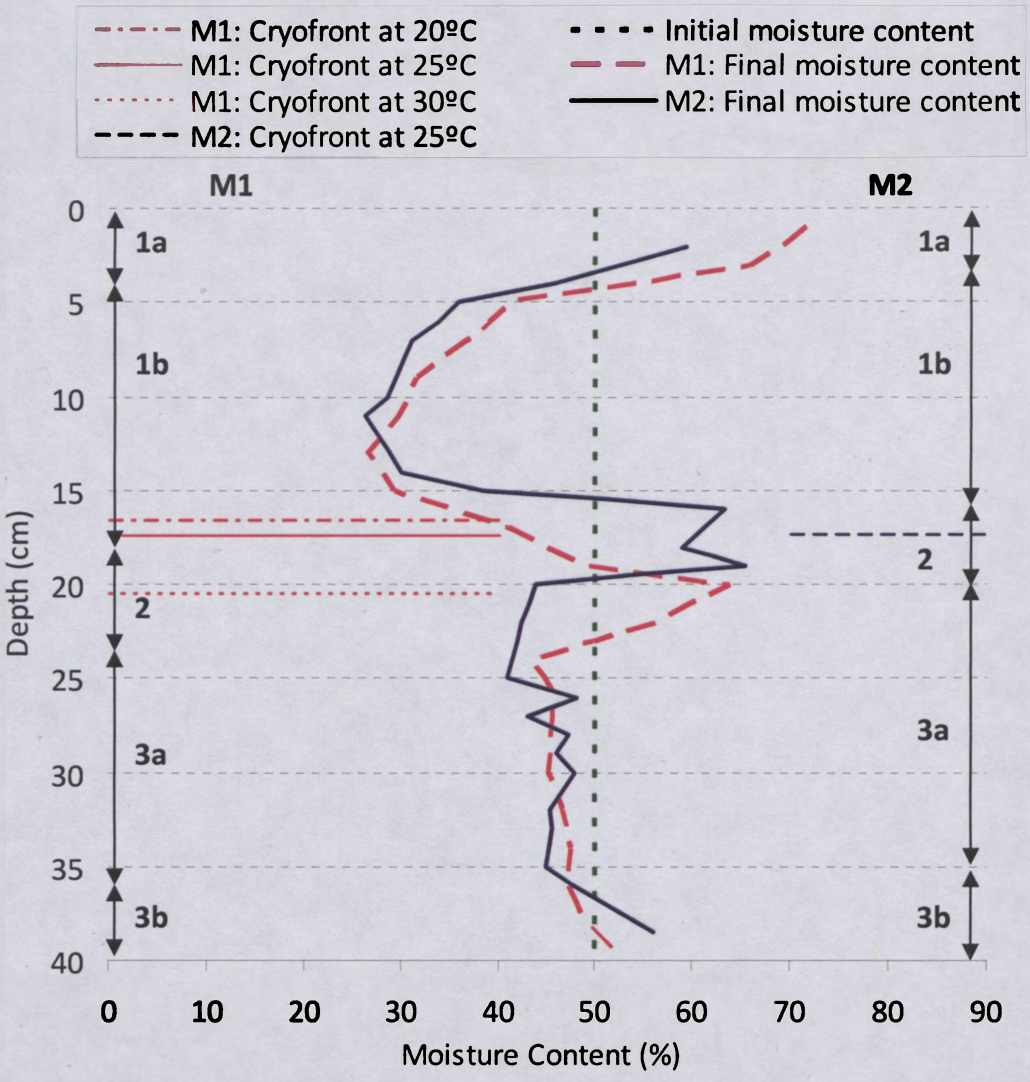

Figure 5.1 Initial and final moisture profiles of M1 and M2

5.2 Interpretation

It is evident that moisture redistribution has occurred in both samples during the eleven cycles of testing. Both models show similar profiles with five distinct moisture zones, from top to bottom:

Zone 1a: the upper zone of the active layer showing increased moisture content;
Zone 1b: the lower zone of the active layer with decreased moisture content;
Zone 2: a layer of moisture surge in the vicinity of the maximum cryofronts;
Zone 3a: a slightly decreased moisture zone in the "long-term permafrost" and
Zone 3b: a slightly increased moisture zone at the bottom boundary of the model.

According to Figure 5.1, both models indicate that the maximum cryofront depths coincide with the depths of moisture surge (20.5 cm in M1 and 17.4 cm in M2). It should be noted that the chemical effect of the pore water was not considered and its analysis is beyond the scope of this study. The final moisture content and change in moisture content for each zone are summarized in Tables 5.1 and 5.2.

Table 5.1 Change of moisture content in M1

Zone	Soil layer	Depth range	Moisture content (%)	Change of moisture content* (%)
1a	Upper active layer	0 – 4 cm	64.9	14.9
1b	Lower active layer	4 – 18 cm	33.1	-16.9
2	Ice-rich layer	18 – 23 cm	53.8	3.8
3a	Long-term permafrost	23 – 36 cm	45.8	-4.2
3b	Long-term permafrost	36 – 40 cm	50.3	0.3

*the change of moisture content after completion of the test is relative to the initial moisture content (50%)

Table 5.2 Change of moisture content in M2

Zone	Soil layer	Depth range	Moisture content (%)	Change of moisture content* (%)
1a	Upper active layer	0 – 3 cm	55.9	5.9
1b	Lower active layer	3 – 15.5 cm	33.2	-16.8
2	Ice-rich layer	15.5 – 20 cm	57.5	7.5
3a	Long-term permafrost	20 – 35 cm	44.6	-5.4
3b	Long-term permafrost	35 – 40 cm	51.8	1.8

*the change of moisture content after completion of the test is relative to the initial moisture content (50%)

Boundary effects explain the moisture conditions in Zones 1a and 3b. The high water content near the top surface is attributed to the addition of water during each thawing cycle. The slight moisture increase at the bottom boundary is due to attraction of moisture to the freezing front where freezing was maintained for the duration of the test. The slightly lower moisture content in Zone 3a (below the ice-rich layer) was most likely caused by moisture migration to the freezing fronts above and below this layer. The moisture in this layer had probably reached or was close to its equilibrium condition after repeated freeze-thaw cycles. This is believed to be true since extensive moisture adjustments would have occurred as evidenced in the active layer and the ice-enriched zone.

The moisture conditions of the Zones 1b and 2 are of great interest. Clearly, moisture has increased significantly in a layer of approximately 5 cm thick (Zone 2) at the bottom of the active layer. Immediately above this high moisture zone, there is a significant drop of moisture despite water supplied at the surface during every thawing cycle. It was observed that the volume of moisture "deficit" in the active layer is greater than that of

moisture "surplus" below. This is likely caused by an alternating two-sided movement of moisture in the active layer. During the thawing period, the moisture in the active layer was attracted to the freezing front below, while during freezing, the unfrozen water in the active layer moved upward due to freezing at the top. These results are consistent with findings reported by others. Cheng (1983) and Mackay (1983) explained the ice accumulation near the permafrost table as a result of water migration during winter and summer in response to a thermal gradient between soil and air surfaces. Moisture is attracted to the cold front and accumulates at a certain depth which creates an ice-rich layer. Ice-enrichment is only present in permafrost terrain due to its two-sided freezing nature (Harris et al. 2008a, b; Kern-Luetschg and Harris 2008) which often leads to a moisture deficit in the active layer (Mackay 1983; Harris and Lewkowicz 2000).

In both models, the soil samples and boundary conditions were identical up to Cycle 8. Extreme temperatures were applied to M1 starting from Cycle 9, while "normal" temperatures were applied to M2. By comparing the results in Figure 5.1, it can be concluded that the "normal" 5 cm thick ice-rich zone above the cryofront under normal conditions in model M1 was altered during the applied extreme temperature. The moisture surplus zone moved downwards by about 3 cm to the new deeper cryofront. This information is critical for understanding the transient layer. It should be noted that the downward shift of the moisture surplus zone took place after only one cycle of extreme thaw. In addition, the moisture conditions in the long-term permafrost may eventually reach equilibrium as demonstrated in Zone 3a described above. Some unfrozen water below the moisture surplus zone may eventually be drawn back to the normal surplus zone under repeated normal freeze-thaw cycles. From these findings, it is believed that the ice-rich zone is likely part of the transient layer.

Generally, moisture content profiles in fine-grained near surface permafrost soils are characterized by a peak in total moisture content. This has been observed extensively in field investigation conducted in the Canadian North (Mackay 1971, 1983; Pollard and French 1980; Harris 1988; Burn and Michel 1988; Kokelj and Burn 2003b, 2005; Wang et al. 2008; Morse et al. 2009). Harris (1988) established several moisture content

profiles in the Northern Canadian Cordillera and determined that there is a concentration of moisture in the upper layers of the permafrost table regardless of profile location or vegetation cover (Fig. 2.5).

A recent Mackenzie valley field study conducted by Wang et al. (2008) established the moisture content profiles for 14 sites. Fine-grained soil samples were extracted from the ground surface down to a depth well into the long-term permafrost. The charts in Figure 5.2 depict typical moisture profiles for two of the 14 sites investigated. Generally, water contents are lower in the active layer (<50%) and increase with depth. A peak in water content at the active layer base and top of permafrost was noted at most sites; findings that agree with the ice-rich zone defined in other field studies (Shur et al. 2005; Bockheim and Hinkel 2005). The shapes of the moisture charts reported by Wang et al. (2008) are very similar to those found in this study (Fig. 5.1).

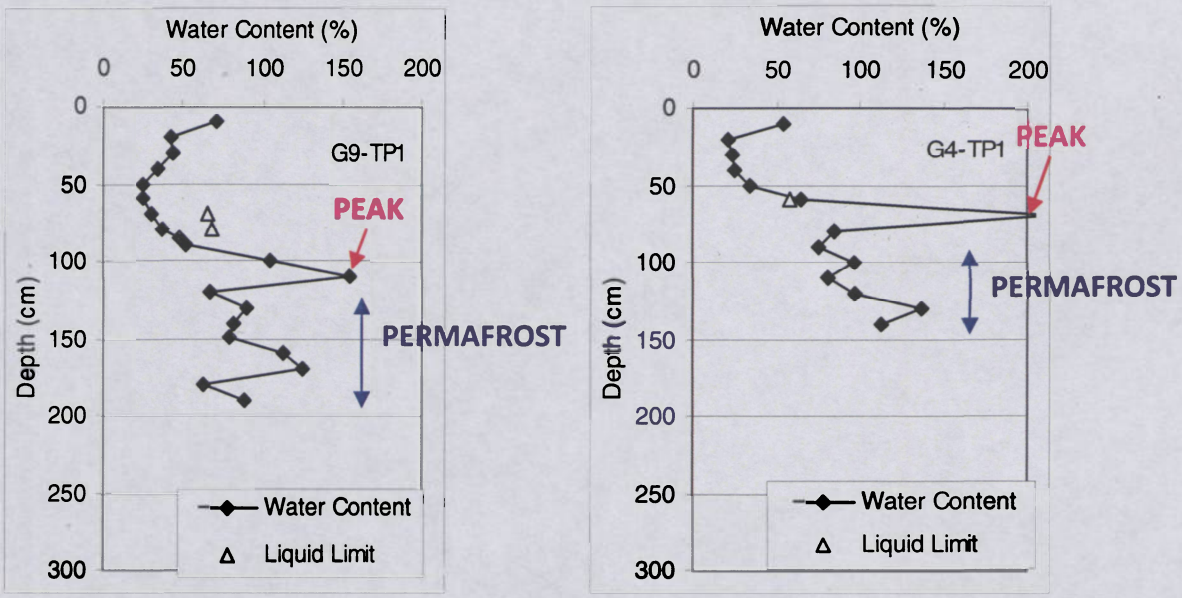

Figure 5.2 Typical soil moisture content profiles for two of the 14 sites (modified from Wang et al. 2008)

6 Cryostructure

6.1 Observations

The cryostructures of each soil column was examined once the test was completed and the samples were opened. Figures 6.1 and 6.2 show the structural conditions of models M1 and M2, respectively. Soil moisture profiles and maximum cryofront depths are shown in Figures 6.1a and 6.2a. The maximum cryofronts are the conditions at the end of thawed cycles with thawing temperatures indicated. In M1, the maximum cryofront depths are 16.7, 17.8 and 20.5 cm for thawing temperatures of 20, 25 and 30°C, respectively; whereas in M2, the maximum cryofront is 17.4 cm. These cryofronts were extrapolated as shown in Figure 4.6. Figures 6.1b and 6.2b depict enlarged areas of the structure at locations marked in Figures 6.1a and 6.2a.

In the active layer, cracks and pore ice crystals were visible in some areas; however, no distinctive ice structures were created in either sample within this zone. This layer extends from the top surface to a depth of 18.0 cm in M1 and 15.5 cm in M2. Below these depths are distinctive cryostructures with ice lenses up to 6 mm in M1 and 9 mm in M2. The ice-rich zone consists of two distinctive structures: (1) the upper half with thinner ice lenses and (2) the lower half with thicker ice lenses. The thicker ice lenses were more horizontal. The division of these two structures coincides in both models. Ice lenses continue below the high moisture zone, although the thickness of the ice lenses is reduced compared to that at the cryofront. The ice lenses taper off at the bottom 4 to 5 cm of both soil columns. The ice lenses become finer and less visible in this bottom layer (Zone 3b).

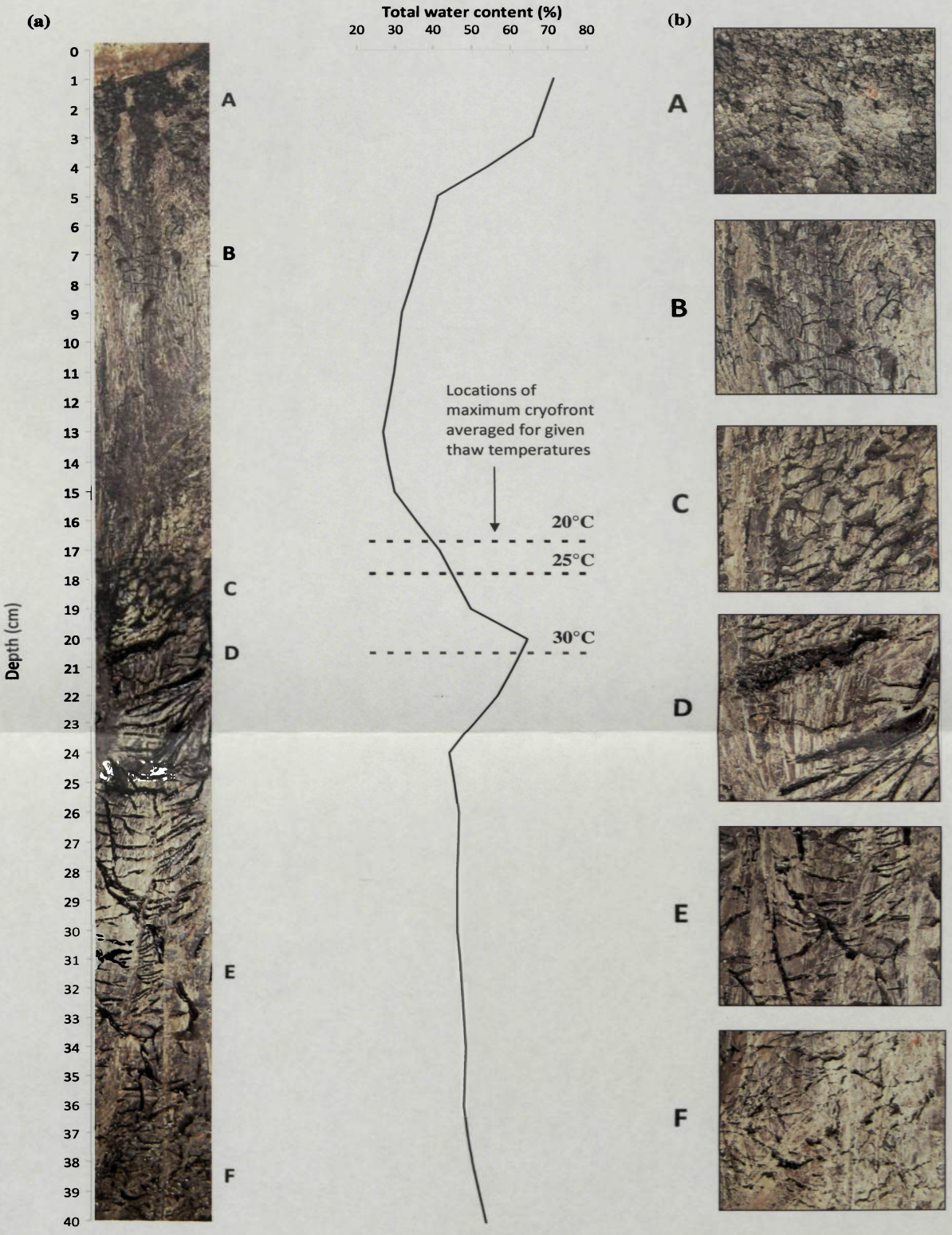

Figure 6.1 Cryostratigraphy of model M1 after eleven freeze-thaw cycles (a) structure and moisture along length of column M1 (b) enlarged areas of selected sections marked on (a). The maximum cryofronts are extrapolated as shown in Figure 4.6.

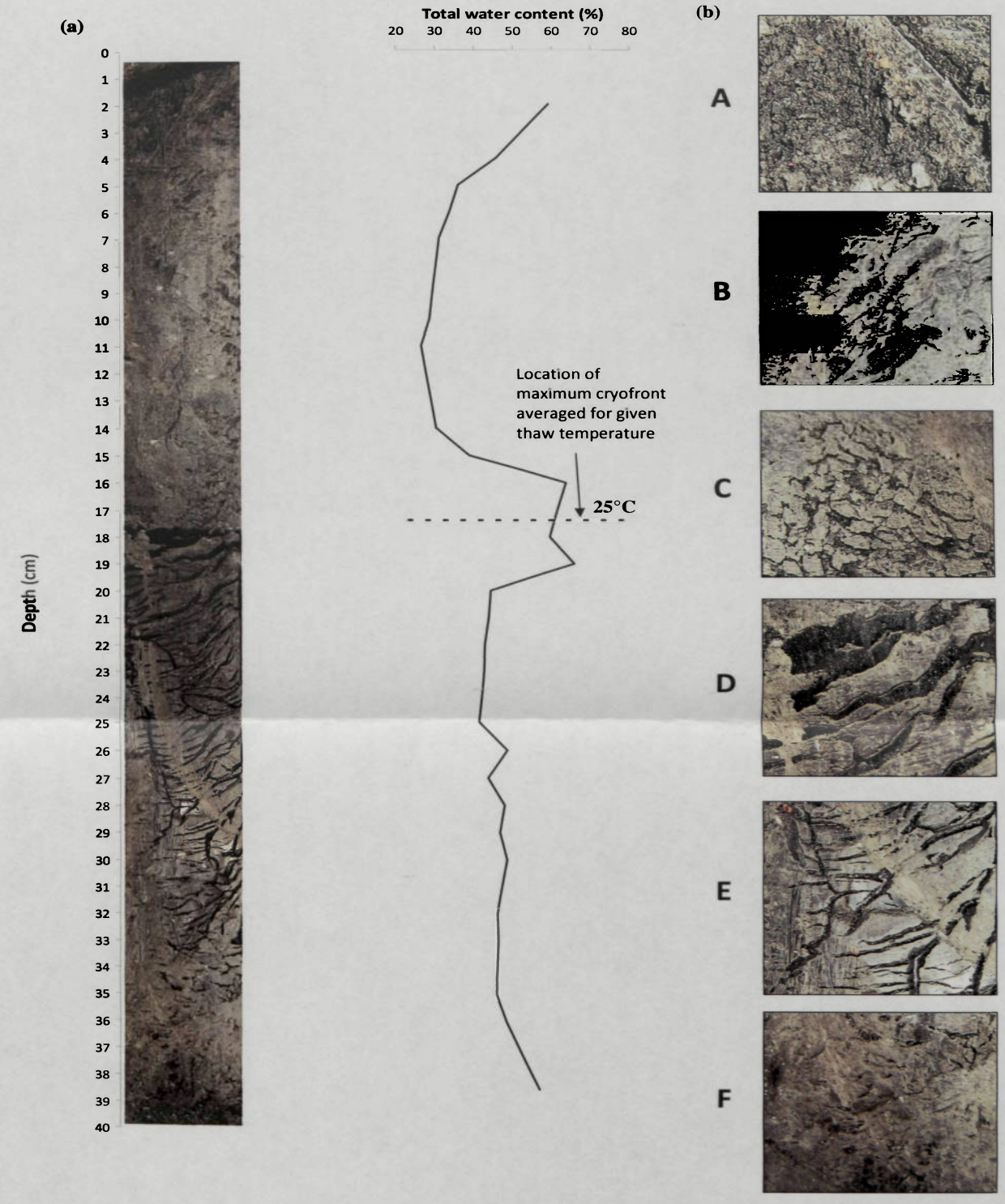

Figure 6.2 Cryostratigraphy of model M2 after eleven freeze-thaw cycles (a) structure and moisture along length of column M2 (b) enlarged areas of selected sections marked on (a). The maximum cryofront is extrapolated as shown in Figure 4.6.

6.2 Interpretation

6.2.1 Cryostructures

The cryostructures observed in this study are compared with the Murton and French (1994) nomenclature (Fig. 2.2). Tables 6.1 and 6.2 list the identification and descriptions of the different cryostructures found in M1 (Fig. 6.1) and M2 (Fig. 6.2) along with corresponding moisture contents. The soil layers identified herein are identical to those referred to in Chapter 5 for moisture descriptions (Table 5.1 and 5.2).

Table 6.1 Identification and description of cryostructures in M1

Zone	Soil layer	Depth range	Moisture content (%)	Cryostructure	Description
1a	Upper active layer	0 – 4 cm	64.9	Structureless	No specific structure. Some visible pore ice crystals.
1b	Lower active layer	4 – 18 cm	33.1	Structureless	No specific structure. Some fine cracks. Some visible pore ice crystals.
2a	Ice-rich layer	18 – 20.5 cm	51.7	Irregular reticulate	Non-parallel net-like structure. Thin ice lenses.
2b	Ice-rich layer	20.5 – 23 cm	57.2	Lenticular or layered	Thick horizontal ice lenses (up to 6 mm thick)
3a	Long-term permafrost	23 – 36 cm	45.8	Lenticular	Fine horizontal ice lenses that are at places layered. Occasional, vertical or diagonal ice lenses.
3b	Long-term permafrost	36 – 40 cm	50.3	Structureless	No specific structure. Fine ice lenses and some visible ice crystals.

Table 6.2 Identification and description of cryostructures in M2

Zone	Soil layer	Depth range	Moisture content (%)	Cryostructure	Description
1a	Upper active layer	0 – 3 cm	55.9	Structureless	No specific structure. Some visible pore ice crystals.
1b	Lower active layer	3 – 15.5 cm	33.2	Structureless	No specific structure. Some fine cracks. Some visible pore ice crystals.
2a	Ice-rich layer	15.5 – 18 cm	59.3	Irregular reticulate	Non-parallel net-like structure. Thin ice lenses
2b	Ice-rich layer	18 – 20 cm	54.5	Lenticular or layered	Thick horizontal ice lenses (up to 9 mm thick)
3a	Long-term permafrost	20 – 35 cm	44.6	Lenticular	Fine horizontal ice lenses that are at places layered. Occasional, vertical or diagonal ice lenses.
3b	Long-term permafrost	35 – 40 cm	51.8	Structureless	No specific structure. Fine ice lenses and some visible ice crystals.

The active layer (Zones 1a and 1b) is described as being structureless with some visible ice crystals with some fine cracks in both samples. In field investigations, Leshchikov and Ryashchenko (1978) also described the active layer as being structureless, whereas Mackay (1983) referred to it as being at times desiccated with the presence of various structures. Gavriliev and Efremov (2003) described the active layer as having cavities and cracks resulting from the melting of ice lenses and streaks. This occurs perhaps because the active layer thaws every year.

In both samples, irregular reticulate ice structures (Zone 2a) are identified in the upper ice-rich layer. Within this region, the ice has a net-like (reticulate) structure and is non-parallel (irregular). Zone 2b is ice-rich and consists of thick lenticular or layered ice structures in both samples. In numerous field investigations, aggradational or segregated ice lenses have been identified near the 0°C isotherm (Mackay 1971, 1972, 1980, 1983;

Pollard and French 1980; Burn et al. 1986; Burn 1988; Harris 1988; Morse et al. 2009). In both samples, the ice-rich layer contains two types of cryostructures: irregular reticulate and lenticular or layered. In a study conducted in the Mackenzie Delta, two kinds of structures were also noted at the active layer and permafrost interface (Fig. 2.3). The authors identified the ice structure located between 7 and 10 cm (on the scale) as segregated ice.

Based on the cryostratigraphy, the transient layer may be ice-enriched and may have a thick lenticular or layered structure. By comparing the cryostructures in models M1 and M2, it is likely that the "normal" ice-rich structures observed in model M2 may have existed in M1 prior to Cycle 11 but were altered during the extreme temperature conditions applied during Cycle 11. Furthermore, the ice-enriched zone moved downwards to the new deeper cryofront. These findings are evidence that the transient layer is a constantly reconditioned zone which may be subjected to significant alterations under varying climate conditions.

In Zone 3a, in the "long-term permafrost" zone, the cryostructure is generally lenticular. This structure consists of fine horizontal with occasional vertical or diagonal ice lenses. No thawing has occurred in this zone during the experiment. The cryostructure described in Zone 3b is structureless within both samples. This can be attributed to boundary effects. In addition, other cryostructures may be slightly distorted due to boundary effects.

6.2.2 Influence of extreme temperatures

The maximum cryofront depths averaged for given thaw temperatures are depicted by dotted lines superimposed on the moisture profiles in Figures 6.1a and 6.2a. For model M2, where only one cryofront depth is reached (Fig. 6.2a), there is a change in cryostructure. The thickest ice lens is approximately located at this depth, which is an indication that moisture migrates toward the cryofront. In model M1, cycles with thawing temperatures of 20°C and 30°C have a different maximum 0°C isotherm than in 25°C thaw cycles. From Figure 6.1a, it can be seen that there is a change in cryostructure

approximately at the 25°C and 30°C cryofront depths. At the 25°C cryofront, the structure gradually changes from structureless to irregular reticulate. During the last cycle of M1, a deeper cryofront was reached due to an air temperature of 30°C. The thickest ice lenses are located at this depth. These findings indicate that the thick ice lenses in the upper portion of the lenticular or layered cryostructure (Zone 2b) were significantly altered and that in the lower portion were enhanced.

7 Pore Water Pressure

Pore water pressures were monitored at depths of 5, 15 and 25 cm in both samples. The soil at the 25 cm depth did not thaw during the entire experiment, therefore results from this sensor will not be presented. In this chapter, the laboratory test data are compared with the theoretical results from Equation [2.3] developed by Morgenstern and Nixon (1971).

7.1 Results

The calibrated total pore water pressure head recorded during the entire test is shown in Figures 7.1a and 7.2a. Figures 7.3a and 7.4a also depict the pore water pressure data, but on a smaller pressure head scale. Figures 7.3a and 7.4a exclude extremely positive and negative values of pore water pressures recorded during the freezing state of the sample. Below all pore pressure data charts is the corresponding chamber temperature (Fig. 7.1b – 7.4b). In previous studies, excessive values of pressure increases have been explained by the result of segregation ice growth (Harris and Davies 1998). However, there are significant uncertainties in the pressure transfer from the heaving soil to the transducer; therefore it cannot be assumed that pressure readings accurately reflect ice pressures. For this reason, only the results obtained during the thawing state of the samples will be discussed.

A chart for each cycle is presented in the discussions section of this chapter.

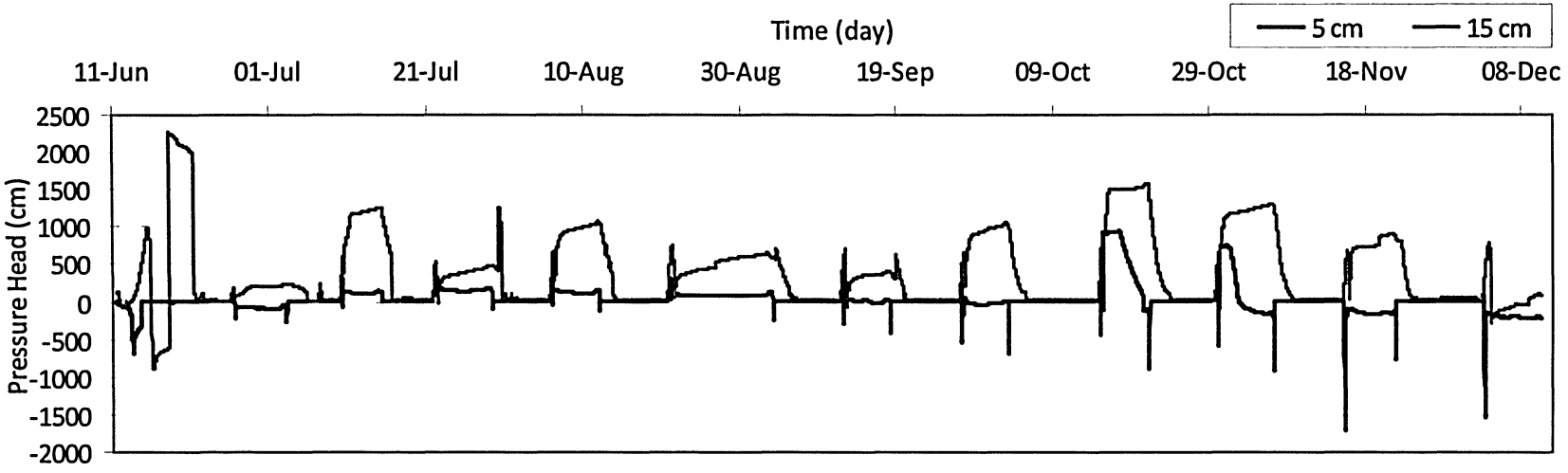

(a) Total pore water pressure history data for model M1

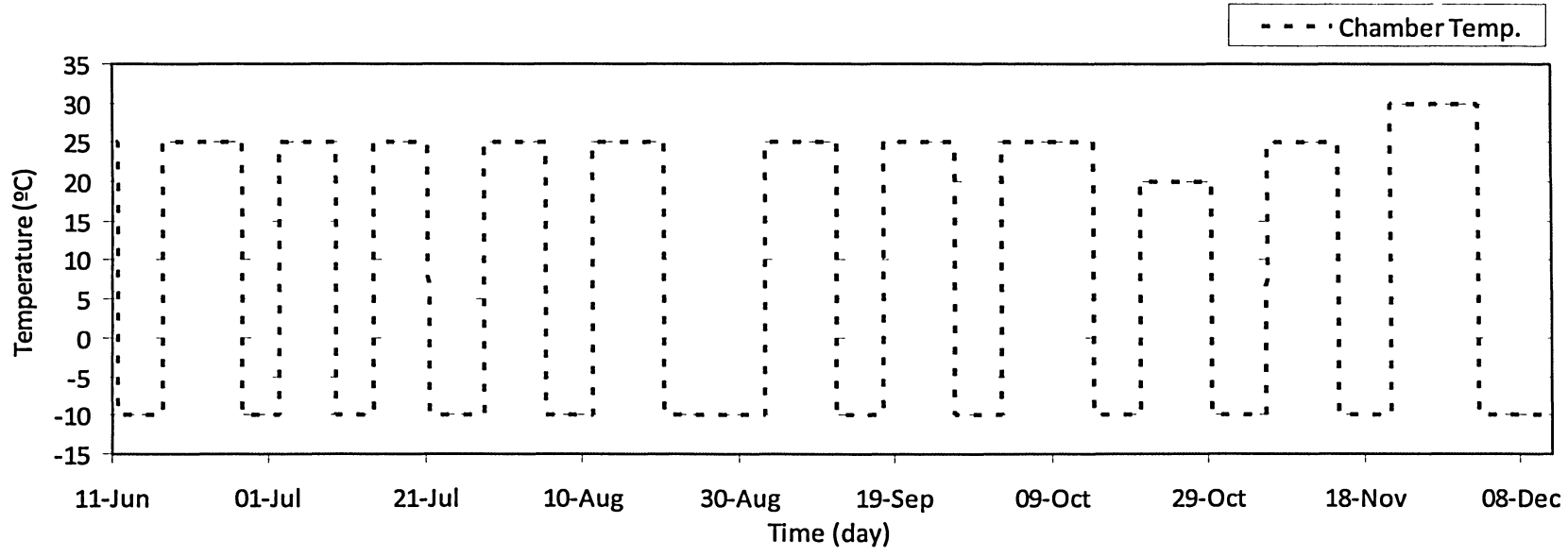

(b) Chamber temperature

Figure 7.1 (a) Total pore water pressure history data for model M1 and (b) chamber temperature

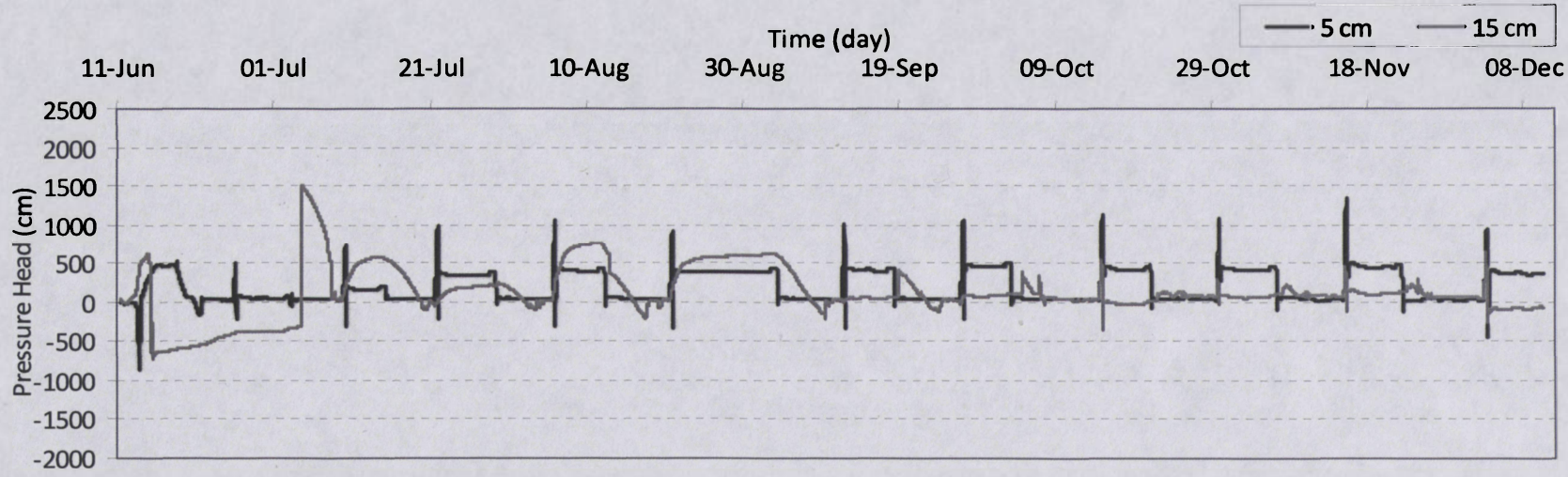

(a) Total pore water pressure history data for model M2

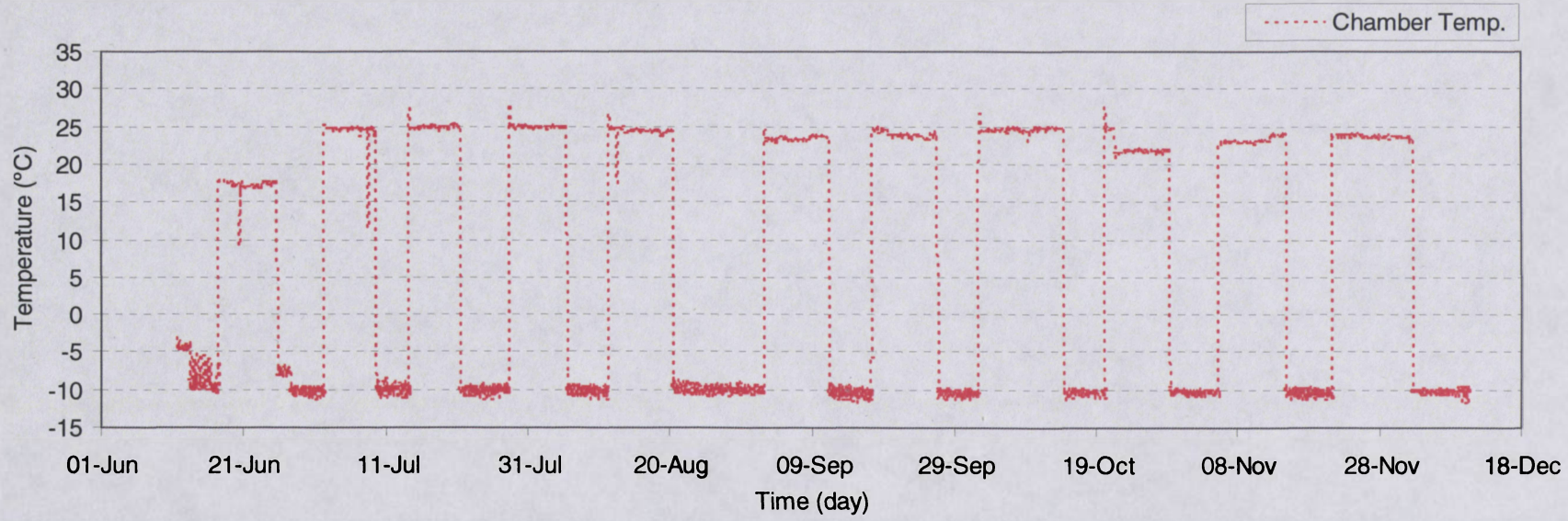

(b) Chamber temperature

Figure 7.2 (a) Total pore water pressure history data for model M2 and (b) chamber temperature

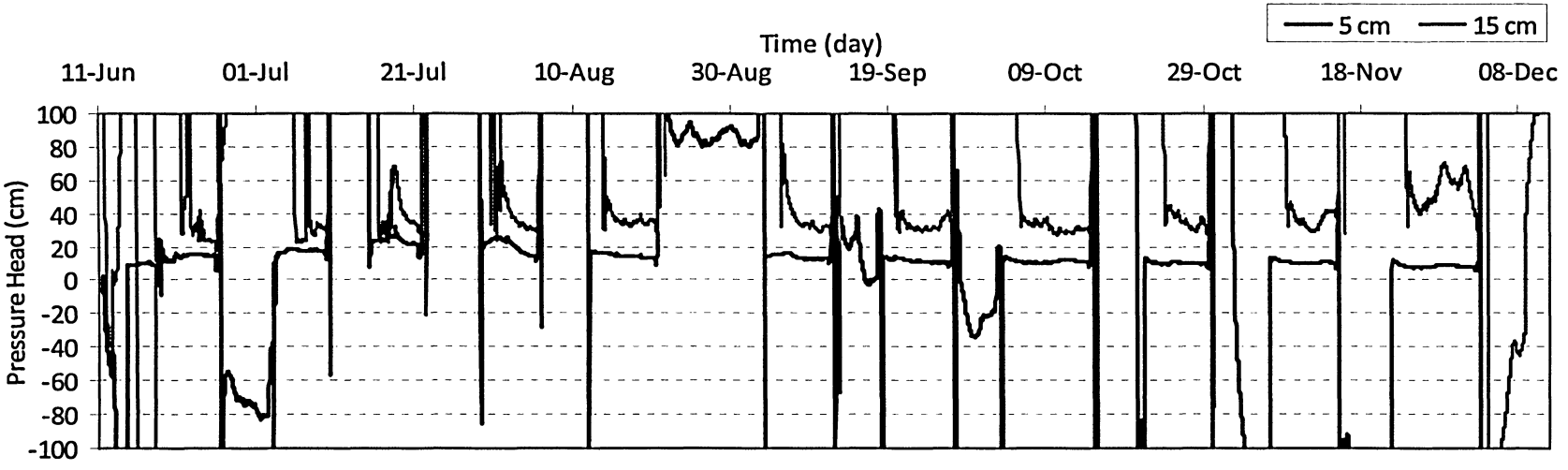

(a) Total pore water pressure history data for model M1 (smaller scale than Fig. 7.1)

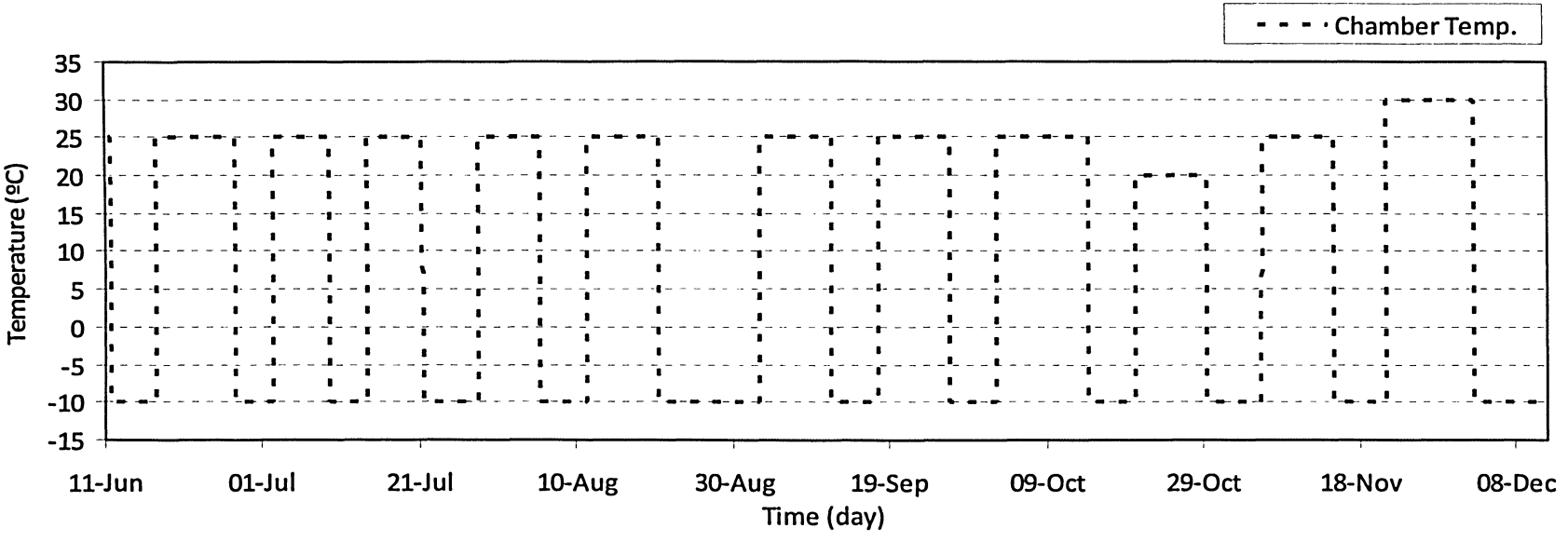

(b) Chamber temperature

Figure 7.3 (a) Total pore water pressure history data for model M1 and (b) chamber temperature

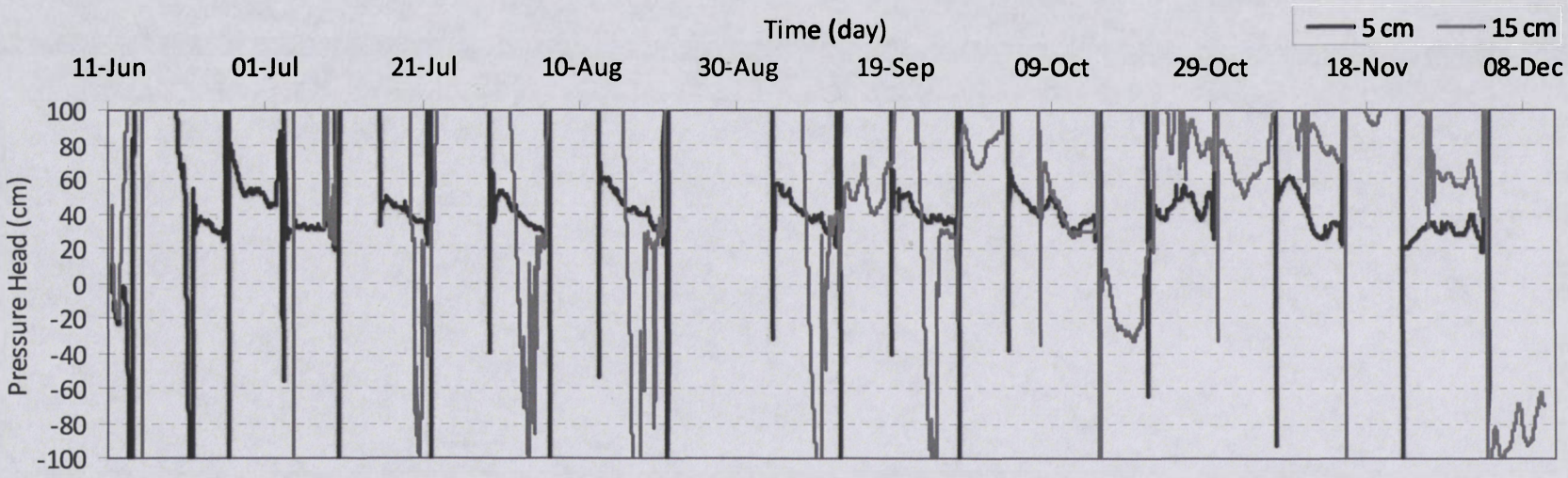

(a) Total pore water pressure history data for model M2 (smaller scale than Fig. 7.2)

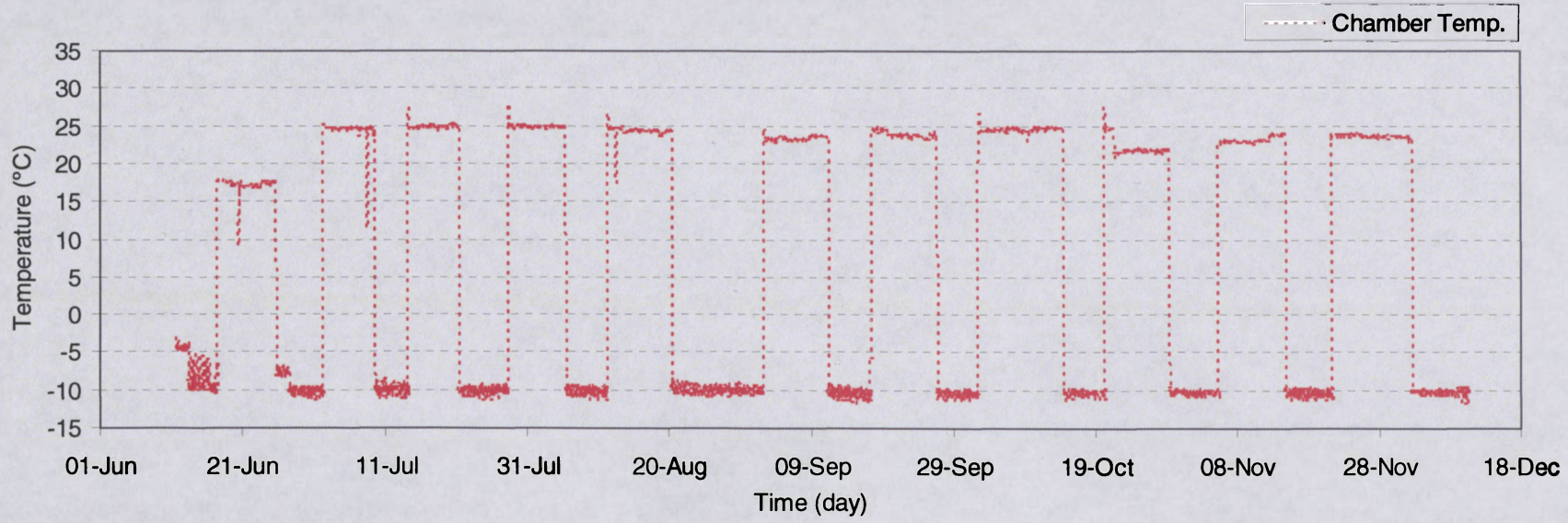

(b) Chamber temperature

Figure 7.4 (a) Total pore water pressure history data for model M2 and (b) chamber temperature

7.2 Theoretical values from Morgenstern and Nixon theory

The thaw consolidation theory developed by Morgenstern and Nixon (1971) estimates the excess pore water pressures generated in a thawing soil. The excess pore pressure under the soil's own weight can be estimated using Equation [2.3]. The excess pressures calculated from this equation is a function of the submerged unit weight of the soil (γ'), the depth at which the excess pore pressures are measured (x) and the thaw consolidation ratio (R). The submerged unit weight of the soil is 6.69 kN/m^3 which was calculated based on the bulk unit weight of the soil (16.5 kN/m^3) determined experimentally. The excess pore water pressures can be calculated for the two depths measured in the laboratory: 5 cm and 15 cm from the soil surface. Equation [2.4] is used to calculate the thaw consolidation ratio which is based on the coefficient of consolidation (c_v) and alpha (α) values.

The coefficient of consolidation was obtained from consolidation tests conducted on the same type of soil used for the freeze-thaw modeling. Figure 7.5 presents the coefficient of consolidation with respect to the load applied during the consolidation test. The black curve is a trend line whereas the dotted line is linear extrapolation.

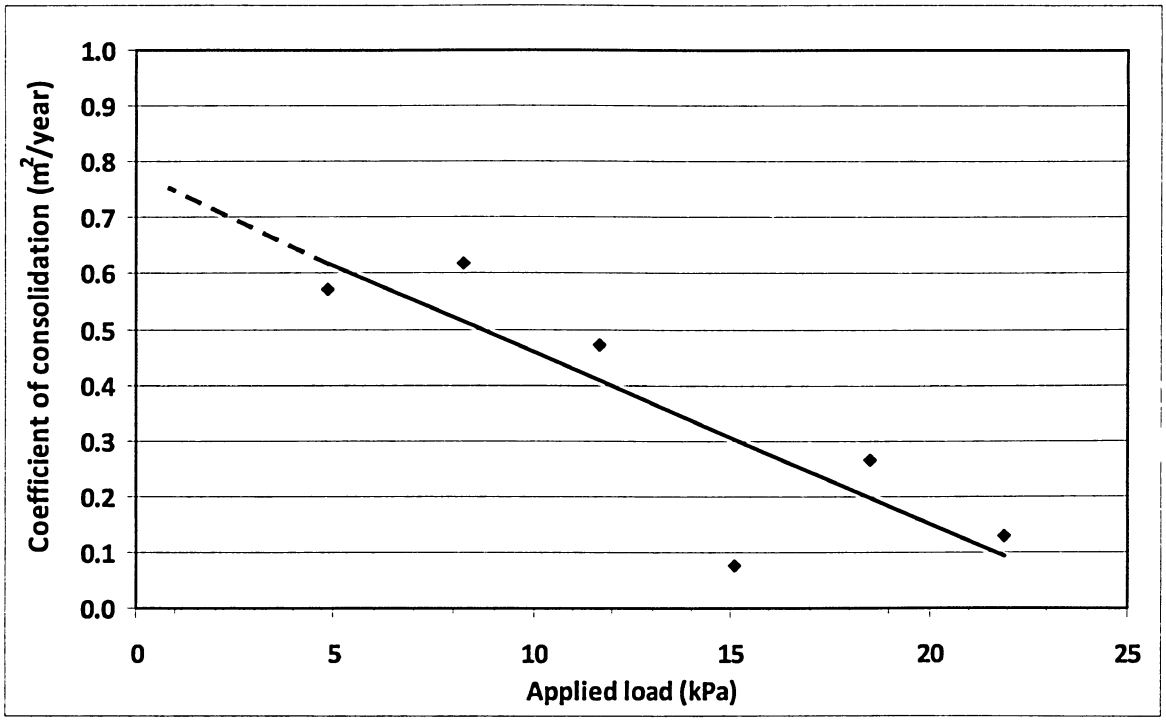

Figure 7.5 Laboratory results for coefficient of consolidation and linear extrapolation

At the sensor depths of 5 and 15 cm, the overburden pressures are calculated to be 0.8 and 2.5 kPa, respectively. For these pressure values, consolidation coefficients were not determined in the consolidation test. Therefore, the c_v values were established by linear extrapolations; 0.74 and 0.68 m^2/year at 5 and 15 cm depth respectively.

In this study, the thermal constant, α, is determined experimentally as discussed hereinafter.

Thermal constant

In order to determine the α value based on experimental results, the Neumann solution (Eq. 2.1) is used. With this equation, it is possible to determine α since the depth and time to reach the sensors are known. The temperature history presented in Figure 4.1 is used to determine the time required for the 0°C isotherm to reach the sensors at 5 and 15 cm depth. Tables 7.1 and 7.2 compare the α values calculated for a depth of 5 and 15 cm, respectively. For M1, three α values are determined – one for each thawing temperature.

Table 7.1 Calculation of α at 5 cm depth

Model	Cycle	Thawing temperature (°C)	X (m)	t (year)	α ($m/y^{1/2}$)
M1	2 to 8 and 10	25	0.05	0.00232	1.04
	9	20	0.05	0.00268	0.97
	11	30	0.05	0.00136	1.36
M2	2 to 11	25	0.05	0.00246	1.01

Table 7.2 Calculation of α at 15 cm depth

Model	Cycle	Thawing temperature (°C)	X (m)	t (year)	α ($m/y^{1/2}$)
M1	2 to 8 and 10	25	0.15	0.00797	1.67
	9	20	0.15	0.01067	1.45
	11	30	0.15	0.01068	1.81
M2	2 to 11	25	0.15	0.00974	1.53

It should be noted that α is dependant of several factors. In Nixon and McRoberts (1973), it is demonstrated that α is a function of seven variables: unfrozen thermal conductivity, frozen thermal conductivity, unfrozen volumetric heat capacity, frozen volumetric heat capacity, initial ground temperature, applied surface temperature and latent heat of soil. The more sophisticated function would lead to more accurate solutions. However, given that the key parameters are unknown and extensive studies of those parameters are beyond the scope of this research, the simple Neumann solution (Eq. 2.1) is used here. This is considered adequate for this study as the results are used to compare the thawing history and the pore pressures of the same model setup.

Theoretical excess pore pressures

Table 7.3 lists the calculated excess and total pore water pressures based on the thaw consolidation theory with respect to thawing temperature. The total water pressure is the

excess water pressure added to the hydrostatic water pressure assuming the free water table at the top surface of the soil column. Theoretically, excess water pressures are higher for higher thawed temperatures (and higher α values) which result in greater consolidation ratios.

Table 7.3 Excess and total pore water pressures

Model	Thawing temperature (°C)	Excess pore water pressure (cm)		Total pore water pressure (cm)	
		at 5 cm	at 15 cm	at 5 cm	at 15 cm
M1	20	1.32	6.22	6.32	21.22
	25	1.45	6.90	6.45	21.90
	30	1.89	7.24	6.89	22.24
M2	25	1.39	6.45	6.39	21.45

The pore pressures in Table 7.3 are discussed in the following subsection.

7.3 Discussions

Figures 7.6 – 7.49 show the total pore water pressure and temperature results compared to the corresponding overburden pressure and that from the Morgenstern and Nixon (1971) theory. In the charts, the experimental data is presented with solid lines and the total theoretical and overburden pressure values are depicted with dotted lines which are plotted throughout the thawed portion of the cycle. The figures consist of one freeze-thaw cycle and are configured as follows:

Figures 7.6 – 7.16: Model M1, Cycles 1 to 11 at 5 cm depth;
Figures 7.17 – 7.27: Model M1, Cycles 1 to 11 at 15 cm depth;
Figures 7.28 – 7.38: Model M2, Cycles 1 to 11 at 5 cm depth;
Figures 7.39 – 7.49: Model M2, Cycles 1 to 11 at 15 cm depth.

In M2 at 5 cm depth, it can be seen that the pore pressures are considerably higher than the predicted total pore pressure values (Table 7.3) and the overburden pressure. The exact reason is unknown, but the sensor data is questionable. In M2, the soil temperature

at 15 cm is very close to the melting point, therefore a significant amount of ice likely existed around the sensor. Thus, pressure data at this depth may be unreliable. It is impossible to compare data of M2 with the thaw consolidation theory. The following discussions are therefore focussed on M1 results.

In model M1 at 5 cm depth, pore water pressures often exceed the overburden pressure (Fig. 7.6-12), but are sometimes close to it (Fig. 7.13-15). At this depth, only the data from Cycle 11 (Fig. 7.16) is close to the theoretical total pore pressure. In M1 at 15 cm depth, some measured thawed readings are close to theoretical results (Fig. 7.17-7.19) while others exceed the overburden pressure.

It should be noted that the thaw consolidation theory assumes a free water table at the top surface of the soil column. However, this is probably not the case in the current experiment. There is most likely an unsaturated zone located in the middle of the active layer due to moisture migration. Furthermore, the theory assumes that ice/water phase change occurs at a given moment and depth, while in reality there is a "zero curtain" or 0°C zone where water is expelled gradually. These discrepancies make it difficult to compare theoretical values and measured data.

During phase change from ice to water, the pressure sensors registered dramatic changes. The changes smoothed out with temperature increase to well above 0°C. Under ideal conditions, the thawed pore water pressure at a given depth should not exceed the overburden pressure at that depth. However, this has not been the case for most of the M1 data and all the data for M2. This could be due to several reasons. For example, the depth of the sensors may not have been at exactly 5 cm or 15 cm due to possible sensor shifting during soil placement. The sensor depth could have been further distorted by soil heaving and settlement during free-thaw cycles. The excessive pressure during freezing may have some residual effect on the sensors for subsequent measurements of low pressures under thawing conditions. Nonetheless, pore water pressure change at the thaw front is a very complex behaviour. This is due to the time lapse occurring during phase change from pore ice to pore water. This is demonstrated by pore pressure fluctuations at

the beginning of almost all thaw cycles. Although the sensors did measure some pressure values close to theoretical values, e.g. Figures 7.16-19, it cannot be concluded that this test confirmed the theory.

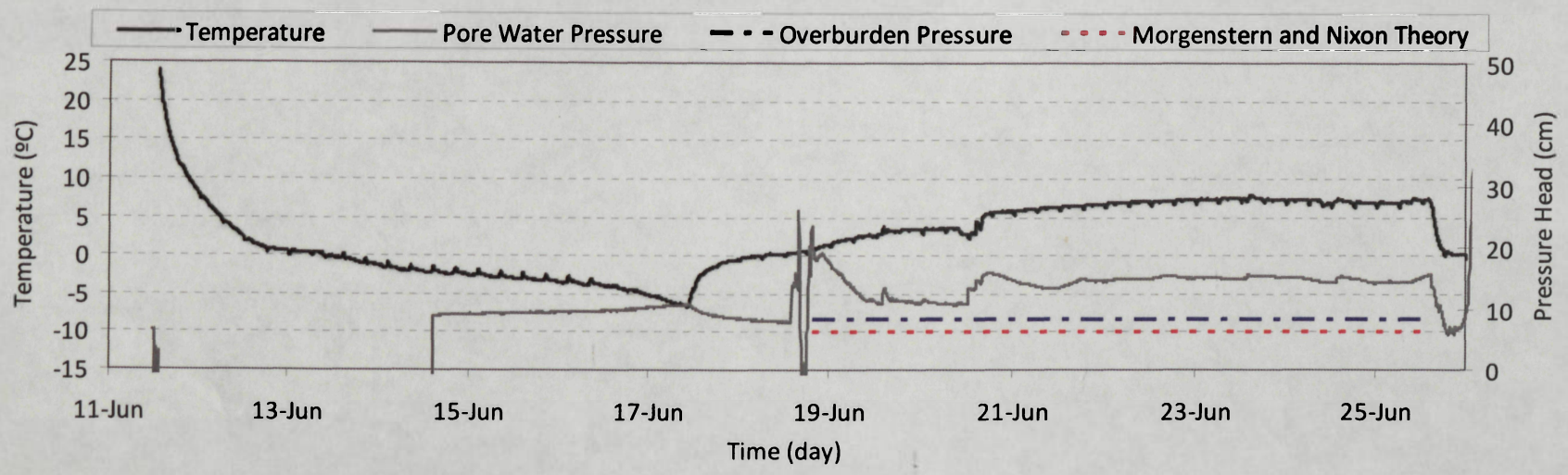

Figure 7.6 Total pore water pressure history, model M1: Cycle 1, depth 5 cm

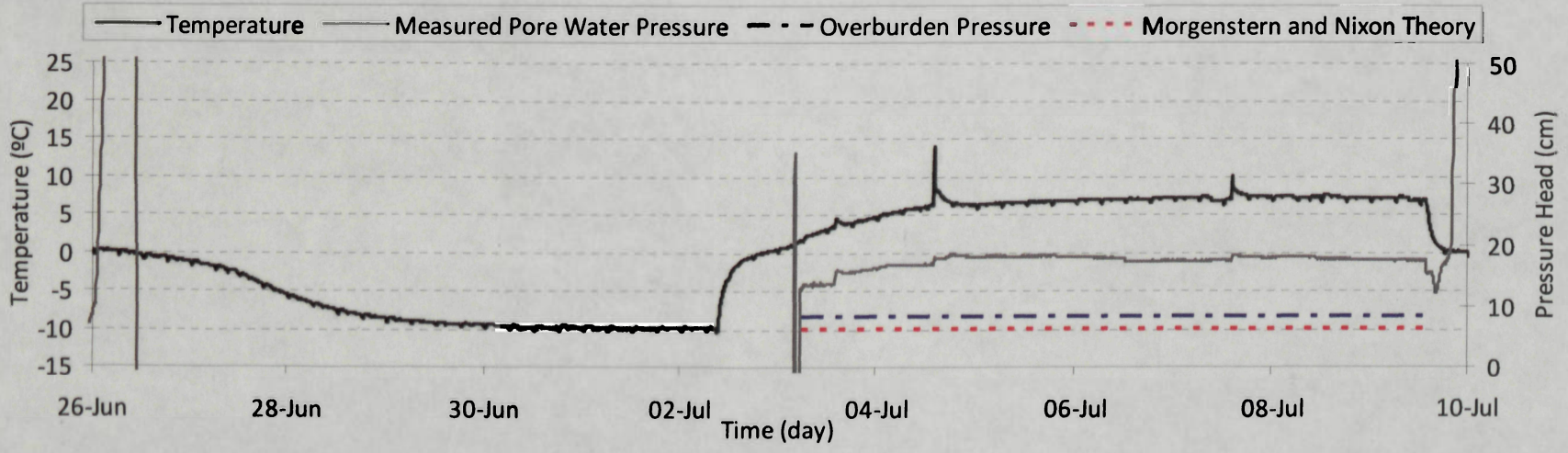

Figure 7.7 Total pore water pressure history, model M1: Cycle 2, depth 5 cm

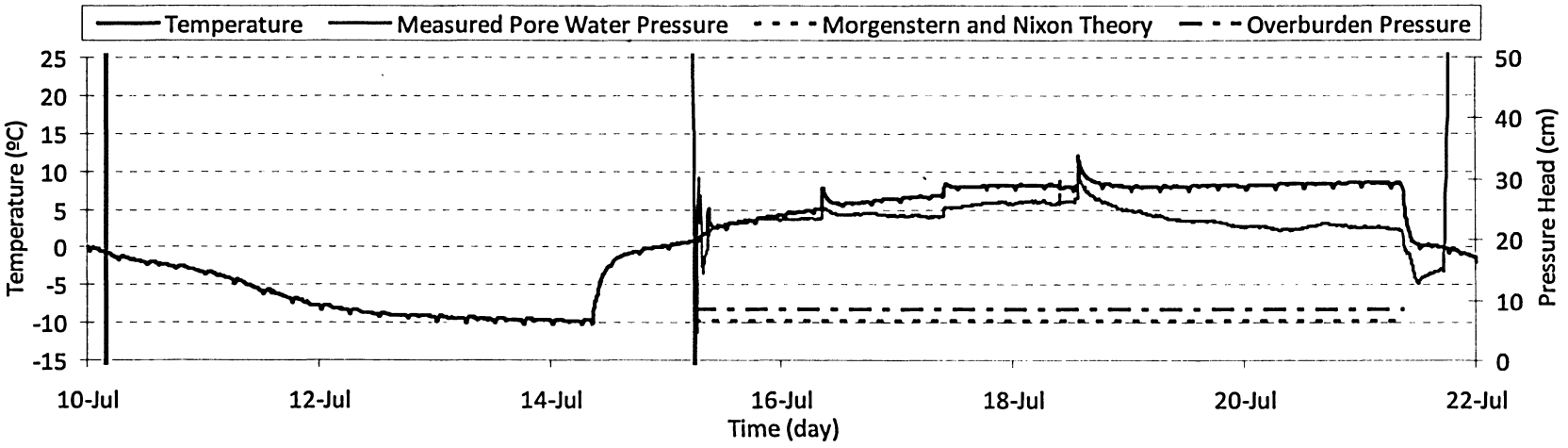

Figure 7.8 Total pore water pressure history, model M1: Cycle 3, depth 5 cm

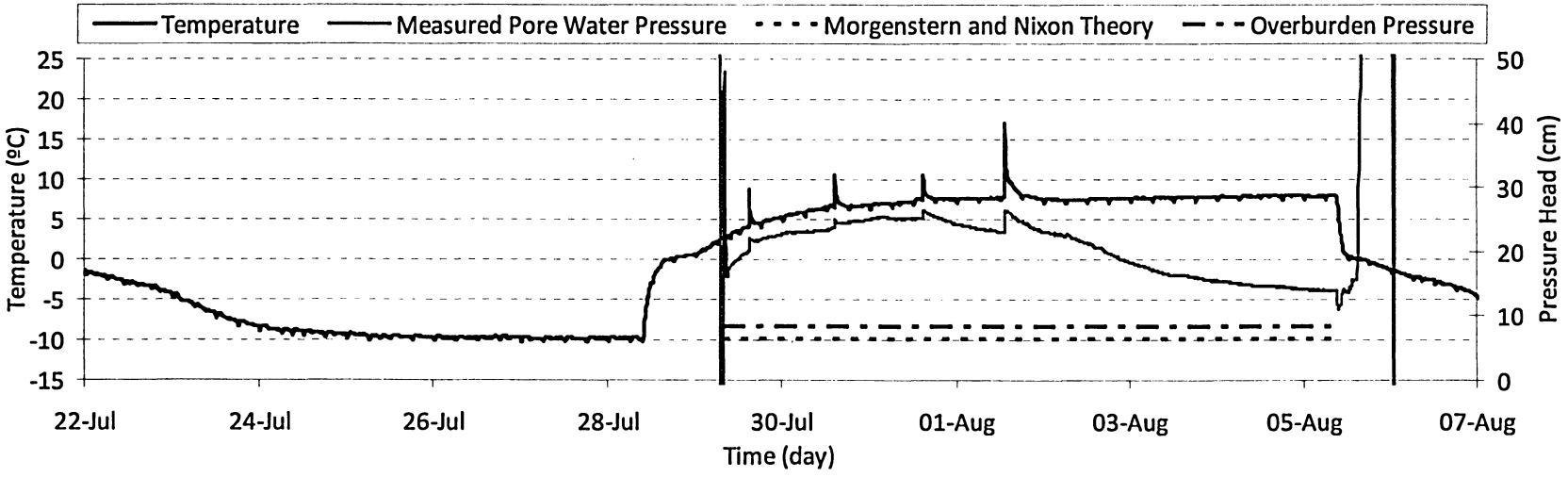

Figure 7.9 Total pore water pressure history, model M1: Cycle 4, depth 5 cm

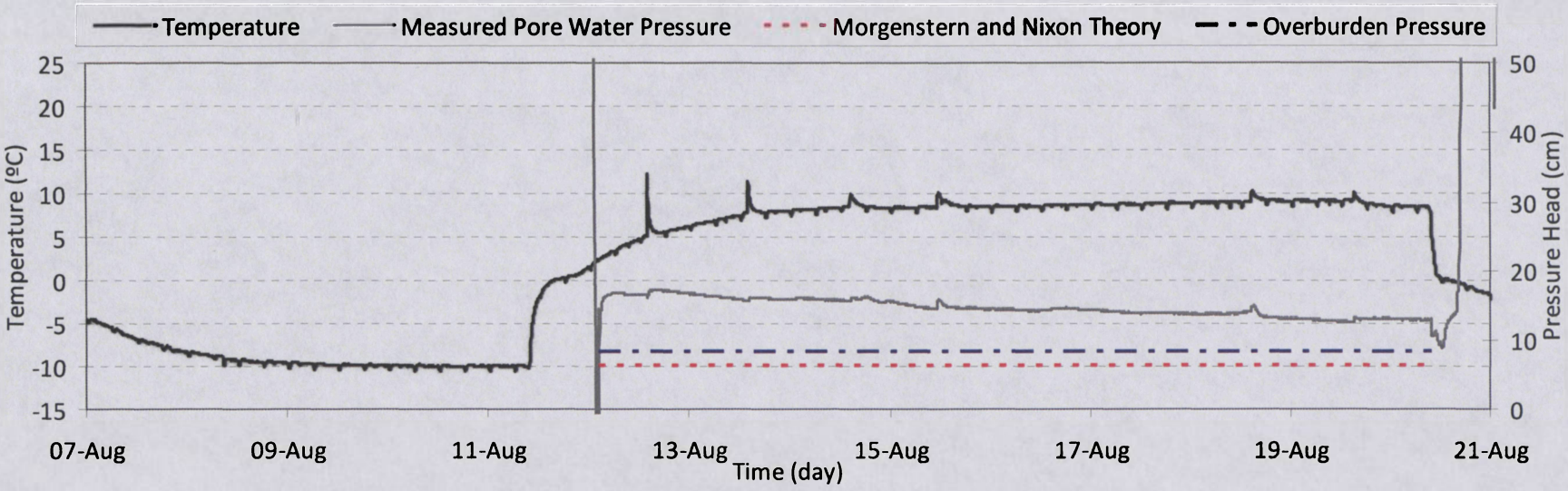

Figure 7.10 Total pore water pressure history, model M1: Cycle 5, depth 5 cm

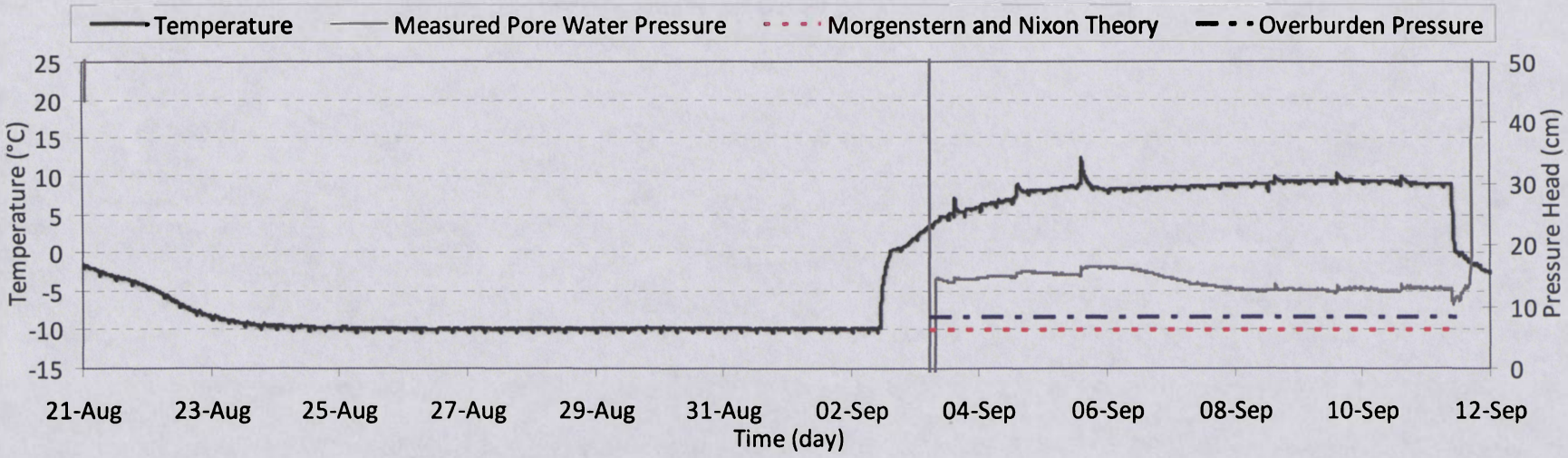

Figure 7.11 Total pore water pressure history, model M1: Cycle 6, depth 5 cm

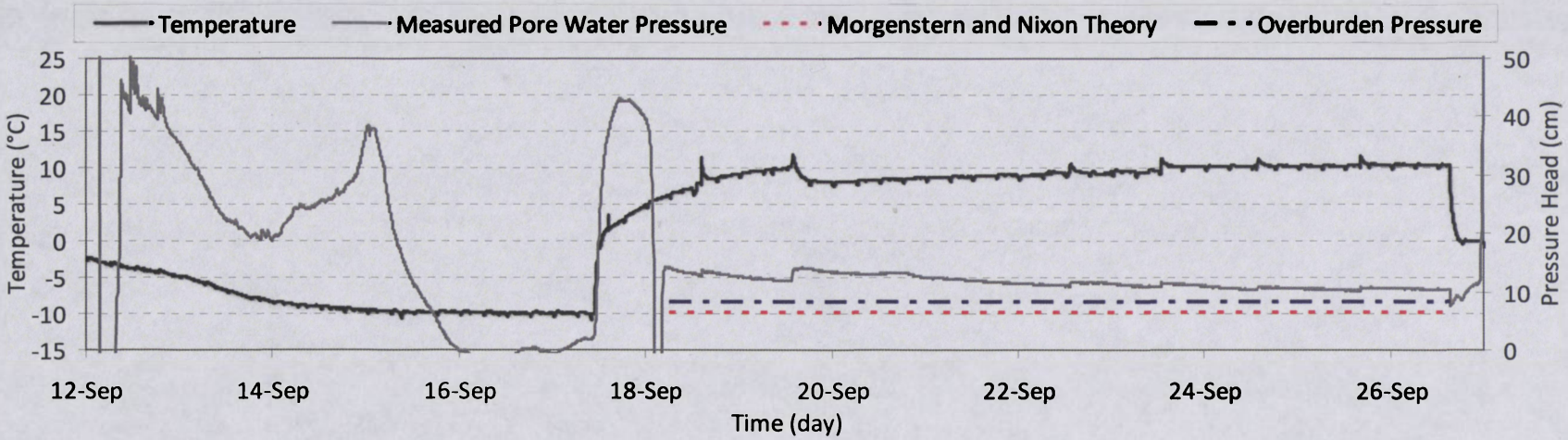

Figure 7.12 Total pore water pressure history, model M1: Cycle 7, depth 5 cm

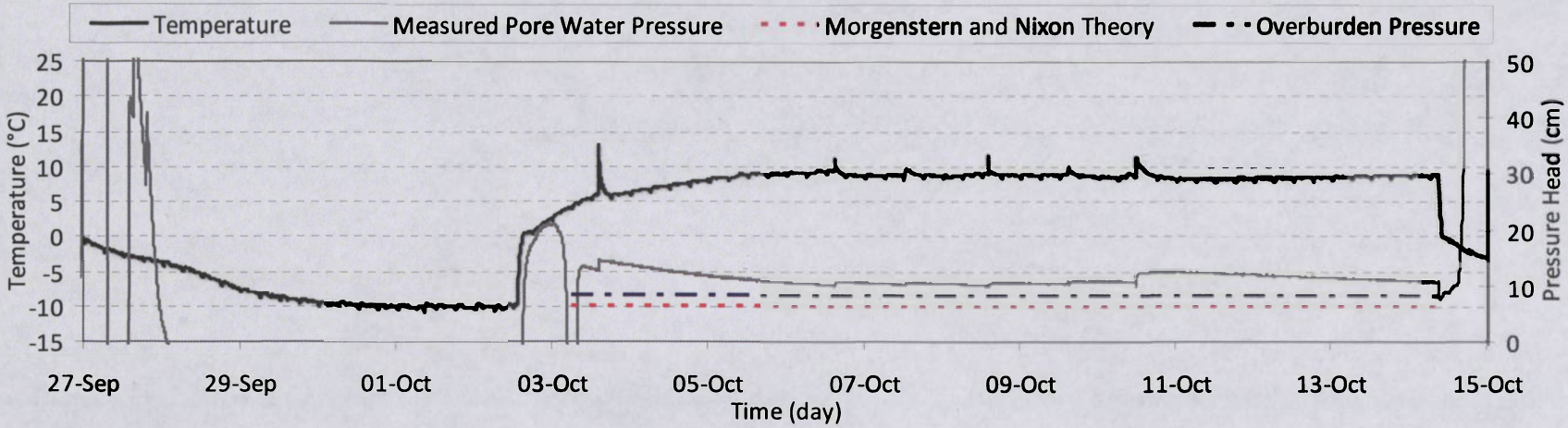

Figure 7.13 Total pore water pressure history, model M1: Cycle 8, depth 5 cm

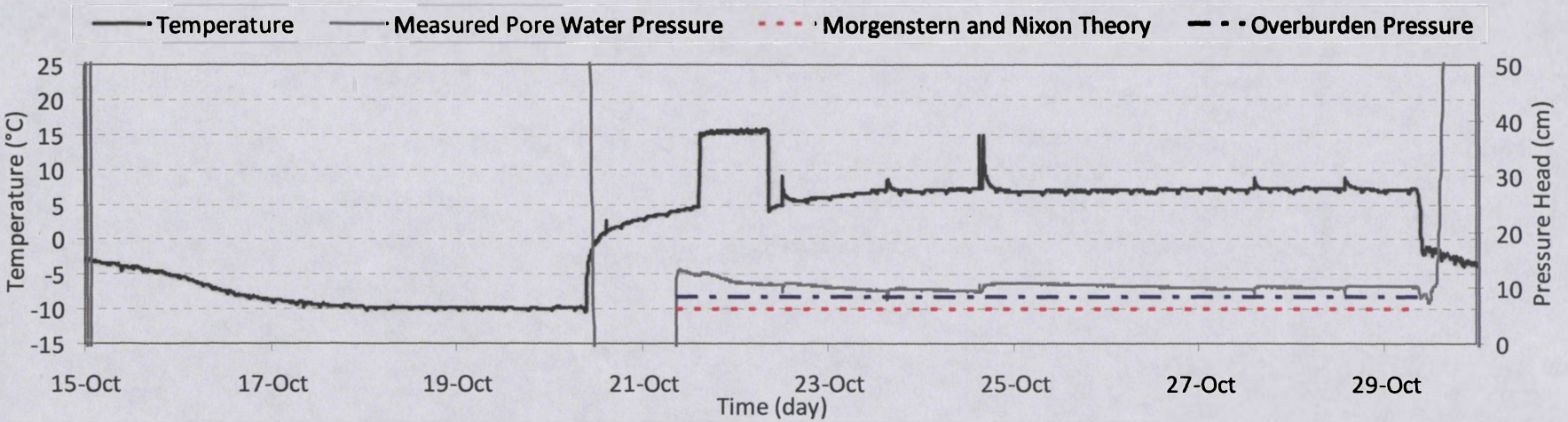

Figure 7.14 Total pore water pressure history, model M1: Cycle 9, depth 5 cm

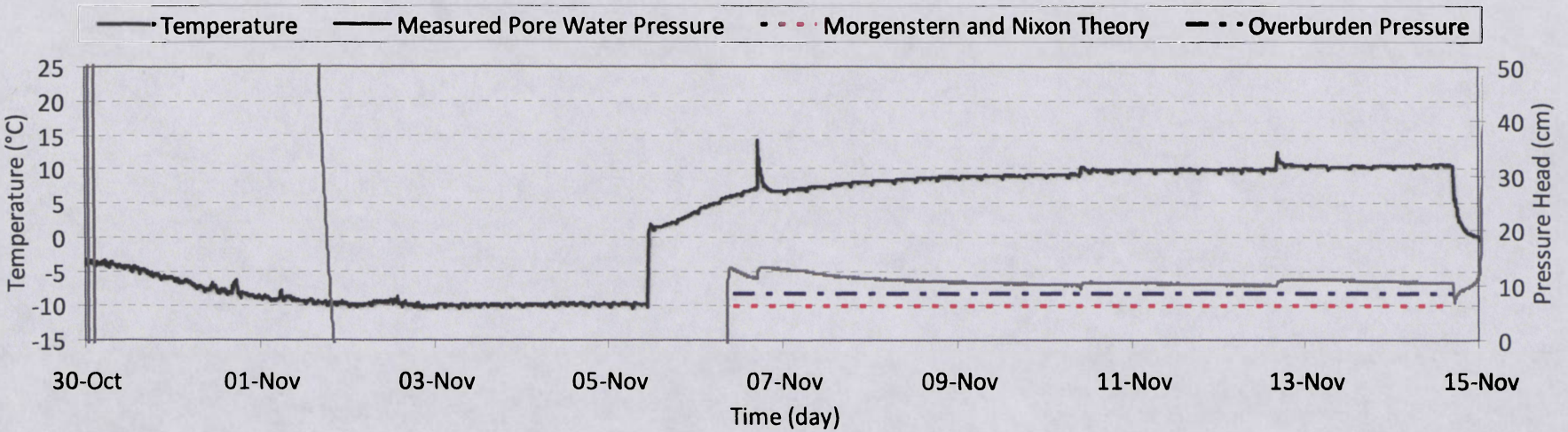

Figure 7.15 Total pore water pressure history, model M1: Cycle 10, depth 5 cm

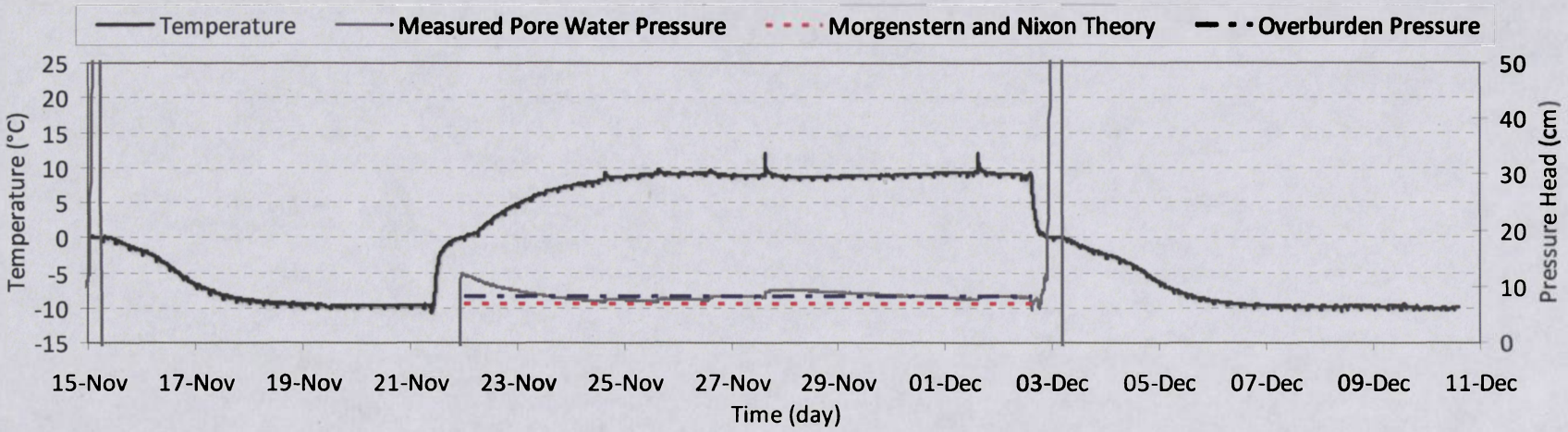

Figure 7.16 Total pore water pressure history, model M1: Cycle 11, depth 5 cm

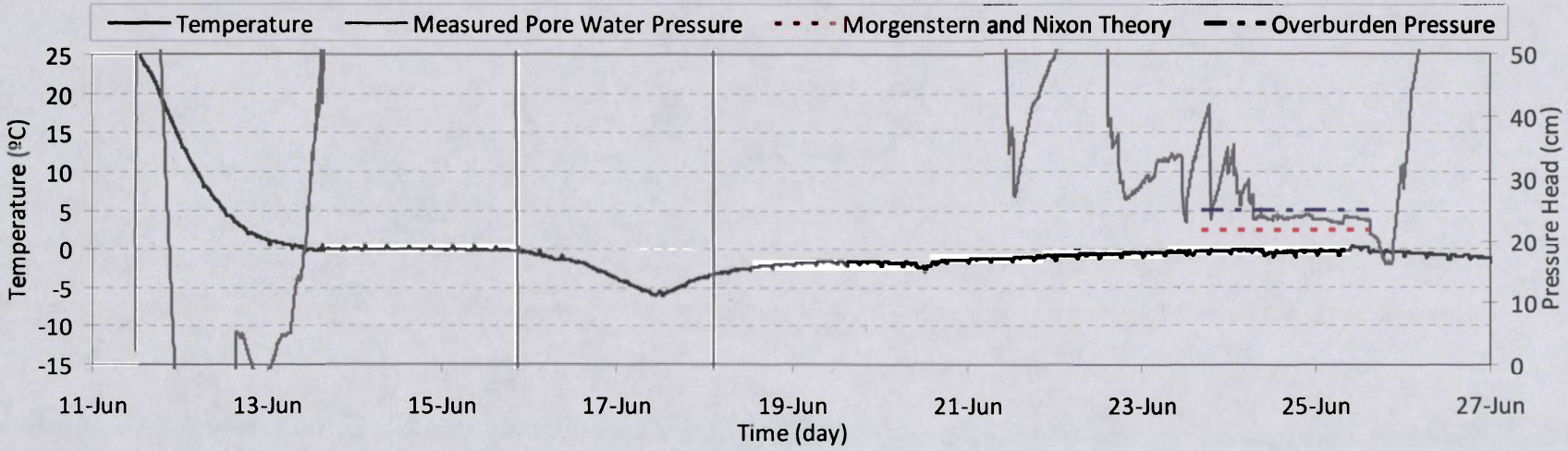

Figure 7.17 Total pore water pressure history, model M1: Cycle 1, depth 15 cm

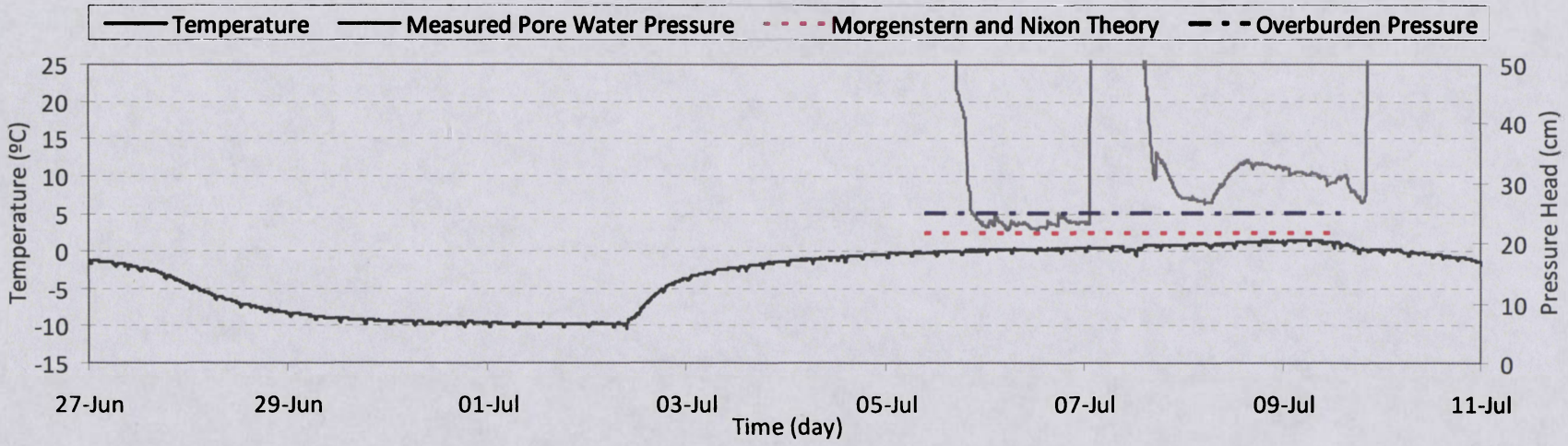

Figure 7.18 Total pore water pressure history, model M1, Cycle 2, depth 15 cm

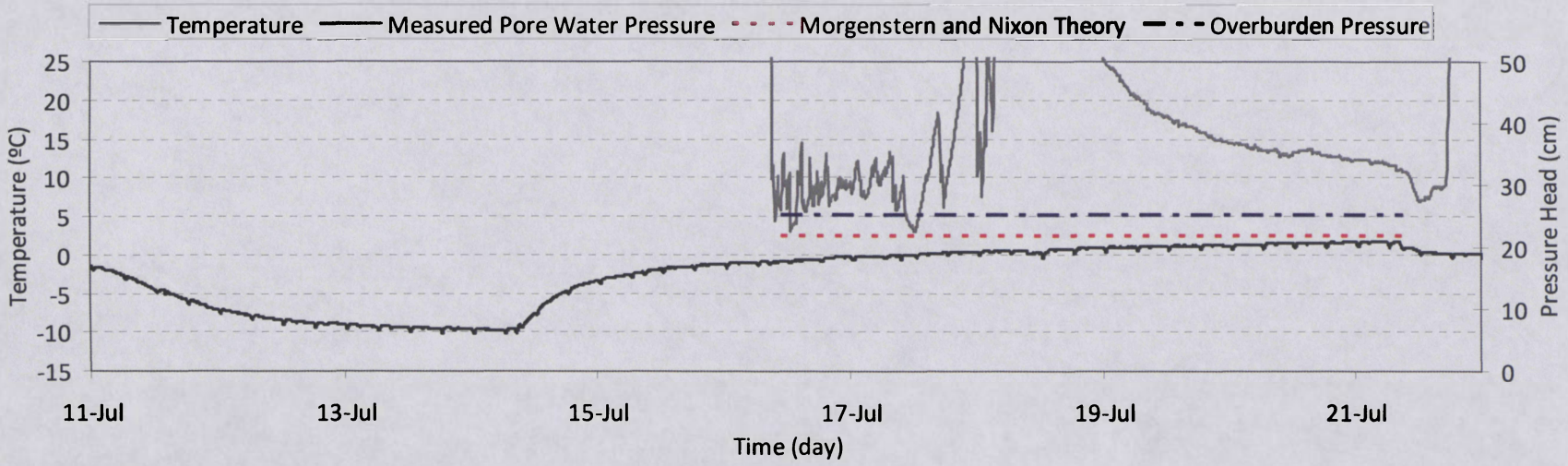

Figure 7.19 Total pore water pressure history, model M1: Cycle 3, depth 15 cm

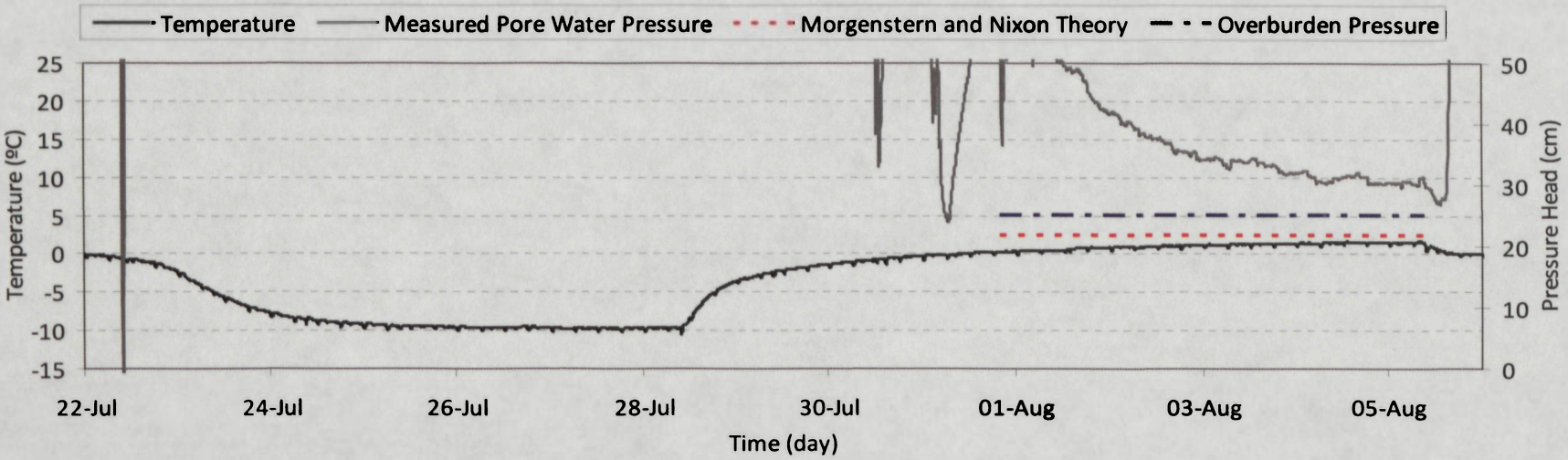

Figure 7.20 Total pore water pressure history, model M1: Cycle 4, depth 15 cm

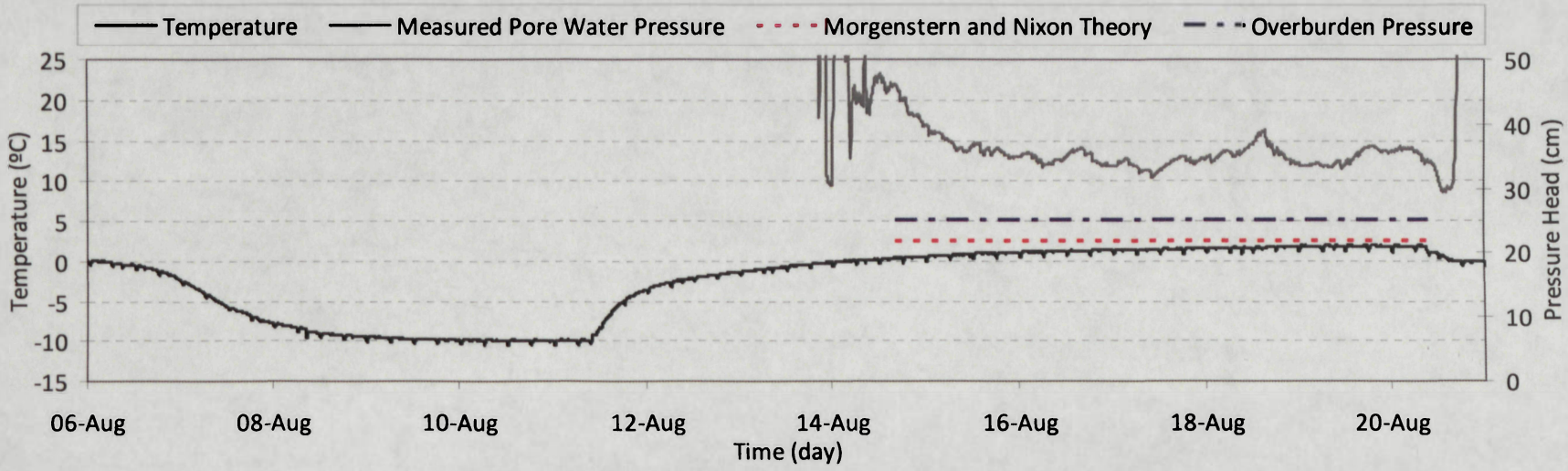

Figure 7.21 Total pore water pressure history, model M1: Cycle 5, depth 15 cm

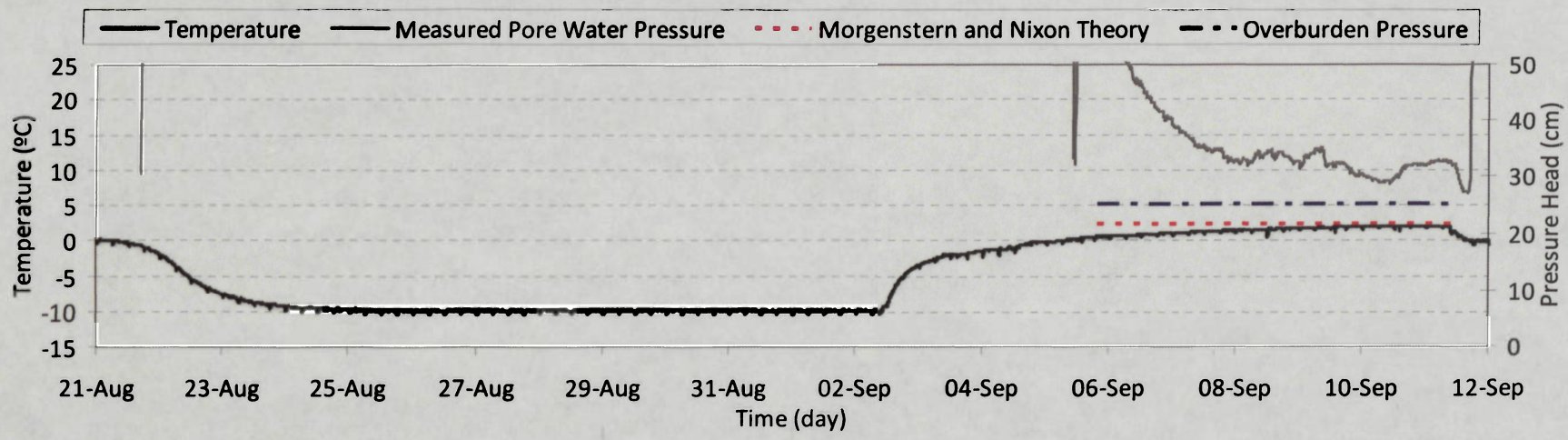

Figure 7.22 Total pore water pressure history, model M1: Cycle 6, depth 15 cm

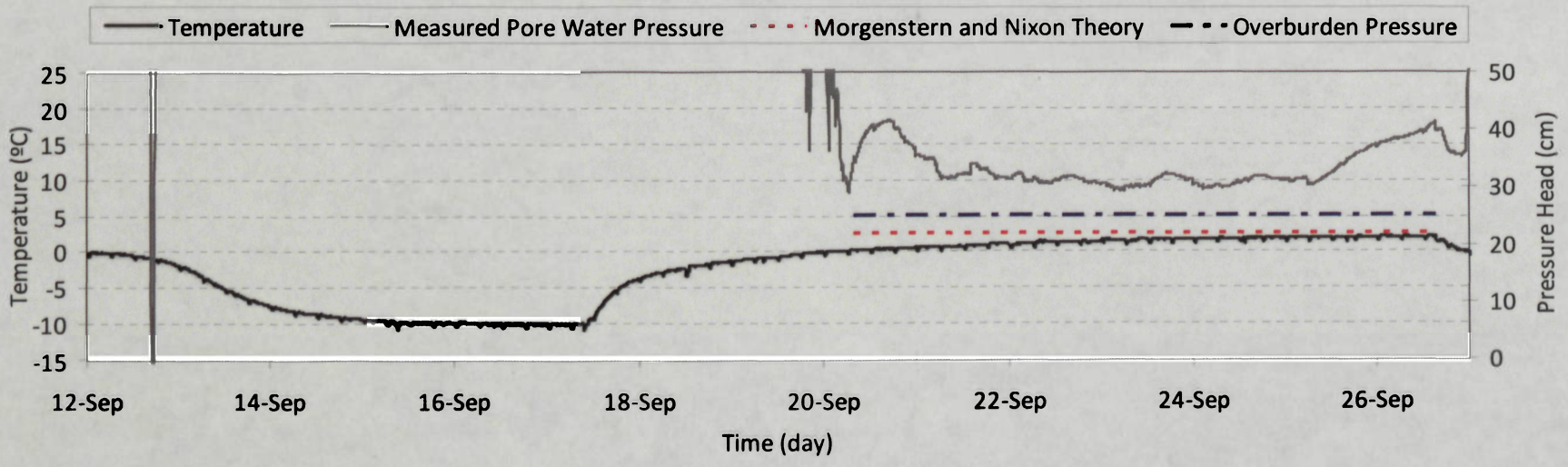

Figure 7.23 **Total** pore water **pressure** history, **model** M1: Cycle 7, depth **15 cm**

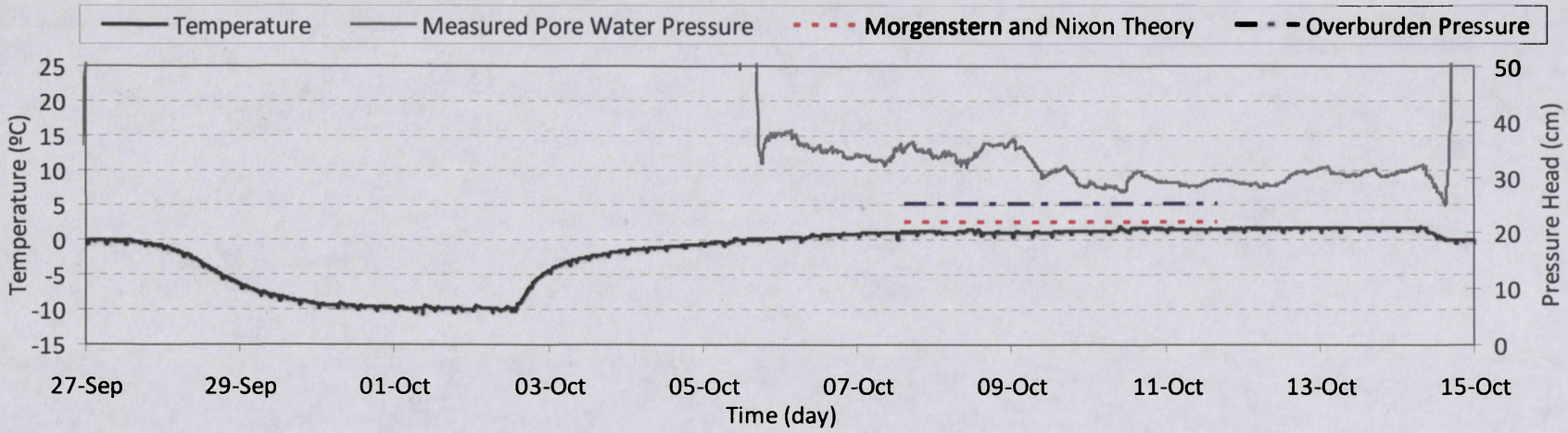

Figure 7.24 Total pore water pressure history, model M1: Cycle 8, depth 15 cm

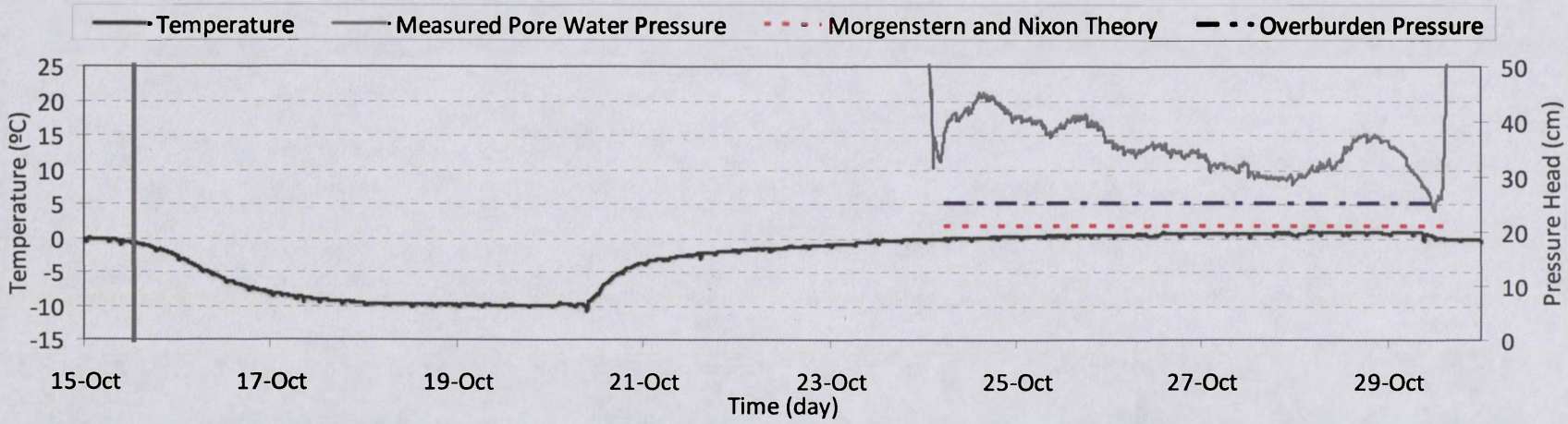

Figure 7.25 Total pore water pressure history, model M1: Cycle 9, depth 15 cm

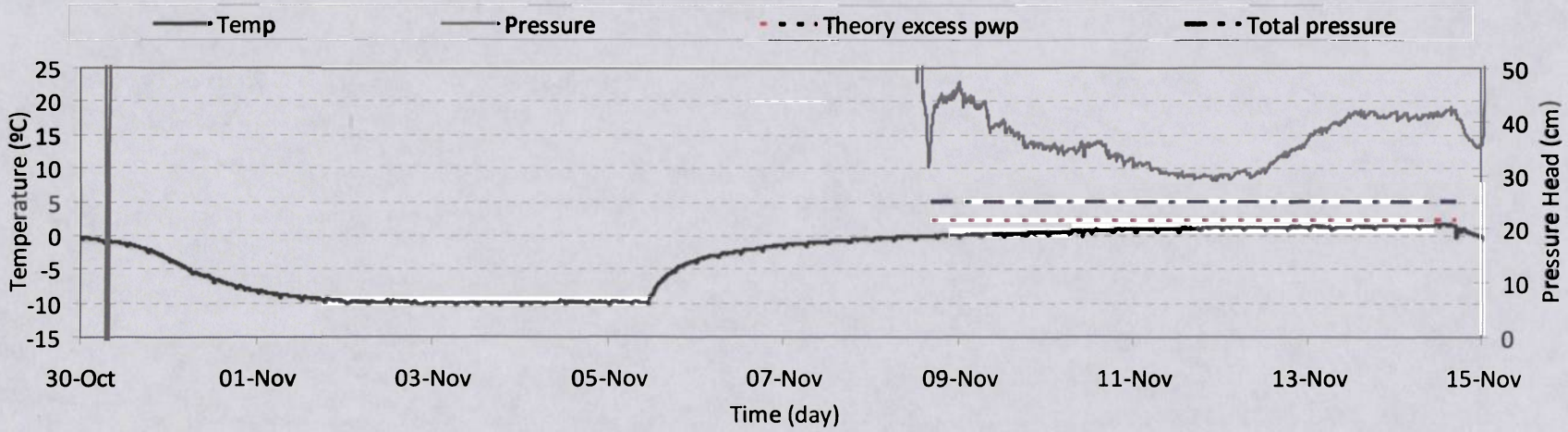

Figure 7.26 Total pore water pressure history, model M1: Cycle 10, depth 15 cm

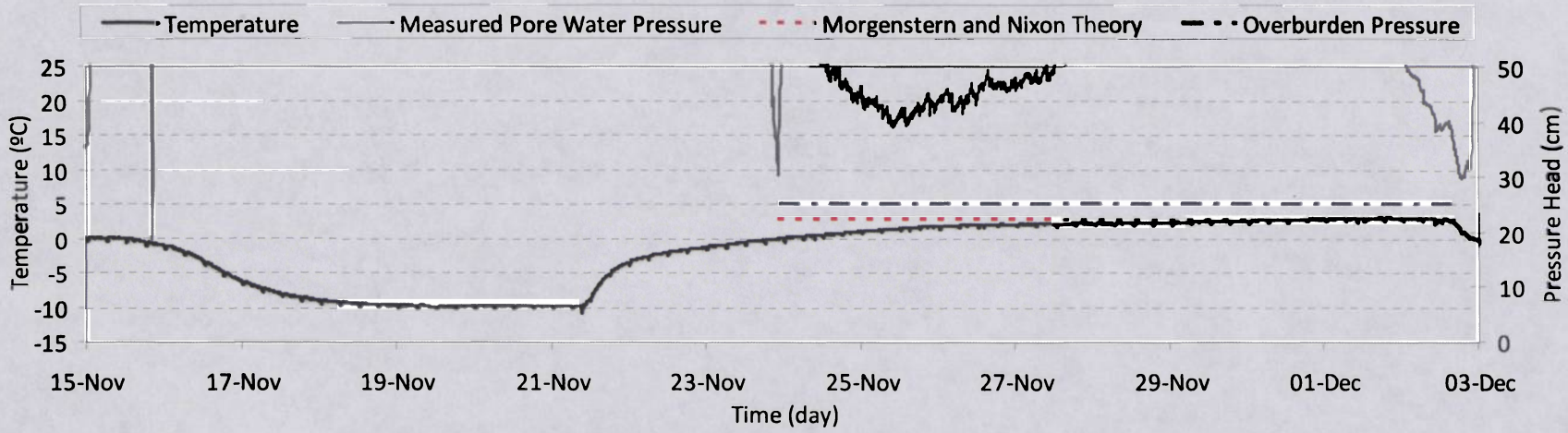

Figure 7.27 Total pore water pressure history, model M1: Cycle 11, depth 15 cm

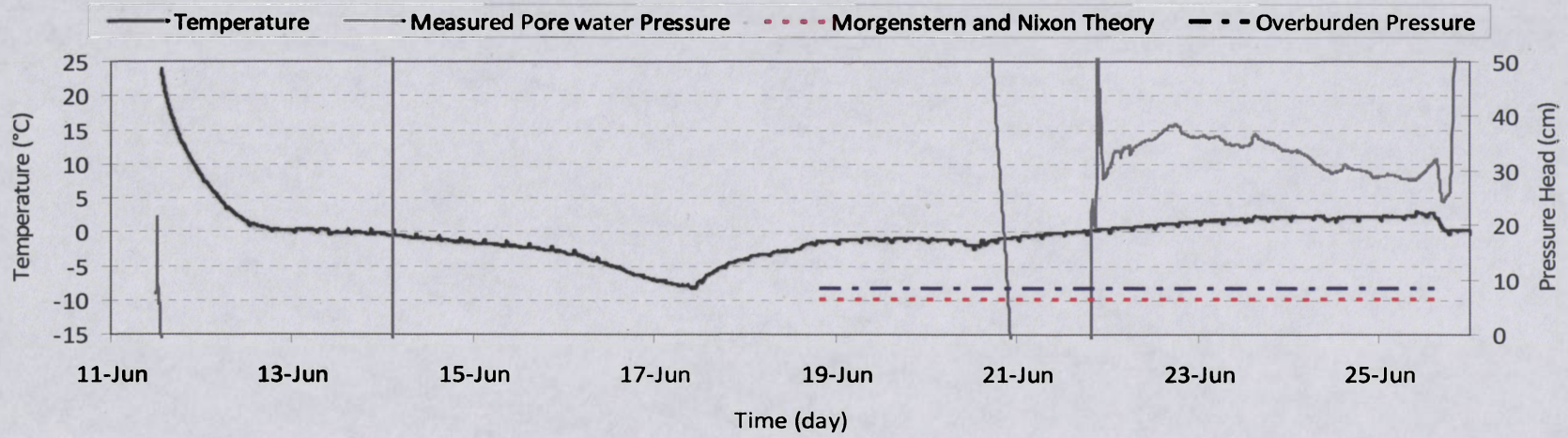

Figure 7.28 Total pore water pressure history, model M2: Cycle 1, depth 5 cm

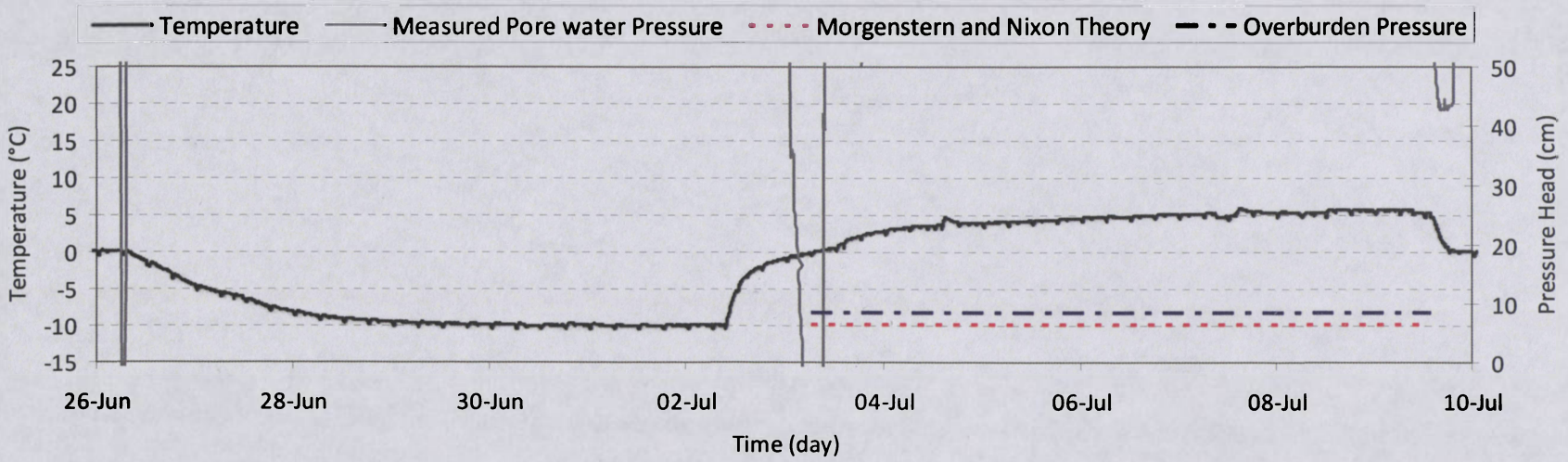

Figure 7.29 Total pore water pressure history, model M2: Cycle 2, depth 5 cm

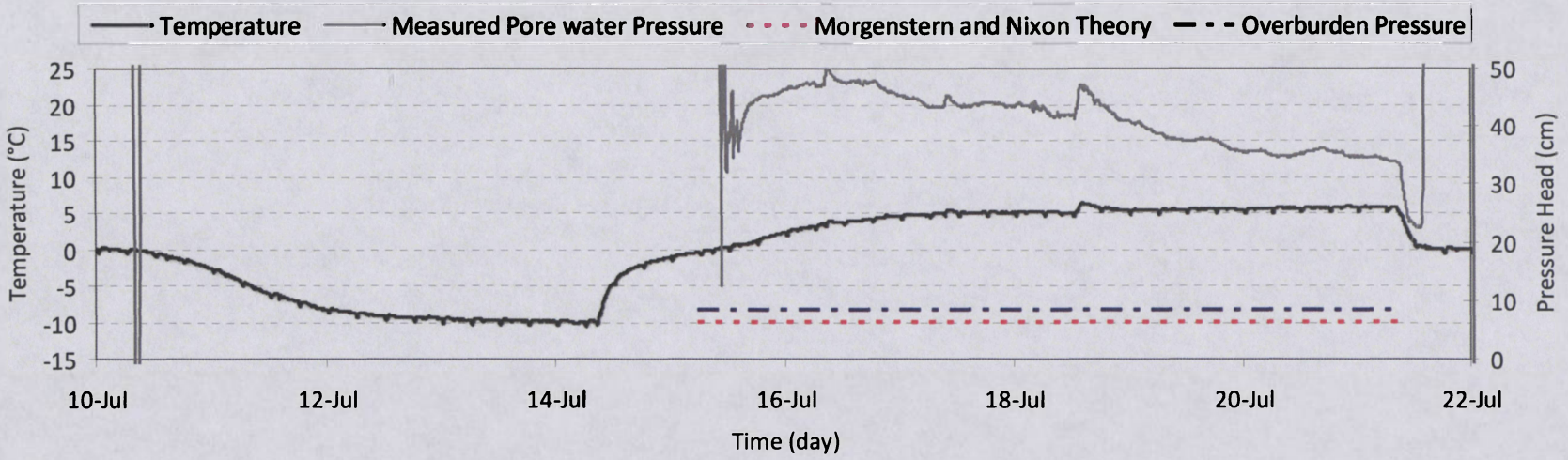

Figure 7.30 Total pore water pressure history, model M2: Cycle 3, depth 5 cm

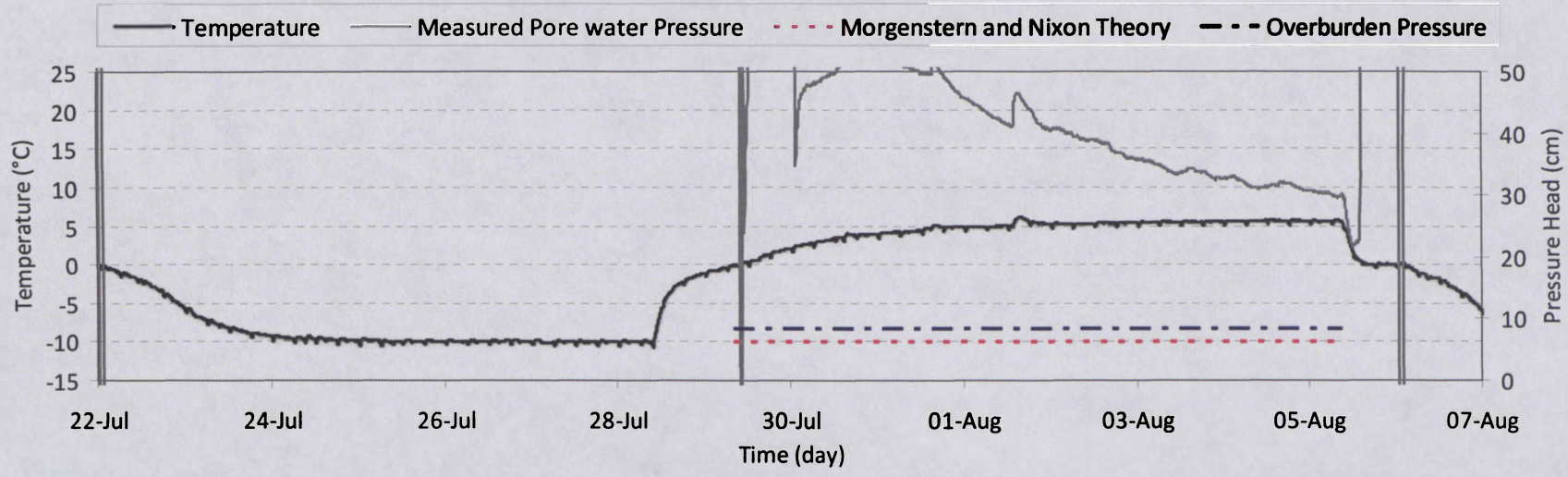

Figure 7.31 Total pore water pressure history, model M2: Cycle 4, depth 5 cm

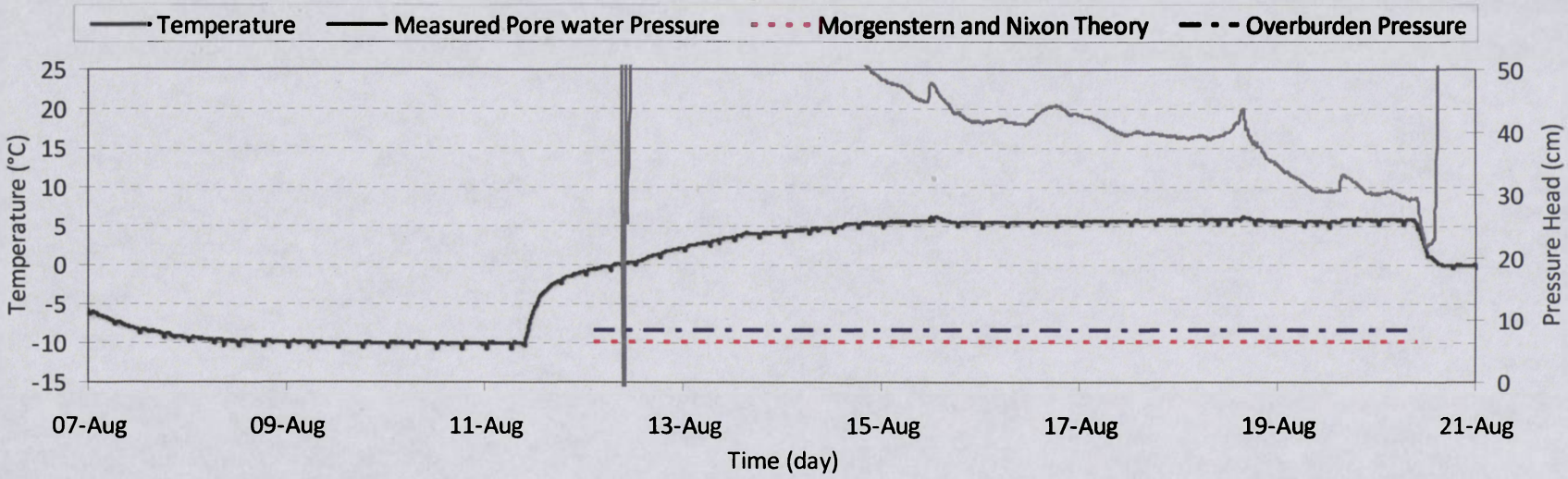

Figure 7.32 Total pore water pressure history, model M2: Cycle 5, depth 5 cm

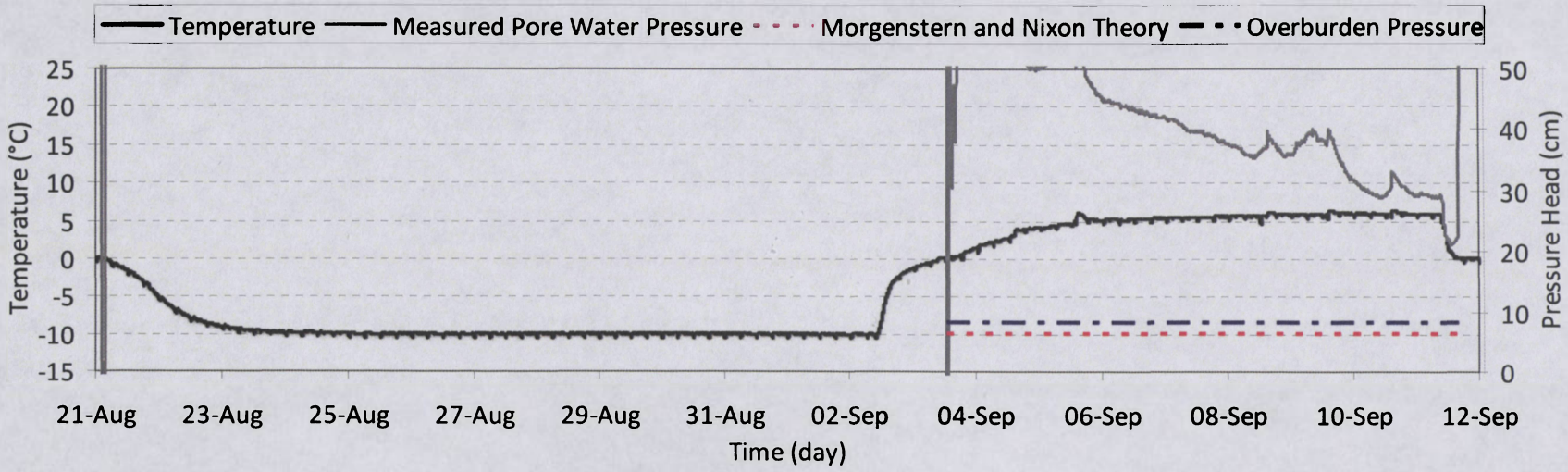

Figure 7.33 Total pore water pressure history, model M2: Cycle 6, depth 5 cm

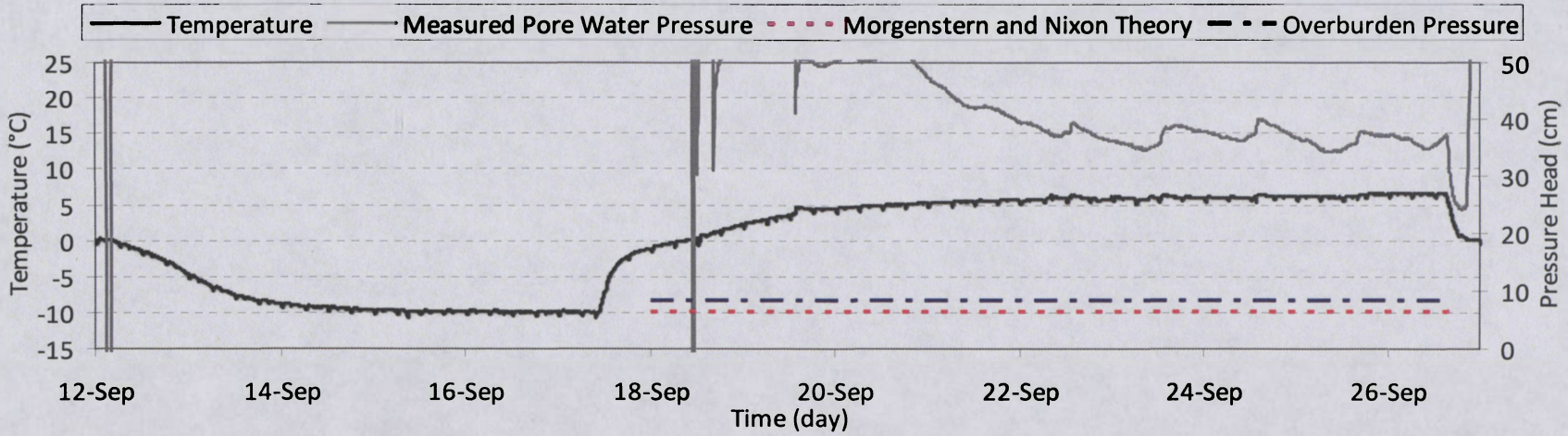

Figure 7.34 Total pore water pressure history, model M2: Cycle 7, depth 5 cm

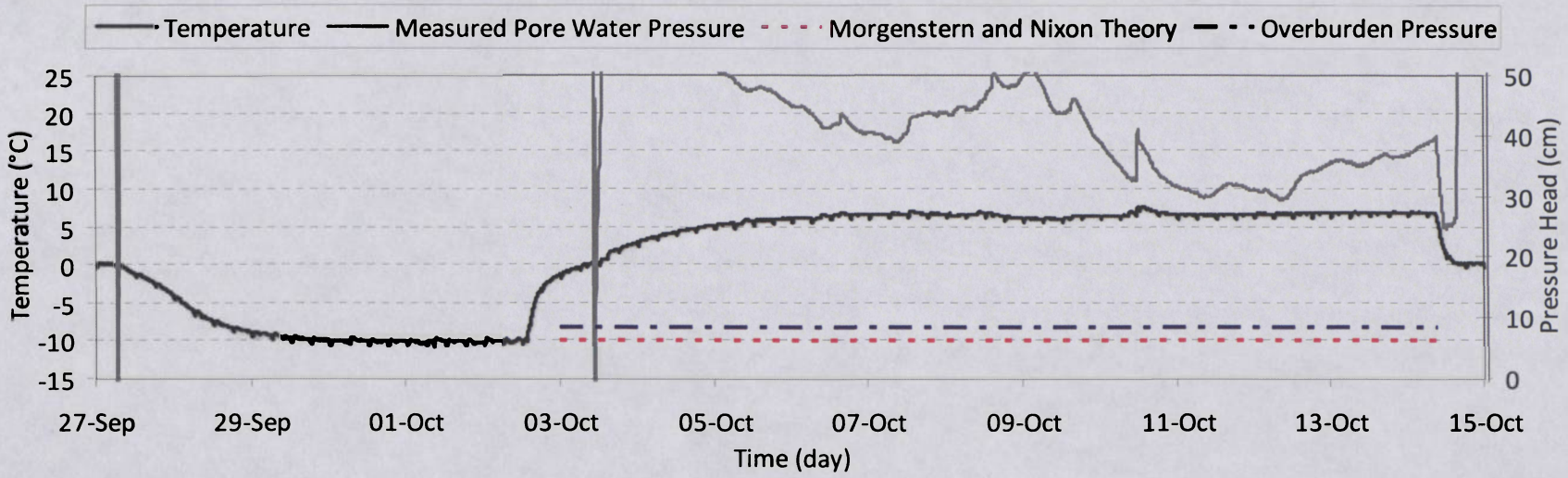

Figure 7.35 Total pore water pressure history, model M2: Cycle 8, depth 5 cm

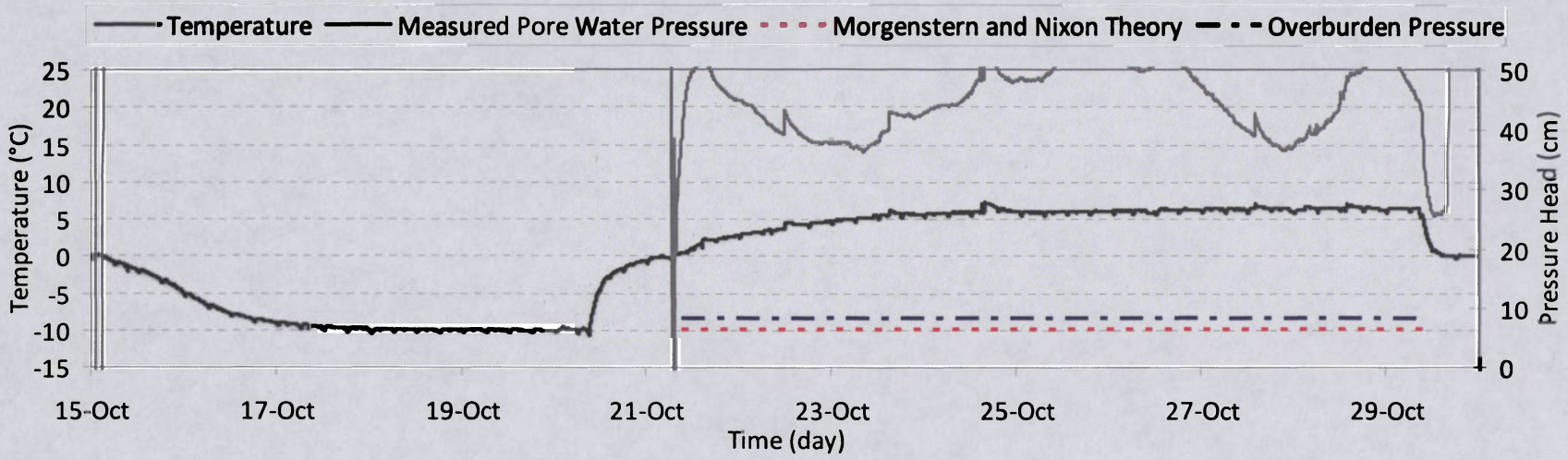

Figure 7.36 Total pore water pressure history, model M2: Cycle 9, depth 5 cm

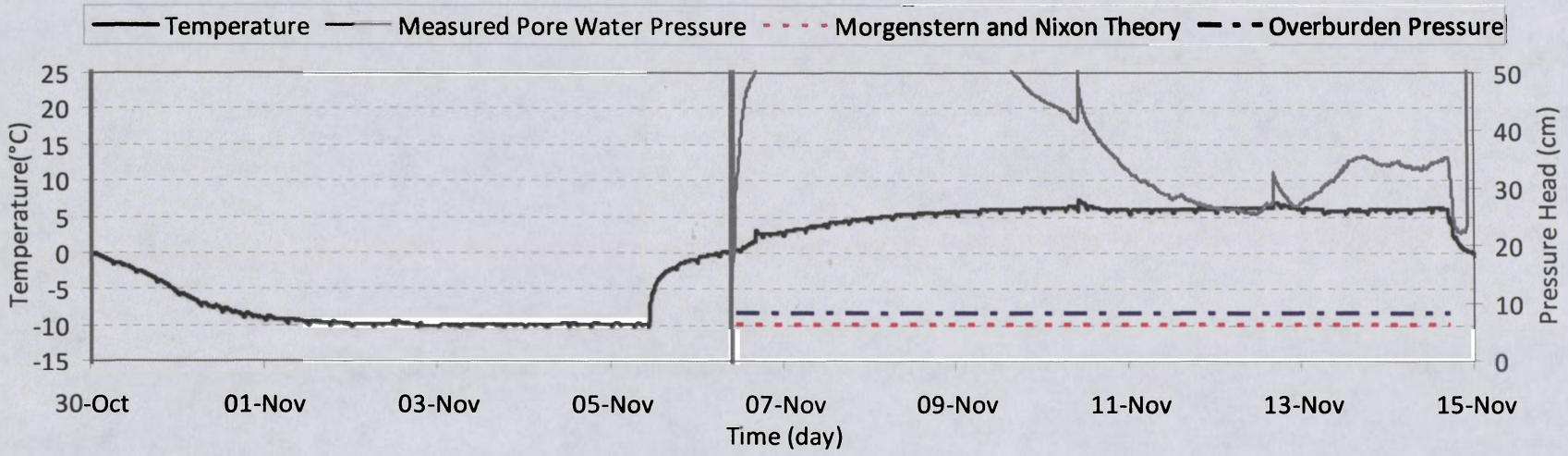

Figure 7.37 Total pore water pressure history, model M2: Cycle 10, depth 5 cm

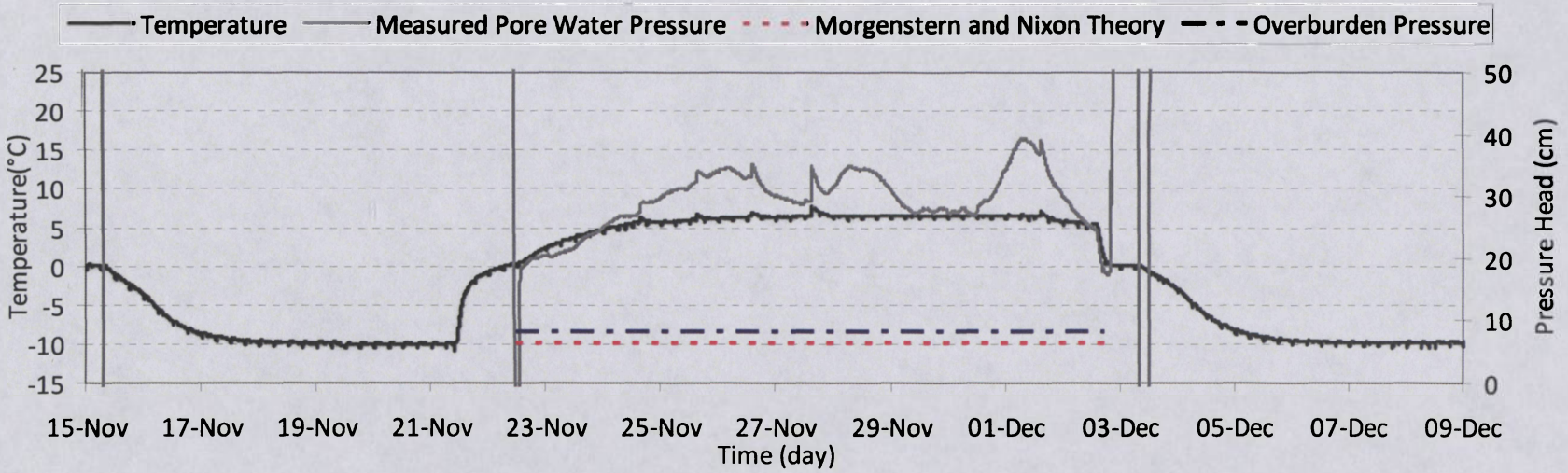

Figure 7.38 Total pore water pressure history, model M2: Cycle 11, depth 5 cm

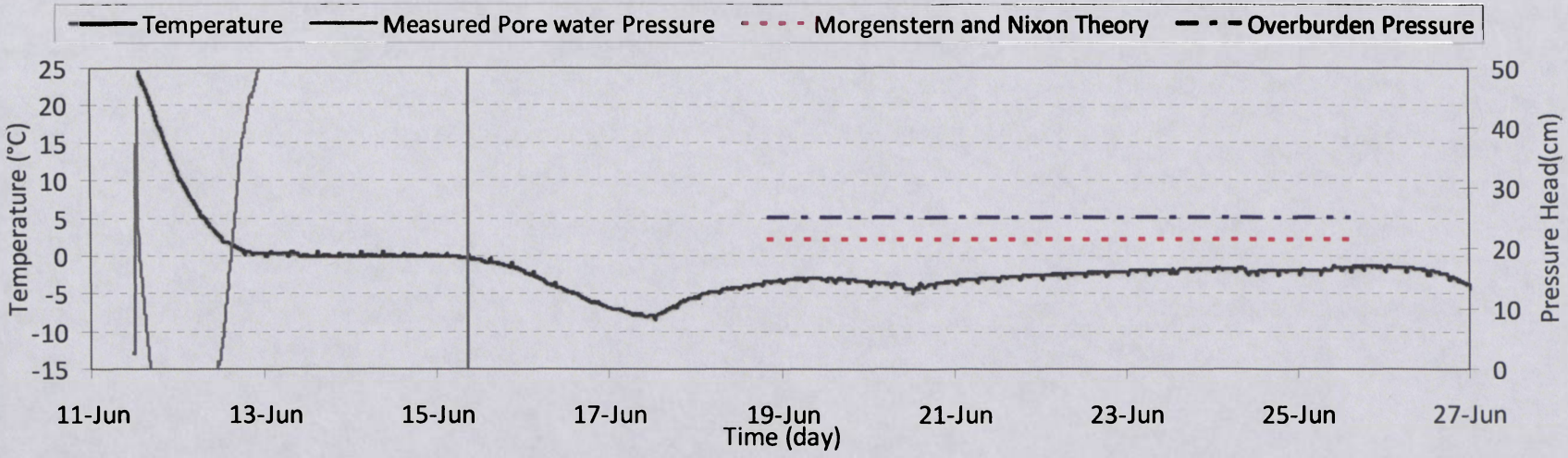

Figure 7.39 Total pore water pressure history, model M2: Cycle 1, depth 15 cm

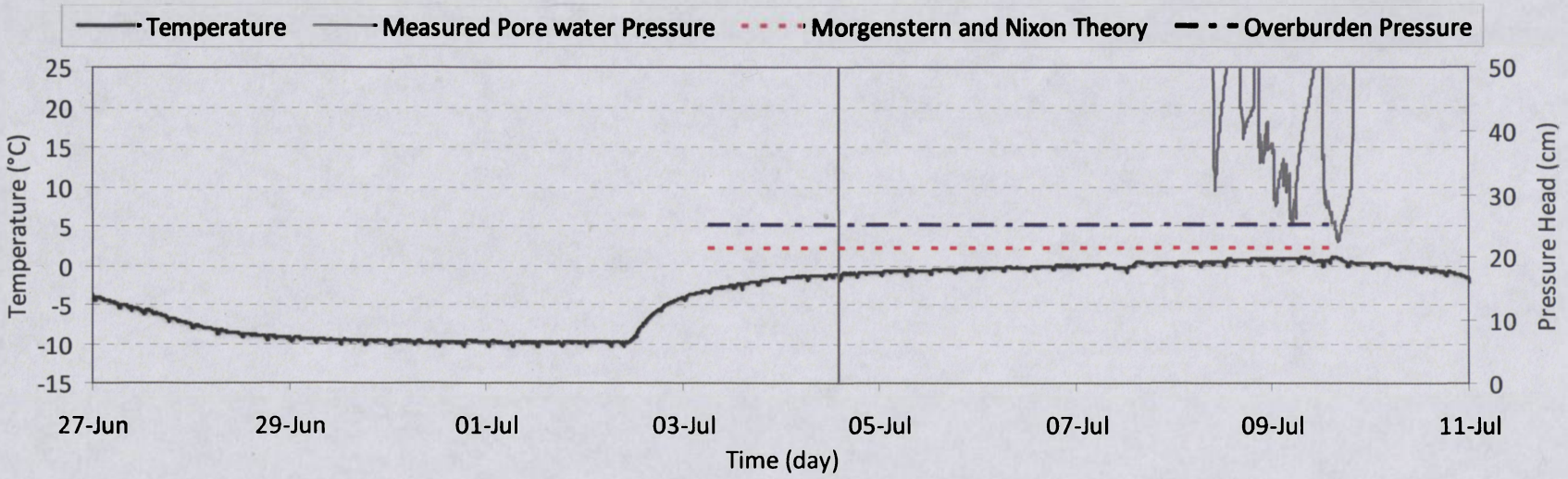

Figure 7.40 Total pore water pressure history, model M2: Cycle 2, depth 15 cm

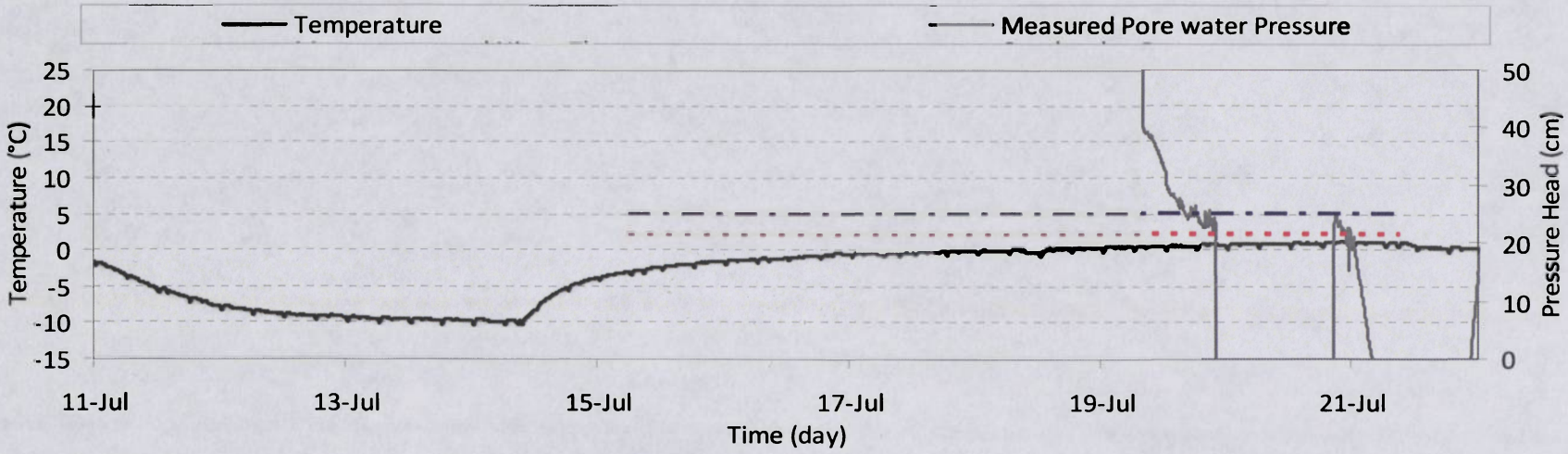

Figure 7.41 Total pore water pressure history, model M2: Cycle 3, depth 15 cm

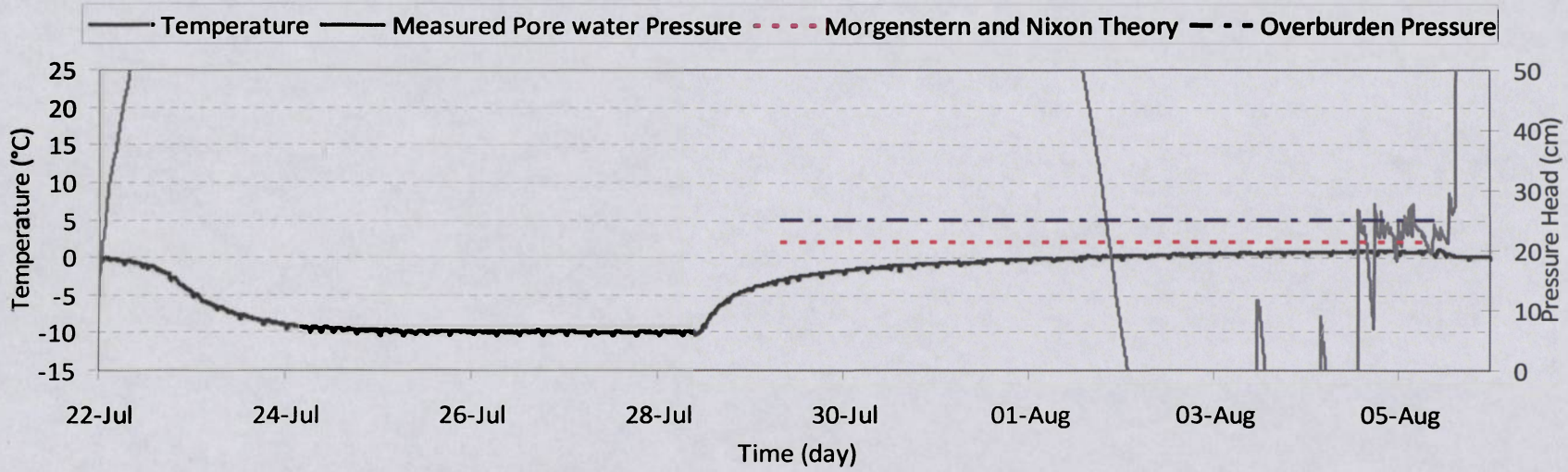

Figure 7.42 Total pore water pressure history, model M2: Cycle 4, depth 15 cm

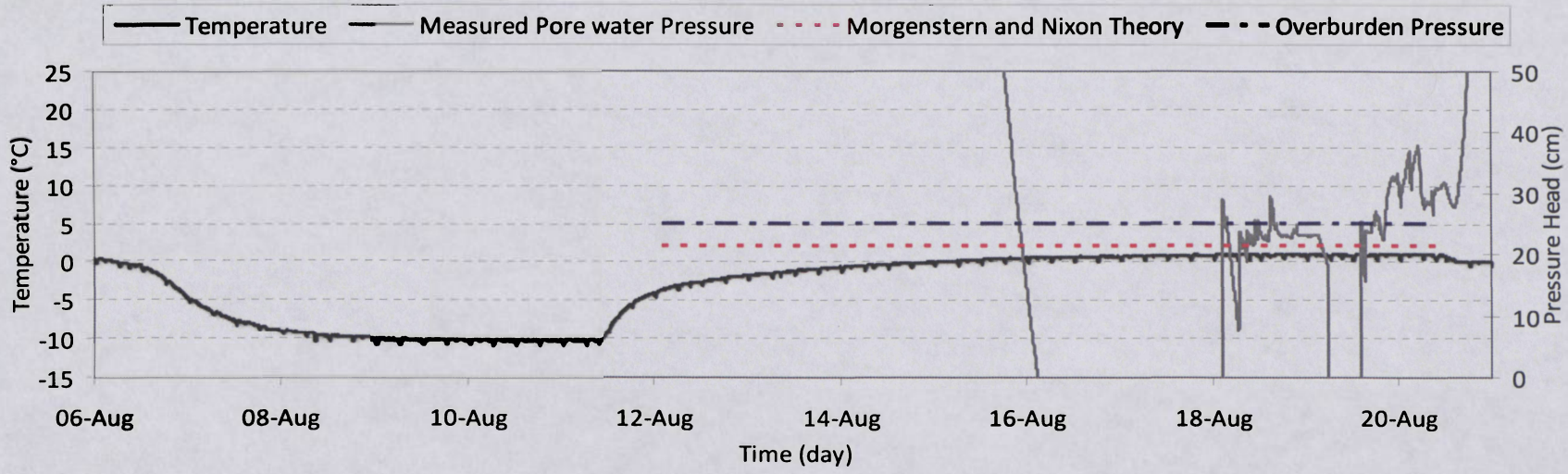

Figure 7.43 Total pore water pressure history, model M2: Cycle 5, depth 15 cm

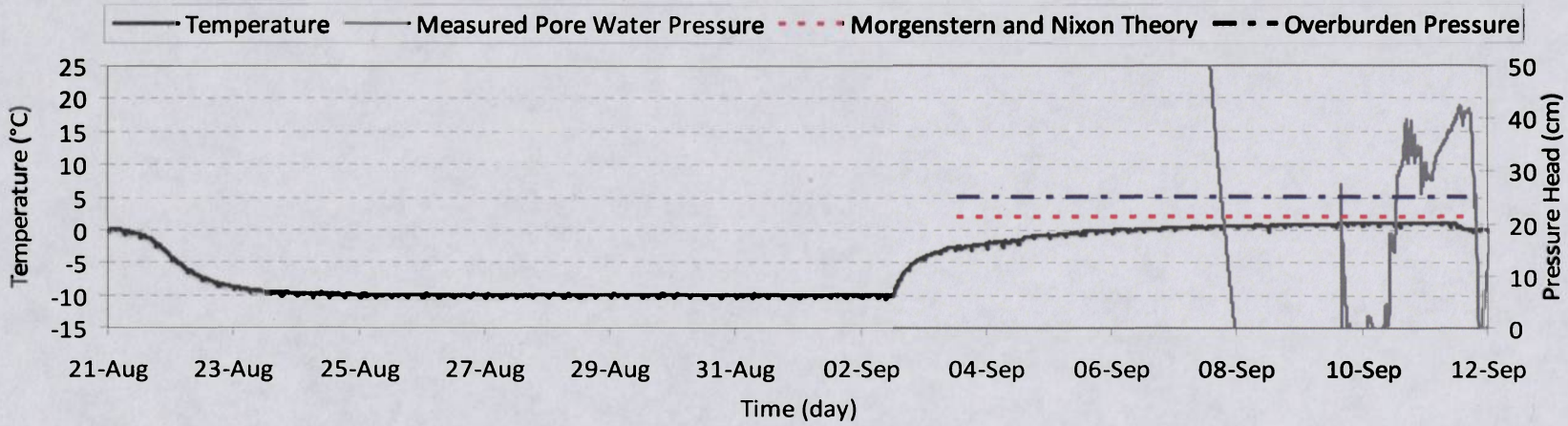

Figure 7.44 Total pore water pressure history, model M2: Cycle 6, depth 15 cm

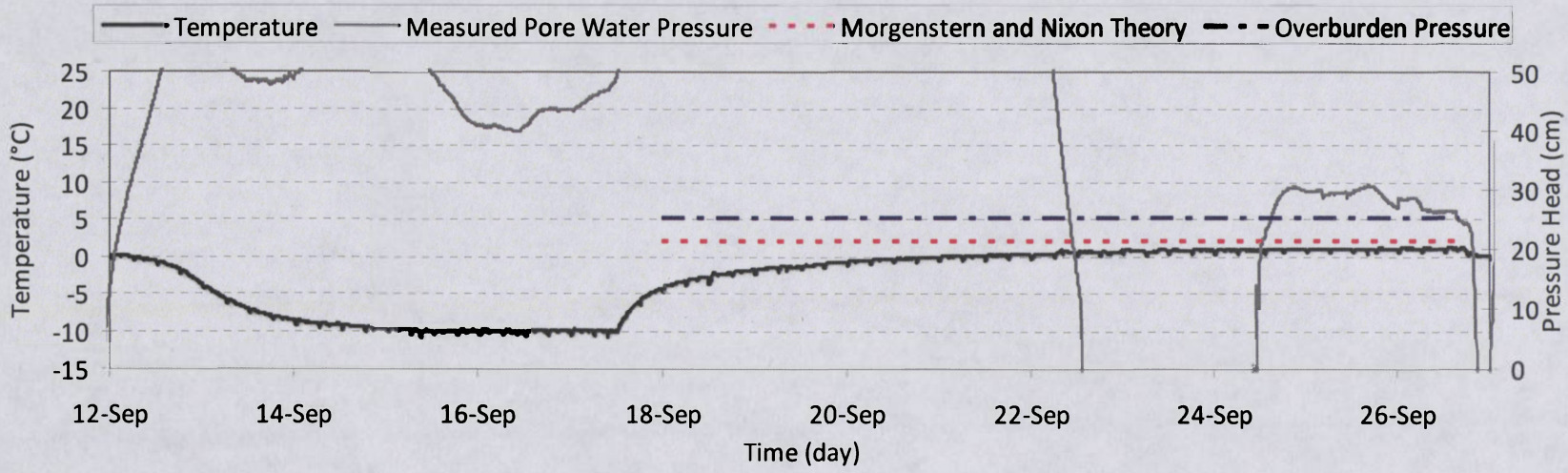

Figure 7.45 Total pore water pressure history, model M2: Cycle 7, detph 15 cm

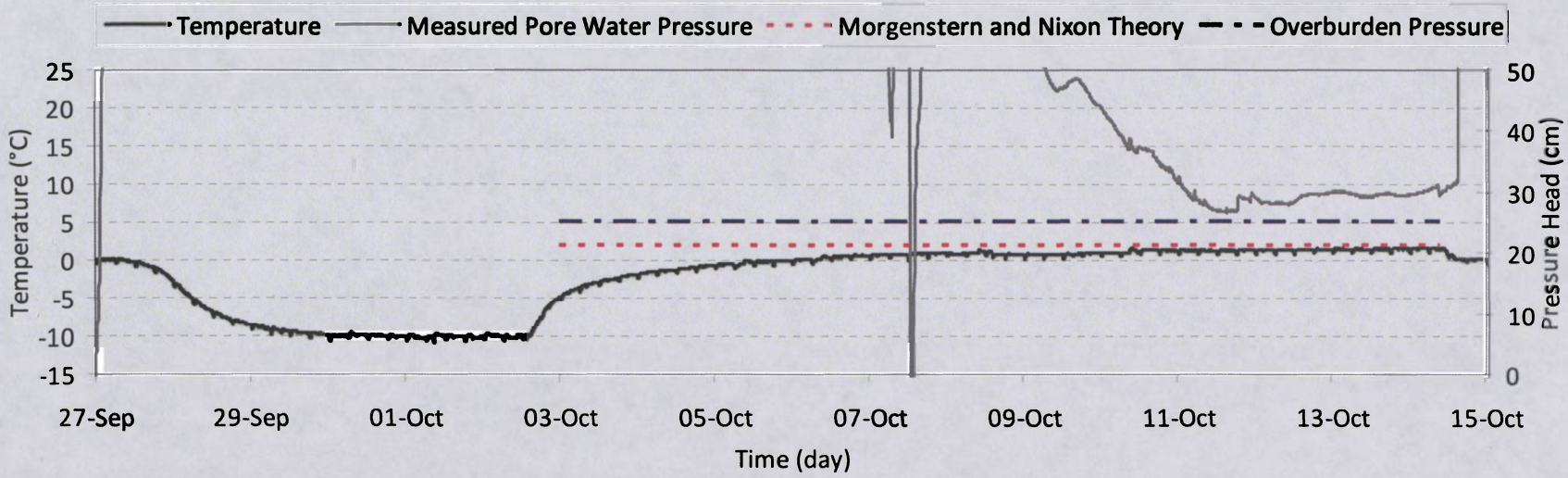

Figure 7.46 Total pore water pressure history, model M2: Cycle 8, depth 15 cm

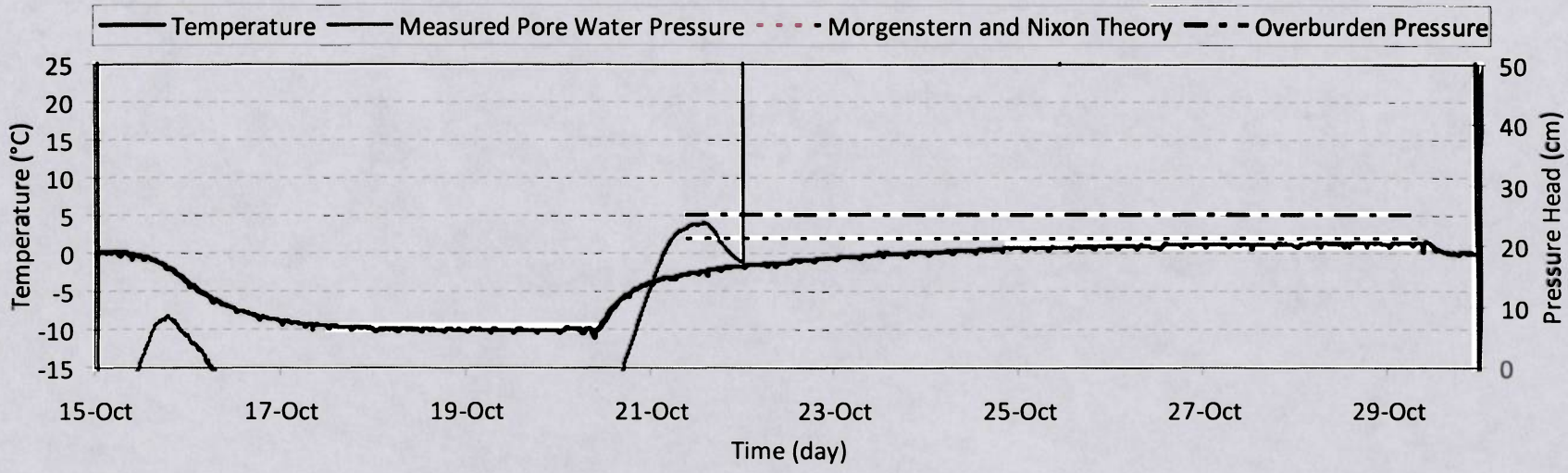

Figure 7.47 Total pore water pressure history, model M2: Cycle 9, depth 15 cm

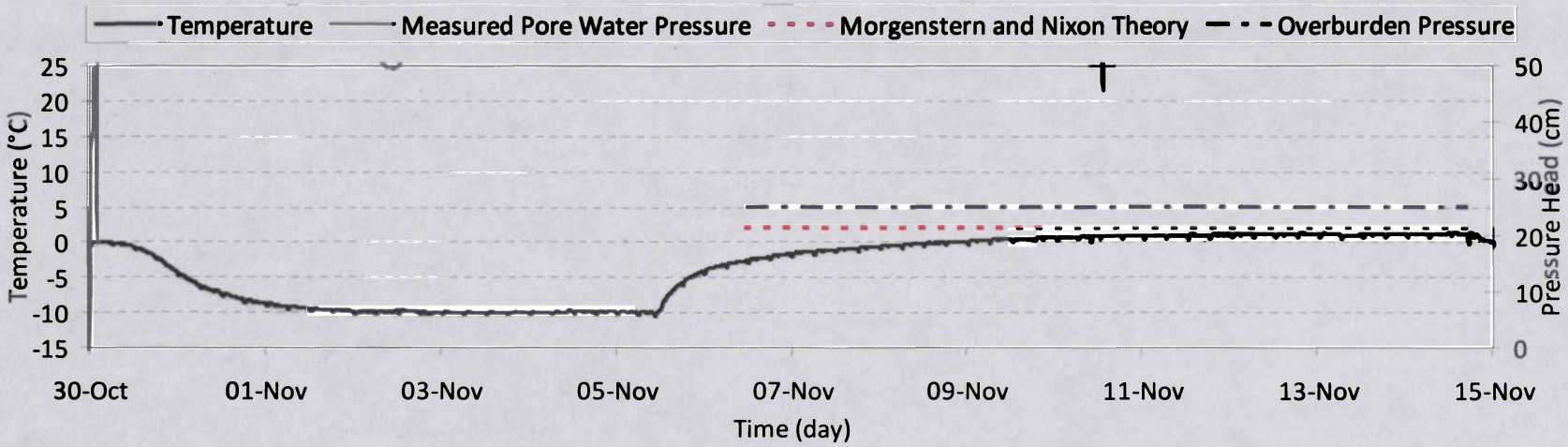

Figure 7.48 Total pore water pressure history, model M2: Cycle 10, depth 15 cm

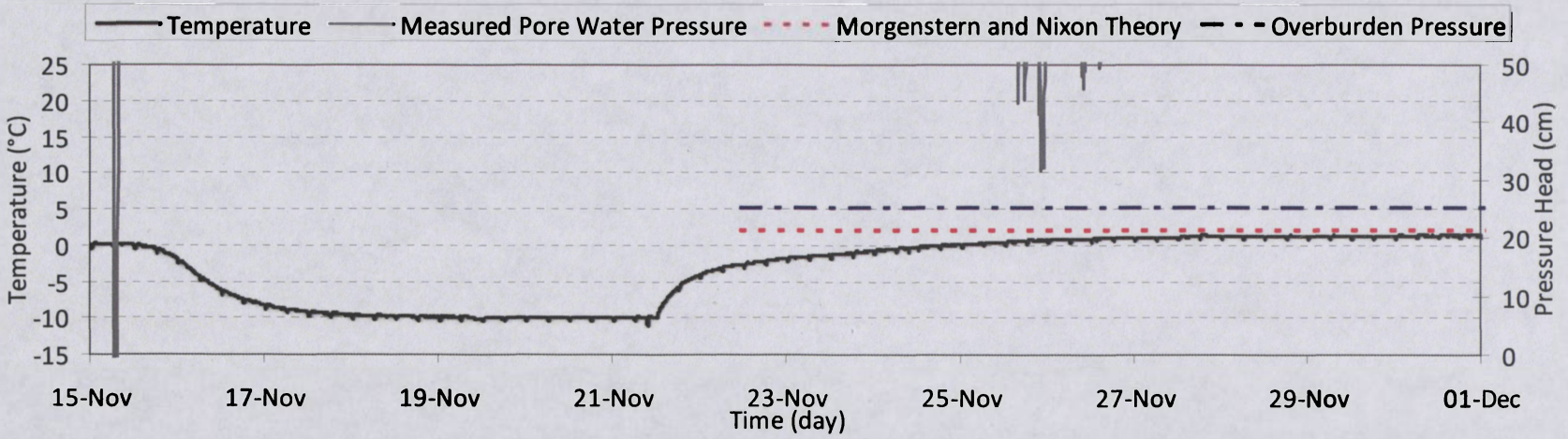

Figure 7.49 Total pore water pressure history, model M2: Cycle 11, depth 15 cm

8 Conclusions

A laboratory study was conducted on fine-grained soils from the Mackenzie valley to study the behaviour of the transient layer under extreme climate conditions. The temperature, moisture, soil structure and excess pore water pressure changes were observed during the eleven cycles of freezing and thawing. Two identical soil samples from the Mackenzie valley were tested under different conditions – one model (M2) was kept at the same freezing and thawing temperatures during all cycles whereas the other model (M1) was subjected to extreme temperature conditions during later thawed cycles. Exposing one sample to elevated air temperatures provided information on the extent of change in soil behaviour and characteristics.

Within both samples, moisture redistribution along the entire soil column was evident. The distinct moisture pattern is believed to be the result of the two-sided freezing of the sample and water migrating towards the freezing front. An ice-rich zone developed at the maximum cryofront depth as a result of the repeated freeze-thaw cycles. The findings indicate that the ice-rich zone can be part of the transient layer. During the last thawing cycle of M1, the air temperature was increased to 30°C while it remained at 25°C in M2. Consequently, the thickness of the ice-rich zone in M1 was reduced and shifted downwards by about 3 cm. The maximum depth of cryofront coincides with the depth of the ice-rich zone as well as with the depth of cryostructure change.

As a result of moisture migration, various cryostructures were created along the soil columns. Both samples have similar cryostratigraphies. Two distinct cryostructures were identified in both samples within the ice-rich zone. The lower part of the ice-rich zone had thicker ice lenses than the upper part. Lenticular cryostructures with mostly horizontal ice lenses were noted in the long-term permafrost zone in both models.

Laboratory results show an active layer increase of 15.2% for an increase in 5°C thawing temperature (from 25°C to 30°C). On the other hand, the active layer depth decreased by 6.2% for a decrease of 5°C thawing temperature (from 25°C to 20°C).

These laboratory findings are evidence that the characteristics of the transient layer are subject to change with increasing number of freeze-thaw cycles. Within this zone, ice may accumulate but can also be destroyed or altered under extreme climate conditions.

The excess pore water pressure data obtained from each thawing cycle were mostly higher than theoretical predictions based on the thaw consolidation theory developed by Morgenstern and Nixon (1971). The measured pore water pressure of some thaw cycles agree with the theory while others do not. The inconsistency between measurements and theoretical calculations can be caused by accuracy or malfunctioning of the sensors, existence of pore ice, or other reasons.

9 References

Andersland, O. and Ladanyi, B. 2004. *Frozen Ground Engineering,* 2nd ed., John Wiley and Sons Inc., Hoboken, NJ, 363 pages.

Aylsworth, J.A., Duk-Rodkin, A, Robertson, T., and Traynor, J.A. 2000a. Landslides of the Mackenzie valley and adjacent mountainous and coastal regions; in The Physical Environment of the Mackenzie Valley, Northwest Territories: a Base Line for the Assessment of Environmental Change, (ed.) L.D. Dyke and G.R. Brooks; Geological Survey of Canada, Bulletin 547, pp. 167-176.

Aylsworth, J. M., Burgess, M. M., Desrochers, D. T., Duk-Rodkin, A., Robertson, T. and Traynor, J. A. 2000b, Surficial geology, subsurface materials, and thaw sensitivity of sediments, The Physical Environment of the Mackenzie Valley, Northwest Territories: A Base Line for the Assessment of Environmental Change, edited by L. D. Dyke and G. R. Brooks, Geological Survey of Canada, 2000, Bulletin 547, pp. 43-47.

Bockheim, J.G. and Hinkel, K.M. 2005. Characteristics and significance of the Transition Zone in Drained Thaw-Lake Basins of the Arctic Coastal Plain, Alaska, *Arctic*, 58(4): 406 - 417.

Bray, M.T. 2008. Effects of soil cryostructure on the long term strength of ice-rich permafrost near melting temperatures. *Proceedings, 9th International Conference on Permafrost*, University of Alaska Fairbanks, June 29–July 3, 2008, 1:183-188.

Bray, M.T., French, H. M. and Shur, Y. 2006. Further Cryostratigraphic Observations in the CRREL Permafrost Tunnel, Fox, Alaska. *Permafrost and Periglacial Processes*, 17: 233–243.

Burn, C.R. 1998. The response (1958-1997) of permafrost and near-surface ground temperatures to forest fire, Takhini River valley, southern Yukon Territory. *Canadian Journal of Earth Sciences,* 35: 184-199.

Burn, C.R. 1988. The development of near-surface ground ice during the Holocene at sites near Mayo, Yukon Territory, Canada, *Journal of Quaternary Science*, 3: 31 - 38.

Burn, C.R. and Michel, F.A. 1988. Evidence for recent temperature-induced water migration into permafrost from the tritium content of ground ice near Mayo, Yukon Territory, Canada, *Canadian Journal of Earth Science,* 25: 909 - 915.

Burn, C.R., Michel, F.A and Smith, M.W. 1986. Stratigraphic, isotopic, and mineralogical evidence for an early Holocene thaw unconformity at Mayo, Yukon Territory, *Canadian Journal of Earth Science,* 23: 794 - 803.

Chamberlain, E.J. and Gow, A.J. 1979. Effect of Freezing and Thawing on the Permeability and Structure of Soils. *Engineering Geology*, 13: 73-92.

Cheng, G. 1983. The Mechanism of Repeated-segregation for the Formation of thick Layered Ground Ice, *Cold Regions Science and Technology*, 8: 57 - 66.

Cheng, G., and Chamberlain, E.J. 1988. Observations of moisture migration in frozen soils during thawing. *Proceedings, 5th International Conference on Permafrost*, Norway, August 2-5, 1: 308-312.

Dyke, L.D. 2000. Stability of Permafrost Slopes in the Mackenzie Valley, Geological Survey of Canada, 2000, Bulletin 547, pp. 177-186.

Dyke, L.D. 2004. Stability of frozen and thawing slopes in the Mackenzie Valley, Northwest Territories, *Proceedings of the 57th Canadian Geotechnical Society*

Annual Conference, Quebec City, 2004.

Eigenbrod, K. D., Knutsson, S. and Sheng, D. 1996. Pore-water pressures in freezing and thawing fine-grained soils. *Journal of Cold Regions Engineering,* 10(2): 77-92.

Everdingen, R. 2002. Multi-language glossary of permafrost and related ground-ice terms, Boulder, CO: National Snow and Ice Data Center/World Data Center for Glaciology, 88 pages.

French, H.M. 2007. *The Periglacial Environment,* 3rd ed. John Wiley and Sons Inc., Chichester, West Sussex, England, 458 pages.

Gavriliev, P.P. and Efremov, P.V. 2003. Effects of cryogenic processes on Yakutian landscape under climate warming. *Proceedings, 8th International Conference on Permafrost*, Zurich, Switzerland, July 20-25, 2003, 1: 277-282.

Geo-Slope International Ltd. 2007. Thermal modeling with TEMP/W – An engineering methodology. Alberta, Canada: TEMP/W Software User's Manual from Geo-Slope International Ltd., 2nd ed., 240 pages.

Goodrich, L. E. 1982. The Influence of snow cover on the ground thermal regime, *Canadian Geotechnical Journal,* 19: 421 - 432.

Grechishchev, S.E. and Grechishcheva, O.V. 1997. Some Details of the Ice Lens Formation Mechanism at the Bottom of a Seasonally Freezing Layer in a Permafrost Zone. Moscow Department, Institute of Earth Cryosphere, Russia.

Harris, C., Kern-Luetschg, M., Murton, J., Font, M., Davies, M.C.R. and Smith, F. 2008a. Solifluction on Permafrost and Non-permafrost Slopes: Results of a Large-scale Laboratory Simulation, *Permafrost and Periglacial Processes*, 19: 359 – 378.

Harris, C., Smith, J.S., Davies M.C.R. and Rea, B. 2008b. An investigation of periglacial slope stability in relation to soil properties based on physical modelling in the geotechnical centrifuge. *Geomorphology,* 93: 437–459.

Harris, C., Kern-Luetschg, M., Murton, J., Font, M., Davies M.C.R and Smith, F. 2008c. Full-scale physical modeling of solifluction processes associated with one-sided and two-sided active layer freezing, *Proceedings, 9th International Conference on Permafrost*, University of Alaska Fairbanks, June 29–July 3, 2008, 1: 663 – 668.

Harris, C., Murton, J.B. and Davies, M.C.R. 2005. An analysis of mechanisms of ice-wedge casting based on geotechnical centrifuge simulations. *Geomorphology,* 71: 328– 343.

Harris, C., Davies, M.C.R. and Rea, B.R. 2003. Gelifluction, viscous flow or plastic creep? *Earth surface processes and landforms,* 28: 1289-1301.

Harris, C. and Lewkowicz, A.G. 2000. An analysis of the stability of thawing slopes, Ellesmere Island, Nunavut, Canada, *Canadian Geotechnical Journal*, 37(2): 449 – 462.

Harris, C. and Lewkowicz, A.G. 1993. Form and internal structure of active-layer detachment slides, Fosheim Peninsula, Ellesmere Island, Northwest Territories, Canada, *Canadian Journal of Earth Science*, 30: 1708 – 1714.

Harris, C. and Davies, M.C.R. 1998. Pressures recorded during lab freezing and thawing of a natural silt-rich soil. *Proceedings, 7th International Conference on Permafrost,* Yellowknife, N.W.T., June 23 - 27, 1998, 1: 433 – 439.

Harris, C., Rea, B.R. and Davies, M.C.R. 2001. Scaled physical modelling of mass movement processes on thawing slopes. *Permafrost and periglacial processes*, 12: 125–135.

Harris, C., Davies, M.C.R. and Coutard, J.-P. 1996. An Experimental Design for Laboratory Simulation of Periglacial Solifluction Processes. Earth Surface Processes and Landforms. 21: 67 – 75.

Harris, S.A. 1988. Observations on the redistribution of moisture in the active layer and permafrost, *Proceedings, 5th International Conference on Permafrost*, Trondheim, Norway, August 1988, 1: 364 – 369.

Heginbottom, J.A. 2000. Permafrost distribution and ground ice in surficial materials; in *The Physical Environment of the Mackenzie valley, Northwest Territories: a Base Line for the Assessment of Environmental Change*, (ed) L.D Dyke and G.R. Brooks; Geological Survey of Canada, Bulletin 547, p. 31-39.

Heginbottom, J.A. and Radburn, L.K. 1992 (map). Permafrost and Ground Ice Conditions of Northwest Canada, Scale 1:1,000,000. Map 1691A. Geological Survey of Canada, Energy Mines and Resources Canada: Ottawa.

Hinkel, K.M., Nelson, F.E. Shur, Y. Brown, J. and Everett, K.R. 1996. Temporal changes in moisture content of the active layer and near-surface permafrost at Barrow, Alaska: 1962-1994, *Arc. Alp. Res.*, 28: 300-310.

Hinkel, K.M. Paetzold, F., Nelson, F.E., Bockheim J.G. 2001. *Patterns of soil* temperature and moisture in the active layer and upper permafrost at Barrow, Alaska: 1993–1999. *Global and Planetary Change*, 29(3-4): 293-309.

Höfle, C.M., Ping, C.L., and Kimble, J.M. 1998. Properties of permafrost soils on the northern Seward Peninsula, northwest Alaska. *Soil Science Society of America Journal,* 62: 1629–1639.

Johnston, G.H. 1981. Permafrost, engineering design and construction, Canada: National Research Council, Associate Committee Geotechnical Research.

Kern-Luetschg, M. and Harris, C. 2008. Centrifuge modelling of solifluction processes: displacement profiles associated with one-sided and two-sided active layer freezing, *Permafrost and Periglacial Processes,* 19: 379 – 392.

Kokelj, S.V. and Burn, C.R. 2003a. 'Drunken forest' and near-surface ground ice in Mackenzie Delta, Northwest Territories, Canada, *Proceedings, 8th International Conference on Permafrost*, Zurich, Switzerland, July 20-25, 2003, 1: 567 – 571.

Kokelj, S.V. and Burn, C.R. 2003b. Ground ice and soluble cations in near-surface permafrost, Inuvik, Northwest Territories, *Permafrost and Periglacial Processes*, 14: 275 – 289.

Kokelj, S.V. and Burn, C. R. 2005. Near-surface Ground Ice in Sediments of the Mackenzie Delta, Northwest Territories, Canada, *Permafrost and Periglacial Processes*, 16: 291 – 303.

Kokelj, S.V., Burn, C. R, and Tarnocai, C. 2007. The Structure and Dynamics of Earth Hummocks in the Subarctic Forest near Inuvik, Northwest Territories, Canada, *Arctic, Antarctic and Alpine Research*, 39(1): 99 – 109.

Konrad, J.M. and Morgenstern, N.R. 1980. A mechanistic theory of ice lens formation in fine-grained soils, *Canadian Geotechnical Journal*, 17: 473-486.

Lesage, K. 2008. Master's Thesis. Experimental studies of thaw consolidation of fine grained permafrost soils from the Mackenzie valley. University of Ottawa.

Lesage, K. and Wang, B. 2008. Experimental studies of thaw consolidation of fine grained permafrost soils from the Mackenzie Valley. *Proceedings, 61rst Canadian Geotechnical Conference*, Edmonton, Alberta, pp. 911-918.

Leshchikov, F.N. and Ryashchenko, T.G. 1978. Changes in the composition and properties of clay soils during freezing. *Proceedings, 2nd International Conference on Permafrost*, Yakutsk, U.S.S.R., July 13-28. Translated from the Russian, 2: 201-203.

Lewkowicz, A.G. and Clarke, S. 1998. Late-summer solifluction and active layer depths, Fosheim Peninsula, Ellesmere Island, Canada, *Proceedings, 7th International Conference on Permafrost,* Yellowknife, N.W.T., Canada, June 23-27, 1998, 1: 641-646.

Luscher, U. and Afifi-Sherif, S. 1973. Thaw consolidation of Alaskan silts and granular soils. *Permafrost; North American Contribution, Second International Conference; Physics, Physical Chemistry, and Mechanics of Frozen Ground and Ice*, pp. 325-334.

Mackay, J.R. 1983. Downward movement into frozen ground, western arctic coast, Canada, *Canadian Journal of Earth Science,* 20: 120-134.

Mackay, J.R. 1981. Active layer slope movement in a continuous permafrost environment, Garry Island, Northwest Territories, Canada, *Canadian Journal of Earth Science*, 18: 1666-1680.

Mackay, J.R. 1980. The origin of hummocks, western Arctic coast, Canada. *Canadian Journal of Earth Science*, 17: 996-1006.

Mackay, J.R. 1972. The world of underground ice. *Annals of the Association of American Geographers,* 62: 1-22.

Mackay, J.R. 1971. Ground ice in the active layer and the top portion of permafrost. In: Brown, R.J.E., ed. *Proceedings, Seminar on the Permafrost Active Layer. Memorandum 103.* Ottawa: National Research Council of Canada, pp. 26-30.

Mackay, J.R. 1971. The Origin of Massive Icy Beds in Permafrost, Western Arctic Coast, Canada, *Canadian Journal of Earth Science*, 8: 397-422.

Mageau, D.W. and Morgenstern, N.R. 1980. Observations on moisture migration in frozen soils, *Canadian Geotechnical Journal*, 17(1): 54-60.

McRoberts, E.C. and Morgenstern, N.R. 1974. The Stability of Thawing Slopes. *Canadian Geotechnical Journal*, 11: 447-469.

McRoberts, E. C. & Morgenstern, N.R. 1975. Pore water expulsion during freezing. *Canadian Geotechnical Journal*, (12):130-141.

Meilani, U., Rahardjo, H., Leong, E. and Fredlund, D.G. 2002. Mini suction probe for matric suction measurements. *Canadian Geotechnical Journal*, 39: 1427-1432.

Morgenstern, N.R. and Nixon, J.F. 1971. One-dimensional consolidation of thawing soils, *Canadian Geotechnical Journal*, 8: 558-565.

Morgenstern, N.R. and Smith, L.B. 1973. Thaw-consolidation tests on remoulded clays. *Canadian Geotechnical Journal*, 10: 25-39.

Morgenstern, N.R. and Nixon, J.F. 1975. An Analysis of the Performance of a Warm-oil Pipeline in Permafrost, Inuvik, N.W.T. *Canadian Geotechnical Journal*, 12: 199-208.

Morse, P.D., Burn, C.R. and Kokelj, S.V. 2009. Near-Surface Ground-Ice Distribution, Kendall Island Bird Sanctuary, Western Arctic Coast, Canada. *Permafrost and Periglac. Process.* 20: 155-171.

Murton, J.B. and Harris, C. 2003. The experimental simulation of ice-wedge casting, *Proceedings, 8th International Conference on Permafrost,* Zurich, Switzerland, July 20-25, 2003, 2: 807-810.

Murton, J.B and French, H.M. 1994. Cryostructures in permafrost, Tuktoyaktuk coastlands, western arctic Canada. *Canadian Journal of Earth Science,* 31: 737-747.

Nelson, F.E., Shiklomanov, N.I., Brown, J. and Hinkel K.M. 2008. Decadal Results from the Circumpolar Active Layer Monitoring (CALM) Program, *Proceedings, 9th International Conference on Permafrost.* University of Alaska Fairbanks, June 29-July 3, 2008, 2: 1273-1280.

Nelson, F.E., Outcalt, S.I., Brown, J., Shiklomanov, N.I. and Hinkel, K.M. 1998. Spatial and temporal attributes of the active-layer thickness record, Barrow, Alaska U.S.A. In Lewkowicz, A. and Allard, M. (eds.), *Proceedings, 7th International Conference on Permafrost.* Yellowknife, N.W.T., June 23 – 27, 1998, 1: 797-802.

Nixon, J.F. 1991. Discrete ice lens theory for frost heave in soils. *Canadian Geotechnical Journal,* 28: 843-859.

Nixon, J.F. 1973. Thaw-consolidation of some layered systems. *Canadian Geotechnical Journal,* 10: 617-631.

Overduin P.P., Kane, D.L., and van Loon, W.K.P. 2006. Measuring thermal conductivity in freezing and thawing soil using the soil temperature response to heating, *Cold Regions Science and Technology,* 45: 8-22.

Penner. E. and Goodrich, E. 1981. Location of segregated ice in frost-susceptible soil. *Engineering Geology*, 18(1-4): 231-244.

Penner, E. 1970. Thermal conductivity of frozen soils. *Canadian Journal of Earth Sciences,* 7: 982-987.

Penner, E., Johnston, G.H. and Goodrich, L.E. 1975. Thermal Conductivity Studies of Some Mackenzie Highway Soils. *Canadian Geotechnical Journal*, 12(3): 271-288.

Pollard, W., and French, H.M. 1980. A first approximation of the volume of ground ice, Richards Island, Pleistocene Mackenzie Delta, Northwest Territories, Canada. *Canadian Geotechnical Journal,* 17: 509-516.

Riseborough, D.W. 2002. The mean annual temperature at the top of permafrost, the TTOP model, and the effect of unfrozen water. *Permafrost and periglacial process,* 13: 137-143.

Riseborough, D.W. 2008. Estimating active layer and talik thickness from temperature data: Implications from modeling results. *Proceedings, 9th International Conference on Permafrost,* University of Alaska Fairbanks, June 29–July 3, 2008, 1: 1487-1492.

Riseborough, D.W and Smith, M.W. 1993. Modelling Permafrost Response to Climate Change and Climate Variability, *Proceedings, 4th International Symposium on Thermal Engineering and Science for Cold Regions*, New Hampshire, United States Army Cold Regions Engineering and Research Laboratory, Special Report 93-22, pp. 179-187.

Ryden, C.G. 1985. Pore pressure in thawing soil. *Proceedings of the 4th international symposium on ground freezing,* 5(7): 223-226.

Shur, Y.L. 1988. The Upper Horizon of Permafrost Soils, *Proceedings, 5th International Conference on Permafrost*, Trondheim, Norway, August 1988, 1: 867-871.

Shur, Y.L. and Jorgenson, M.T. 1998. Cryostructure development on the floodplain of Colville River Delta, Northern Alaska. *Proceedings, 7th International Conference on Permafrost*, Yellowknife, NWT, June 23 - 27, 1: 993-999.

Shur, Y.L. and Ping, C.L. 1994. Permafrost Dynamics and Soil Formation, *Proceedings of the meeting on classification, correlation, and management of permafrost-affected soils.*

Shur, Y.L. and Zhestkova, T. 2003. Cryogenic structure of glacio-lacustrine deposit. *Proceedings, 8th International Conference on Permafrost,* Zurich, Switzerland, July 20-25, 2003, 2: 1051-1056.

Shur, Y.L., Hinkel, K.M. and Nelson, F.E. 2005. The Transient Layer: Implications for Geocryology and Climate-Change Science, *Permafrost and Periglacial Processes*, 16: 5 – 17.

Smith, M.W. 1985. Observations of soil freezing and frost heave at Inuvik, NWT, Canada. *Canadian Journal of Earth Science*, 22: 283-290.

Smith, S.L. and Burgess, M.M. 2000. Ground Temperature Database for Northern Canada. Geological Survey of Canada Open File Report 3954 October, 2000.

Smith, M.W. and Riseborough, D.W. 2002. Climate and the Limits of Permafrost: A Zonal Analysis. *Permafrost Periglac. Process.* 13: 1-15.

Solomatin, V.I. and Xu, X. 1994. Water migration and ice segregation in the transition zone between thawed and frozen soil. *Permafrost and Periglac. Process.*, 1994, 5: 185-190.

Su, X., Wang, B., Nichol, S. 2006. Back analysis of a slope failure in permafrost in the Mackenzie valley, Canada, GSC, 601 Booth St., Ottawa, ON, Canada.

Taylor, A.E. and Judge, A.S. 1983. Climate and Permafrost. In: French, H.M., and Heginbottom, J.A., eds. Northern Yukon Territory and Mackenzie Delta, Canada: Guidebook to permafrost and related features. Guidebook 3. Fairbanks, Alaska: *International Conference on Permafrost*, pp. 21-34.

Viklander, P. 1998. Permeability and volume changes in till due to cyclic freeze-thaw. *Can. Geotech. J.* 35: 471-477.

Wang, B., Nichols, S. and Su, X. 2005. Geotechnical field investigations of landslides in fine-grained permafrost soils in the Mackenzie Valley, Canada, Submitted to the *Symposium on landslide risk analysis and sustainable disaster management*, Washington, D. C., October 2005.

Wang, B. and Lesage, K. 2007. Impact of climate change on slope stability in permafrost regions. *Proceedings, 8th International Symposium on Cold Region Development*, Tampere, Finland, Sept. 25-27, 2007.

Wang, B. and Saad, B. 2007. In-Situ Measurements of Ground Response to Heat Penetration Induced by Removal of Organic Cover in Fine-Grained Permafrost Soils, *Proceedings of the First North American Landslide Conference*, Vail, Colorado, June 2007.

Wang, B., Li, H. and Paudel, B. 2008. The transient layer and slope stability in permafrost soils. *Proceedings, 61rst Canadian Geotechnical Conference*, Edmonton, Alberta.

Wong, L.C. and Haug, M.D. 1991. Cyclical closed-system freeze-thaw permeability testing of soil liner and cover material. Department of Civil Engineering, University of Saskatchewan, Saskatoon.

Wu, Q. and Tong, C. 1991. Thaw-consolidation process and calculation of frozen clayey soil. *Proceedings, 6th international symposium on ground freezing,* 6: 89-92.

Yong, R.N. Boonsinsik, P. and Yin, C.W.P. 1985. Alteration of soil behaviour after cyclic freezing and thawing. *Proceedings, 4th International Symposium on Ground Freezing*, Sapporo, Aug. 5-7, 1985.

Yong, R.N. Boonsinsik, P. and Murphy, D. 1982. Short-term cyclic freeze-thaw effect on strength properties of a sensitive clay.

Zhao, S.-P., Zheng, J.-F., Ma, W. and Pu, Y.-P. 2008. Impact of Freezing on Water Migration in Silty Clay Samples. *Proceedings, 9th International Conference on Permafrost*, University of Alaska Fairbanks, June 29–July 3, 2008, 2: 2077-2081.

Appendix A – Thaw consolidation theory

Morgenstern and Nixon (1971) presented the following derivation for their thaw consolidation theory, starting with the movement of the thaw plane, given by the Newmann solution:

$$X(t) = \alpha\sqrt{t} \qquad [1]$$

Where:

- X: distance to the thaw plane from the soil surface;
- α: a thermal constant;
- t: time.

In the thawed region, it is assumed that the soil is compressible and that the theory of consolidation is valid.

$$c_v \frac{\partial^2 u}{\partial x^2} = \frac{\partial u}{\partial t} - \frac{\partial \sigma}{\partial t} \qquad [2]$$

Where:

- u: excess pore pressure;
- x: depth measured from the ground surface;
- σ: total stress applied;
- c_v: coefficient of consolidation.

If the stress does not vary with time, the equation becomes:

$$c_v \frac{\partial^2 u}{\partial x^2} = \frac{\partial u}{\partial t} \qquad [3]$$

Boundary Conditions:

$$t = 0; \quad X = 0 \qquad [4]$$

$$t > 0; \quad u = 0; \quad x = 0 \qquad [5]$$

From Darcy's Law, the volume of pore fluid expelled from a small layer ΔX as the thaw line advances through an increment in time Δt is

$$\Delta V = -\frac{Ak\dfrac{\partial u}{\partial x}(X,t)}{\gamma_w}\Delta t \qquad [6]$$

Where:

ΔV: change in volume in a layer of thickness ΔX;

A: cross-sectional area of a soil element;

k: hydraulic conductivity of the soil;

$\dfrac{\partial u}{\partial x}(X,t)$: excess pore pressure gradient at the thaw interface;

γ_w: unit weight of water.

The volumetric strain is given by:

$$\frac{\Delta V}{V} = \frac{\Delta V}{A\Delta X} = -\frac{k\dfrac{\partial u}{\partial x}(X,t)}{\gamma_w \dfrac{dX}{dt}} \qquad [7]$$

For a compressible soil:

$$\frac{\Delta V}{V} = -m_v \Delta \sigma' \qquad [8]$$

Where m_v is the coefficient of volume compressibility.

From Equations [7] and [8]:

$$\Delta \sigma' = \frac{c_v \dfrac{\partial u(X,t)}{\partial x}}{\dfrac{dX}{dt}} \qquad [9]$$

The total stress at x = X is:

$$\sigma(X,t) = P_0 + \gamma X \qquad [10]$$

Where P_0: load applied to the surface;

γ: unit weight of soil.

At x = X the pore pressure is

$$P_w(X,t) = u(X,t) + \gamma_w X \qquad [11]$$

And therefore the effective stress is

$$\sigma'(X,t) = P_0 + \gamma' X - u(X,t) \qquad [12]$$

Where γ' is the submerged unit weight of the soil.

$$\Delta \sigma' = \sigma'(X,t) - \sigma_0' \qquad [13]$$

Where σ_0' is the initial effective stress in the soil

It is assumed that in ice-rich soils, σ_0' is zero. Therefore, from Equations [12] and [13]:

$$\Delta\sigma' = P_0 + \gamma' X - u(X,t) \qquad [14]$$

From Equations [14] and [9], the following equation is derived:

$$P_0 + \gamma' X - u(X,t) = \frac{c_v \frac{\partial u}{\partial x}(X,t)}{\frac{dX}{dt}} \qquad \begin{matrix} x = X(t) \\ t > 0 \end{matrix} \qquad [15]$$

Analytical solution:

A solution to [3] subject to the boundary conditions expressed by [4], [5] and [15] is assumed in the form:

$$u(x,t) = A\,erf\left(\frac{x}{2\sqrt{c_v t}}\right) + Bx \qquad [16]$$

Where $erf(\ )$: error function

The constants A and B may be found from the boundary conditions and are:

$$A = \frac{P_0}{erf(R) + \frac{e^{-R^2}}{\sqrt{\pi} R}} \qquad [17]$$

$$B = \frac{\gamma'}{1 + \frac{1}{2R^2}} \qquad [18]$$

Where $R = \frac{\alpha}{2\sqrt{c_v}}$ is the thaw consolidation ratio

Therefore the complete solution is:

$$u(x,t) = \frac{P_0}{erf(R) + \frac{e^{-R^2}}{\sqrt{\pi}R}} * erf\left(\frac{x}{2\sqrt{c_v t}}\right) + \frac{\gamma' x}{1 + \frac{1}{2R^2}} \qquad [19]$$

It is convenient to introduce the dimensionless variables:

$$Z = \frac{x}{X(t)} \quad \text{and} \quad W_r = \frac{\gamma' X(t)}{P_0} \qquad [20]$$

[19] becomes:

$$u(Z,t) = \frac{u(Z,t)}{P_0 + \gamma' X} = \left(\frac{1}{1+W_r}\right) \frac{erf(RZ)}{erf(R) + \frac{e^{-R^2}}{\sqrt{\pi}R}} + \frac{z}{\left(1 + \frac{1}{2R^2}\right)\left(1 + \frac{1}{W_r}\right)}$$

[21]

Where W_r is the ratio of the relative magnitude of the applied load and the effective overburden pressure at the thaw line

For a weightless material ($W_r = 0$):

$$\frac{u(Z,t)}{P_0} = \frac{erf(RZ)}{erf(R) + \frac{e^{-R^2}}{\sqrt{\pi}R}} \qquad [22]$$

For a soil consolidating under its own weight ($W_r = \infty$):

$$\frac{u(Z,t)}{\gamma' X} = \frac{Z}{\left(1+\frac{1}{2R^2}\right)} \qquad [23]$$